DOI: 10.1002/((please add manuscript number))
Article type: Review

Graphene and related materials for resistive random access memories

By *Fei Hui*, *Enric Grustan-Gutierrez*, *Shibing Long*, *Qi Liu*, *Anna K. Ott, Andrea C. Ferrari*, and *Mario Lanza*[*]

Ms. Fei Hui, Dr. Enric Grustan-Gutierrez, Prof. Mario Lanza[*]
Institute of Functional Nano and Soft Materials (FUNSOM), Collaborative Innovation Center of Suzhou Nanoscience and Technology, Soochow University, 199 Ren-Ai Road, Suzhou, 215123, China
[*] Corresponding author Email: mlanza@suda.edu.cn
Fei Hui and Enric Grustan-Gutierrez contributed equally to this work

Prof. Shibing Liu, Prof. Qi Liu
Key Laboratory of Microelectronic Devices & Integrated Technology, Institute of Microelectronics of Chinese Academy of Sciences, Beijing 100029, China

Dr Anna K. Ott, Prof. Andrea C. Ferrari
Cambridge Graphene Centre, University of Cambridge, Cambridge, CB3 0FA, UK

Keywords: RRAM, GRM, graphene, resistive switching, non-volatile memory

Abstract

Graphene and related materials (GRMs) are promising candidates for the fabrication of resistive random access memories (RRAM). Here, we analyze, classify and evaluate this emerging field, and summarize the performance of the RRAM prototypes using GRMs. Graphene oxide, amorphous carbon films, transition metal dichalcogenides, hexagonal boron nitride and black phosphorous can be used as resistive switching media, in which the switching can be governed either by the migration of intrinsic species or penetration of metallic ions from adjacent layers. Graphene can be used as electrode to provide flexibility and transparency, as well as an interface layer between the electrode and dielectric to block atomic diffusion, reduce power consumption, suppress surface effects, limit the number of conductive filaments in the dielectric, and improve device integration. GRMs-based RRAMs fit some non-

volatile memory technological requirements like low operating voltages <1V and switching times <10 ns but others, like retention >10 years, endurance $>10^9$ cycles and power consumption ~10 pJ/transition still remain a challenge. More technology-oriented studies including reliability and variability analyses may lead to the development of GRMs-based RRAMs with realistic possibilities of commercialization.

List of acronyms

a-C	amorphous-Carbon
ALD	Atomic Layer Deposition
APTES	3-Aminopropyltriethoxysilane
BD	Dielectric Breakdown
BLG	Bilayer Graphene
BP	Black Phosphorous
CAFM	Conductive Atomic Force Microscopy
CBRAM	Conductive Bridge Random Access Memory
CF	Conductive Filament
CL	Current Limitation
CMOS	Complementary Metal Oxide Semiconductor
CVD	Chemical Vapor Deposition
CVS	Constant Voltage Stresses
1D1R	One Diode One Resistor
DRAM	Dynamic Random Access Memory
ECM	Electrochemical Metallization
FET	Field Effect Transistor

GB	Grain Boundary
GFET	Graphene Field Effect Transistor
GIG	Graphene/Insulator/Graphene
GO	Graphene Oxide
GODs	Graphene Quantum Dots
GO-PVK	Poly (N-vinylcarbazole) derived Graphene Oxide
GRMs	Graphene and Related Materials
h-BN	Hexagonal Boron Nitride
HRS	High Resistance State
ITO	Indium Tin Oxide
ITRS	International Technology Roadmap for Semiconductors
LM	Layered Material
LPE	liquid phase exfoliation
LRS	Low Resistance State
MC	Micromechanical Exfoliation
MIM	Metal/Insulator/Metal
MLG	Multilayer Graphene
MRAM	Magnetoresistive Random Access Memory
NVM	Non-Volatile Memory
PCBM	6-Phenyl-C61 Butyric acid Methyl ester
PCRAM	Phase Change Random Access Memory
PET	Poly(ethylene Terephthalate)
PMC	Programmable Metallization Cells
PMMA	Polymethyl Mechacrylate
PVP	Polyvinylpyrrolidone

RGO	Reduced Graphene Oxide
RRAM	Resistive Random Access Memory
RS	Resistive Switching
SLG	Single Layer Graphene
STTM-RAM	Spin Transfer Torque Magnetic Random Access Memory
ta-C	tetrahedral amorphous-Carbons
TEM	Transmission Electron Microscopy
TMDs	Transition Metal Dichalcogenides
TMO	Transition Metal Oxide
TPAPAM	Triphenylamine-based Polyazomethine
VCM	Valence Change Memory
ReRAM	Redox Random Access Memory
XPS	X-ray Photoelectron Spectroscopy
ZnONRs	ZnO Nanorods

1. Introduction

The impressive technology-driven development of modern societies during the last half-a-century has been possible thanks to the creation of new electronic devices (computers, smart phones, vehicles, medical equipments), which allow performing multiple complex operations (calculations, interpolations, statistics), leading to the apparition of new services (Email, GPS, data mining) that create new jobs and.[1] Non-volatile memories (NVM) are essential elements in most modern electronic devices and integrated circuits, as they allow storing enormous amounts of data (5.62×10^{10} Bits/cm^2)[2] in a fast (< ns/bit)[3] and cheap (~ 0.019 $/GB)[4] way. For this reason, the memory market has been estimated to reach 47 billion USD in 2016.[5] The most used

NVM device nowadays is called *NAND Flash*. [6] It stores one bit of information in a capacitor (integrated in the floating gate of a field effect transistor, FET).[6] The charge/discharge of the capacitor can be used to simulate the ones/zeros of the binary code, therefore to store information. Over the past 25 years technological advances have been linked to the scaling down of the *NAND Flash* memory, a process that enormously improved its size (from 2 μm node in 1980 to 7 nm node in 2015),[7] switching speed (from 1MB/s in 1985 to 10GB/s in 2012)[8] and cost (from 437,500 $/GB in 1980 to 0.019 $/GB in 2016).[4] As the size approaches the nanometer range, leakage currents in the capacitor become prohibitive, leading to severe information loss.[9-10] Therefore, in order to continue the exponential growth of information storage, new devices using non-capacitive working principles need to be developed.

According to the International Technology Roadmap for Semiconductors (ITRS), [2] the *performance requirements* for any NVM technology are (see Table 1): *i)* low operating voltages (< 1V); *ii)* low power consumption (~ 10 pJ per state transition); *iii)* high operation speed (< 10 ns/transition); i*v)* high endurance >10^9 cycles. This is defined as the number of times a NVM can be switched on/off before one of the states becomes irreversible;[2] *v)* long state retention time >10 years (>3 10^8 s). This is defined as the time before the state is lost (i.e. a state change without the application of any electrical stress happens);[2] *vi)* small size below 600 nm^2 (this refers to the cell that stores 1 bit of information, not the whole NVM); *vii)* good integration, with a capacity density larger than 10^{11} bits/cm^2; and *viii)* simple structure, which usually brings associated low fabrication costs. Several new memory concepts are being developed to achieve these targets,[1-2] including dynamic RAM (DRAM), [11-12], ferroelectric RAM, [13-14] phase change RAM (PCRAM), [15-16] magnetoresistive RAM (MRAM), [17-18] resistive RAM (RRAM), [19-20] conductive bridge RAM, [21-22]

carbon nanotube RAM, [23-24] spin transfer torque magnetic RAM (STTM-RAM), [25-26] molecular memories, [27-28] and Mott memories. [29-30] A comparative review of the different technologies being considered for future information storage can be found in Ref. [1] Until now the RRAM has shown the most advanced performances (see Table 1).[2, 31-33]

RRAM is a simple and industry-compatible structure formed by a matrix of metal/insulator/metal (MIM) nanojunctions,[34] in which the sandwiched dielectric enables reversible electrical resistance changes (see **Fig. 1**). This phenomenon, called resistive switching (RS), [34] can be used to induce two logic states: the high resistance state (HRS) and the low resistance state (LRS).[35] Cyclic transitions between these two resistive states can also be used to simulate the ones and zeros of the binary code, without the need of a capacitor, making possible the storage of digital information.[36] Before stable cycling between HRS and LRS can be achieved (i.e. 50 electrical pulses applied to the MIM cell produce 50 state changes without resistance mismatch), most RRAMs require a one-time activation process called forming.[34] This is defined as the first generation of a reversible dielectric breakdown (BD) in the insulator.[2] The RS phenomenon can be classified in: *i)* unipolar/bipolar if the electrical stresses that produce the state change are of the same/opposed polarity;[37] and *ii)* local/distributed if the atomic rearrangements that produce the state change take place at few/most locations within the area under stress.[36, 38]

State of the art RRAMs use transition metal oxides (TMO) as insulator, including HfO_2,[39-42] Al_2O_3,[43-46] TiO_2 [47-50] and TaO_X.[51-52] In these cells the RS is related to the formation and dissolution of a nanosized conductive filament (CF) across the insulator,[35] leading to an effective connection/separation of the two electrodes. In this case the RS is a local phenomenon. The physical mechanisms inducing the

formation/dissolution of the CF depend on the materials that compose the MIM cell (not only the insulator, but also the metal),[53] and it is thought that mainly two phenomena are predominant.[54-58] The first is the movement of oxygen vacancies in the TMO as a consequence of the applied field, leaving behind an oxygen-free metallic path.[54] These devices have been called valence change memories (VCM)[55] and/or redox random access memory (ReRAM)[56]. And the second is the generation of a CF made of metallic ions from the adjacent electrodes, which can penetrate into the dielectric when the MIM structure is polarized; [57] these devices are called electrochemical metallization (ECM) memories, [55] programmable metallization cells (PMC)[58] and/or conductive bridge random access memory (CBRAM)[59], even though all these names refer to the same device structure.

Over the last decade many RRAM prototypes with different characteristics have been reported. [39-52] Amongst them, the most remarkable performances are: *i)* Ultra fast (< 20 ns) logic state transitions; [31-32,44-45,60] the reset (LRS-to-HRS transition) process is usually much slower (60 ns) than the set (HRS-to-LRS transition) one. [61-62] Ref.[32] achieved sub-nanosecond (300 ps) set/reset transitions in HfO_X-based RRAMs. *ii)* Energy consumption per state transition as small as 0.1 pJ,[31,44] lower than that of other technologies, such as PCRAM [63] and MRAM.[64] *iii)* Long cycling endurance up to 10^{12} cycles. Ref.[33] achieved 10^{12} cycles using Ta_2O_{5-X}/TaO_{2-X} bilayer structures coupled with Pt electrodes. *iv)* Long data retention.[46] Ref. [65] indicated that RRAMs can retain the resistive state even at high temperatures (up to 200 ºC). *v)* As the switching takes place though nanosale CFs,[35] the area of the cell is just limited by the area of the CF (typically tens nm).[31] E.g., Ref. [31] reported a 10 nm × 10 nm TiN/Hf/HfO_X/TiN RRAM with fast ns-range on/off switching times at low-voltages below 3V, switching energy < 0.1 pJ/bit, excellent endurance > 5×10^7 cycles, current

on/off ratios (I_{ON}/I_{OFF}) > 50. The devices also showed 30 h retention at 200 ºC. RS has been observed in even smaller areas (~10 nm^2) using the tip of a conductive atomic force microscope (CAFM);[35] *vi)* Simple fabrication process, as the structure basically consists of a capacitor. The materials that form the RRAM have been used in the complementary metal oxide semiconductor (CMOS) technology for years. This favours their three dimensional integration.[66] RRAM have also shown potential multi bit storage per unit cell,[43,67] highly desired for future NVM technologies.[2]

All these performances, which can be found summarized in Table 1, have been observed in RRAMs made of different materials (e.g. TaO_X provides the highest endurance, HfO_X the fastest transitions and lowest power consumption), but no single RRAM device has yet shown all NVM technology requirements simultaneously.[1-2] The most critical tradeoffs in RRAM technology are speed-retention, power-speed and endurance-retention.[1] Crossbar Inc.[68] claimed the development of RRAMs covering all these capabilities, but no details about the composition of the core cell have been revealed to date. ITRI,[65] NEC,[69] and Fujitsu[70] have also announced similar devices, with no commercial device yet available. Panasonic has commercialized the *MN101L RRAM Embedded 8-bit* microcontroler unit,[71] Adesto is distributing their *Mavriq* 45 nm CBRAM,[72] and Nantero developed a RRAM memory using MIM cells integrated on CNTs, but their use is still limited to few applications (mainly sensors). [73] More information about commercial RRAMs can be found in Ref. [1]

Despite these developments, reliability issues (endurance, retention) and variability (cycle-to-cycle and device-to-device) of essential parameters like set/reset voltages (among others), as well as the understanding of failure mechanisms are still hindering RRAM large scale manufacturing.[1-2] Therefore, the reproducibility and uniformity of RS in RRAMs still remains an area of active research, with the need to

optimize the materials that form MIM cells.

One promising approach consists in replacing the metallic and/or insulating films of the MIM structures by novel materials with enhanced capabilities which, at the same time, could provide new features to the devices, such as transparency and flexibility. [74-75] Along these lines, graphene and related materials (GRMs) are at the centre of an ever increasing research area due to their unique electronic,[76] physical,[77] chemical,[78] mechanical,[79] optical,[80] magnetic[81] and thermal[82] properties.[83] The term GRMs encompasses graphene, graphene oxide (GO), transition metal dichalcogenides (TMDs), hexagonal boron nitride (*h*-BN), black phosphorous (BP) and any other layered material (LM) atomically thin (less than 20 layers) relative to graphene, with independency of its fabrication method, sheet size and thickness.[83] Furthermore a variety of thin carbon films have been considered for the implementation of RRAMs, ranging from sp^2 rich amorphous carbons (a-C),[84-87] to sp^3 rich tetrahedral amorphous carbons (ta-C). [88-89]

Here we will review the use of GRMs to build RRAMs, providing a working tool for many microelectronic engineers and materials scientists. In the following sections we describe the fabrication process of RRAM devices using GRMs (section 2), the advantages of using graphene as top/bottom electrode (section 3), the performances achieved using graphene oxides (section 4) and amorphous carbons (section 5), as well as recent observations of RS in other novel LMs, including TMDs, *h*-BN and BP, among others (section 6). The status and prospects of GRMs-based RRAM technology are discussed in section 7.

2. Fabrication of RRAMs using GRMs

A detailed description of the different approaches for the preparation of GRMs

can be found in Refs. [83, 90]. The aim of this section is to emphasize which methods have been used to implement GRMs-based RRAMs, with special emphasis on those that are scalable. We also include practical information for device integration.

2.1. Device architecture

Different device architectures to achieve NVM using GRMs have been suggested. The first used NVM configuration based on graphene-FETs (GFETs), such as floating gate and charge-trap memories.[91-99] RRAMs based on redox-switchable functionalized graphene nanoribbons,[100] stripes of thin (< 10 nm) graphitic material grown by chemical vapor deposition (CVD)[101] and graphene/metal contacts[103] were also proposed.

The first reports using GRMs in MIM-like RRAMs did not use the vertical MIM structure, but planar configurations containing a transversal insulating nanogap.[101-105] (see **Figs. 2a** and 2b). Ref. [103] fabricated a planar device with two electrodes connected by a single layer graphene (SLG) placed on a 300 nm SiO_2 / Si substrate by micromechanical exfoliation (MC), very similar to a single back gate GFET.[106] By applying between 2.5 and 4 V, the breakdown of the SLG channel (physical fracture) was induced.[103] By applying a reverse bias from 0.1 up to 5 V, reproducible transitions between a HRS and LRS could be observed. Ref.[104] improved this performance using 5–10 nm thick films of graphitic material (consisting of discontinuous graphene sheets grown by CVD) and reported bistability in current vs. voltage (*I-V*) curves with I_{ON}/I_{OFF} up to 10^7 and switching times as fast as 1 μs. Ref. [105] further enhanced the capabilities of planar bilayer graphene (BLG) switching devices by coating a 10 nm layer of conducting 3-Aminopropyltriethoxysilane (APTES) molecules over the surface of the insulating region (SiO_X). Nevertheless, the difficulty in controlling the size of the

nanogap [104-106] and the probably large device-to-device variability (statistical information has never been reported), made most works concentrate on the vertical MIM-like RRAMs (like that shown in Fig. 2b), which is by far the most widespread and competitive device architecture developed until now for RS-based NVMs. [107-112]

The core cell of state-of-the-art RRAMs consist of a matrix of vertically aligned MIM structures[34-35] (see Fig. 2b). These can be fabricated by sequentially depositing each material on a desired substrate, using standard industrial processes such as atomic layer deposition (ALD), [113] sputtering [107] and/or electron-beam evaporation. [114] GRMs can be used in multiple parts of RRAMs (see Figs. 2c-2f): *i)* replacing one/all layers in the MIM structure, leading to alternative configurations such as, e.g., graphene/insulator/graphene (GIG) or metal/*h*-BN/metal structures; and *ii)* introducing one/few additional GRM layer/s within the standard MIM cell, leading to MGIM, MIGM, MGIGM, GMIM, MIMG and GMIMG (where *G* denotes a generic GRM). Another possible configuration is the MI**G**IM structure, in which the GRM is used for charge trapping purposes [115-116] (see Fig. 2g). In all cases, the goal is to improve the NVM performance (i.e. switching speed, retention time, endurance, power consumption) as well as to provide the device with some of the genuine properties of the GRM (i.e. transparency [74] and flexibility; [75] enhanced thermal heat dissipation,[117] and chemical stability has been achieved using GRMs in other devices like FETs,[118] meaning that these properties may be also achieved in RRAMs).

2.2. Insertion of GRMs in the RRAM structure

The main challenge associated to the fabrication of vertical RRAMs using GRMs is that the GRM cannot be introduced in the MIM structure using the conventional fabrication tools above mentioned. First, a large portion of the reports on

GRMs used non-scalable techniques, like MC.[119-120] MC can produce flakes with a very low amount of defects,[121-122] but this is not industrially scalable yet. This strongly limits its application in RRAMs, and only allows RS studies using local techniques, such as CAFM.[124] Industrially scalable GRM production methodologies,[83] such as liquid phase exfoliation (LPE) [83,90,124] and CVD [90,124-125] are now available, and are the most used for the fabrication of RRAMs.[126-129]

LPE gives GRMs flakes of different sizes and thicknesses (with sizes typically below 1 μm in diameter and 1-20 layers thick) [83,90,124,130]. They have been introduced in RRAMs by drop casting,[131] spin coating,[132] or ink-jet printing,[133] which leads to 15-500 nm thick films. [126-129] LPE is cheap and scalable,[83] but the rough surface of the samples obtained by this method (typically RMS > 20nm) [134] may be an important source of variability, [135-137] which is one of the main concerns of RRAM technology. [1] The lack of variability analyses in all LPE based-RRAM reports published to date [138-141] indicates the need of further studies.

CVD is the most widely used technology to produce GRMs for electronic devices, as it allows wafer scale production.[83] GRMs can be grown by CVD on different substrates. In the case of SLG, metals with low carbon solubility and catalytic activity (such as Cu, Ir, Co, Ni) are necessary.[142-144] Some reports claim direct CVD growth on SiO_2 [145-147]. For MoS_2, [148-152] TiS_2,[153] TaS_2,[154] WS_2,[155], $MoSe_2$[156-157] and WSe_2[158] direct CVD growth on insulating substrates like SiO_2 and Al_2O_3 is preferred because their lattice constants offer a good match to that of the GRM. [148-158] CVD-growth of *h*-BN was also reported on Cu,[159] Fe, [160] and Pt.[161] Ref. [162] reported the CVD growth of BP on a Si substrate using a red phosphorous powder source.

When working with insulating GRMs (like *h*-BN) grown by CVD, the metallic substrate used for the CVD growth can be used as bottom electrode. [163] This facilitates

the fabrication of the RRAM device, and the top electrode can be then deposited by photolithography or shadow mask, plus metal evaporation. However, the underlying metal can have large roughness (RMS ~30nm)[164] due to the polycrystallization suffered during the CVD growth at high temperatures, usually not below 800 ºC.[142-144,148-152] Therefore, the growth of insulating GRMs on ultra-flat metal-coated wafers is of utmost importance to avoid roughness-induced variability, as well as to offer better integration with the industry. In general, the thermal budget may be an issue for the fabrication of GRMs-based RRAMs. On the contrary, when working with conductive GRMs (like graphene), the metallic substrate used during the CVD growth is a burden for RRAM fabrication because sometimes the presence of the GRM is required on substrates that are not favourable for its CVD growth, *e.g.* HfO_2 and other TMOs).[106] One approach is to transfer the GRM on the desired substrate using polymer scaffolds, being polymethyl mechacrylate (PMMA) the most commonly used.[83,90,165-167] The problems associated with this technique are: *i)* local physical breakdown of the GRM,[168-169] producing cracks within its area, which may locally alter the properties of the devices. [170-171] E.g., a MGIM device in which the GRM contains holes may lead to local MIM structures; and *ii)* polymer residuals on the GRM surface. Although this may not produce the failure of the device, since the polymer is insulating, this can be understood as a decrease of the effective area of the MIM device (capacitor). The introduction of annealing processes (at ~ 300 ºC) [172] may contribute to the removal of these impurities, but may produce the polycrystallization of TMOs in the RRAM (if any), leading to unwanted inhomogeneities and thickness fluctuations.[135-137] Polymer-free transfer techniques, such as electrostatic graphene/substrate attraction can be used,[173] but this may increase the complexity of the process.[174-175]

Other methodologies to grow GRMs are physical vapour deposition, [176] growth

on SiC, [177] and hydrothermal method [178] but, to the best of our knowledge, their use in the RRAM technology has not been reported yet.

The deposition of insulators on GRMs is also problematic. According to Ref. [179] TMOs cannot be deposited directly by atomic layer deposition (ALD) on defect-free SLG, due to the lack of dangling bonds or functional groups. Ref.[180] observed that, when trying to grow HfO_2 by ALD on MoS_2, HfO_2 did not form a homogeneous film, but islands on the MoS_2 surface, probably located at MoS_2 defects (where there are dangling bonds that allow HfO_2 agglutination).[181] One possible approach is the functionalization of the GRM surface, [182-185] which may enhance the homogeneity of the TMO film at the interface. The most common strategies to achieve a uniform SLG/high-k interface are: functionalization with NO_2,[182] metal seed layer,[183] organic seed layers[184] and ozone (O_3).[182-184] An interesting method to generate a SLG-TiO_x/Al_2O_3/TiO_2-SLG cell was proposed in Ref.[185] A seed Ti layer was first deposited on the bottom SLG electrode by e-beam evaporation and then oxidized to TiO_x in air. Then the Al_2O_3/TiO_2 stack was deposited by ALD, and the top SLG electrode was transferred. Another similar GIG device was fabricated in Ref. [186] by depositing a bilayer insulating film made of Ta_2O_{5-x}/TaO_y on a CVD-SLG using radio-frequency and reactive sputtering (respectively), followed by another CVD-SLG transfer.

For devices designed to be tested in a probe station, the use of top metallic electrodes is unavoidable, as placing the large tip on a SLG top electrode may damage it. Therefore, the GI interface is in fact a MGI. One method able to measure the SLG electrodes without the need of metal deposition is the use of CAFM, which controls very accurately the tip/sample contact force and does not damage the GRM surface.[187] CAFM can also allow the investigation of ultra scaled RRAMs. [35]

3. Use of graphene as top/bottom electrode

3.1. Transparency

One motivation for using graphene in electronic devices is to provide them with flexibility [75] and transparency.[74] For transparent devices, indium tin oxide (ITO) has been traditionally the most preferred electrode material,[188-190] but its brittle nature makes it unsuitable for flexible/foldable devices. One alternative is using organic materials, such as conductive polymers,[191] but in this case the NVM performance (i.e. retention times of just 10^4 s and endurance below 100 cycles) are usually much lower than the state-of-the-art TMO-based RRAMs. [1, 31-33]

Ref.[192] fabricated transparent MLG/Dy_2O_3/ITO structures by transfer of CVD-grown multilayer graphene (MLG) patterned in a subsequent photolithography step. The devices showed forming-free unipolar RS with $I_{ON}/I_{OFF} \sim 10^5$, low set and reset voltages (0.4 and 0.2V respectively), endurance >100 cycles, retention time > 10^4 s and typical switching power and speed of 4.4 μW and 60 ns. Furthermore, the devices showed a transparency ~ 80%. The performance as RRAMs of these devices overcomes that of other graphene-free cells, such as ITO/ZnO/ITO,[188] ITO/AlN/ITO,[189] ITO/Gd_2O_3/ITO,[190] and other transparent prototypes like Ga-doped ZnO.[193] Ref.[105] further improved the optical performance by building BLG/SiO_X/BLG structures, with a transmittance > 90% (see **Figs. 3a-3c**). Ref.[74] also achieved good RRAM functionality with an overall light absorptance < 25% in devices made of ITO/SLG/ZnO/ITO, which also showed better RS uniformity than its graphene-free counterparts. Ref. [75] used MLG with a transmittance up to 92% to fabricate a flexible organic memory device. The characteristics of transparent and flexible graphene-based RRAM devices found in the literature are summarized in Table 2. Coupling graphene electrodes with organic RS media seems to provide the highest transparency ~ 92%, [194] maintaining high $I_{ON}/I_{OFF} \sim 10^6$ and long retention ~ 10^4 s. All graphene based

transparent devices were fabricated by CVD plus transfer (see Table 2).

3.2. Flexibility

Graphene can be used to increase the flexibility of RRAM cells. Ref. [105] reported BLG/SiO_X/BLG cells with no RS degradation after bending >300 times at a bending radius (r_b) ~ 1.2 cm (see **Fig. 3d**). Ref. [195] presented a flexible organic device based on SLG sandwiched by two insulating poly(ethylene terephthalate) polymer (PET) layers.[195] A Ni/PMMA/SLG/PMMA/ITO/PET cell fabricated by transferring a CVD-SLG and spin-coating the PMMA layers. In this case SLG was used as a charge storage medium. The electric measurements indicate a good memory performance including endurance > 1.5×10^5 cycles, I_{ON}/I_{OFF} > 10^6, and retention time > 1×10^5 s. Especially significant was the lack of interference observed for scaled-down devices with SLG, as well as the ability of the devices to maintain similar switching characteristics (set/reset voltages and I_{ON}/I_{OFF}) even after being bent (r_b ~ 1cm) over 1.5 × 10^5 times. Ref.[75] designed 8 × 8 cross-bar array-type flexible organic RRAMs on PET using MLG electrodes coupled with two different active layers: one polyimide and the other 6-phenyl-C_{61} butyric acid methyl ester (PCBM). Typical write-once-read-many characteristics and high I_{ON}/I_{OFF} up to 10^6 were achieved; for > 1000 mechanical cycles (r_b between 4.2 and 27 mm) the devices maintained a retention time > 10^4 s with < 12.5 % resistance fluctuations in both HRS and LRS.[75] Comparing the RS performance of all flexible RRAMs exposed to mechanical stresses is complex because these may have been applied using different bending radius and times. The influence of the bending time in flexible RRAM was not reported to date, while most works report r_b.[75,105,195-196] Smaller r_b should produce more damage to the devices, as they introduce higher stresses. Therefore, from Table 2 it can be concluded that the RRAMs with the

best performance under bending are those in Ref. [195]

3.3. Blocking layer for atomic diffusion

The most common electrode materials in RRAMs are Al, Pt, Au, Cu, Ti and Ni.[197-202] These not only serve as contacts, but they play an essential role on the physics,[53] kinetics [202] and statistical distribution [203-204] of the RS. E.g., different metallic electrodes can alter the number of CFs in the RS media, which has an impact on the shape (sharp or progressive) of the reset process, among others.[53] One strategy to tune the switching characteristics of RRAMs is the use of active metal electrodes (like Ti or Zr) that can interact with the species from the insulator. E.g. in Pt/Ti/HfO_2/Pt cells [205-207] oxygen atoms from the HfO_2 layer can interact with the Ti electrode. This allows the observation of bipolar RS thanks to the movement of oxygen in-and-out of the HfO_2 film, forming an O-vacancies based CF with the narrower end at the cathode side.[206] On the contrary, in Pt/HfO_2/Pt devices [205-207] the O-vacancies movement towards the electrode is difficult, generating a CF that can only be disrupted by applying large currents, [205-206] which melt the filament by Joule effect.[208] In this case, the forming event is sharper, which leads to a higher $I_{ON}/I_{OFF} \sim 10^4$ for Pt/HfO_2/Pt instead of ~ 12 for Pt/Ti/HfO_2/Pt, but the endurance may be worse due to the generation of avalanche current,[209] BD spot propagation,[210] thermal heat,[211] insulator contamination by metal migration[212] and dielectric breakdown induced epitaxy[213]. Comparing the performance of Pt/Ti/HfO_2/Pt and Pt/HfO_2/Pt cells Refs. [205-217] observed that, while the LRS currents in Ti-free devices were linear and the filament was symmetric, those including inserted Ti layers drove exponential currents representative of partially formed conical filaments, with the narrower end at the HfO_2/Ti interface. This was confirmed by fitting the experimental *I-V* curves to the

Quantum Point Contact model. [214] Moreover, at larger electrical fields, the movement of metallic ions may also be activated, allowing their penetration in the TMO and producing even larger changes in the device conductivity than the motion of oxygen vacancies.[40] Therefore, as SLG is impermeable[77,215], introducing SLG between metal and insulator alters these interactions.[108, 216]

Ref.[107] observed that inserting CVD-SLG in Al/WO_3/Al structures *stabilized* the characteristics of the RRAM devices (see **Figs. 4a,b**), reducing the variability of the set/reset voltages and currents, as well as enhancing the endurance. In the SLG-free cells, when positive bias is applied to the top electrode, oxygen ions from the Al/WO_3 interface are pushed into the oxide bulk, leading to the formation of CFs rich in oxygen vacancies (which can be charged by electrons). During the reset process, the oxygen-deficient region is reoxidized. Ref. [107] suggested that SLG blocks the diffusion of oxygen ions into the reactive Al layer, which reduces the cycle-to-cycle variability in *I-V* curves. The dissolution of oxygen in SLG is very scarce and it presents a high potential barrier for oxygen diffusion.[56] Both factors impede the diffusion of oxygen ions through SLG, avoiding the interaction with the metallic top electrode. Ref. [217] suggested that the electric field applied during the set operation can move the oxygen ions towards the metal/oxide interface, but they cannot penetrate into the Ti electrode due to the presence of the interfacial SLG (see **Fig. 4c**). At most, the oxygen ions could form covalent bonds with the SLG defects (missing atoms and/or dangling bonds [185,217]), leading to a p-type doping that can be released during the reset transition. However, Ref.[55] reported the migration of metallic ions from the electrode into the dielectric in ECMs, even with the presence of interfacial SLG. Ref.[55] reported that, in ECM cells based on Ta/SLG/TaO_X/Pt stacks, the switching is influenced by the formation of Ta ions and their interaction with the TaO_X active layer. Nevertheless, Ref.

[55] used large device areas ranging between 25 × 25 and 1000 × 1000 μm^2. The presence of cracks and leaky grain boundaries is something usual in CVD-grown and transferred SLG[218], thus MLG may provide a better protection than SLG.

3.4. Lowering power consumption

The out-of-plane SLG contact resistance is larger than that of metallic electrodes,[219] which can be used to reduce the currents in both resistive states of the RRAMs, lowering power consumption. Ref.[217] analyzed bipolar RS in TiN/Ti/SLG/HfO_X/Pt RRAMs. The cyclic voltammograms obtained indicated a reduction of the reset current by a factor ~11 compared to the SLG-free device (Fig. 5a), further corroborated using cumulative probability plots. Despite this improvement, the plots indicate that the HRS currents under positive polarity for the SLG-based devices increase, which is an unwanted effect. Ref.[217] pointed out that comparisons between SLG-based and SLG-free cells using similar current limitations (CL, defined as the threshold current used during the forming/set processes to limit the BD truculence) were not reliable due to the low endurance of SLG-free cells at such low (100 μA) current levels. To solve this problem, Ref.[217] compared the typical RS cycles using the optimal CL for each cell (10 μA for the SLG-based cell and 100 μA for the SLG-free one), understanding *suitable* as the one that produces a lower cycle-to-cycle variability (Fig. 5b), and concluded that: *i)* The CL needed to stabilize RS in the SLG-based device is lower, which from the power consumption point of view is an advantage. Despite the current in HRS being the same, the LRS current was reduced more than one order of magnitude. This implies that, when the filament is completely formed in LRS, its size (diameter) is much smaller using SLG-based electrodes. *ii)* The reduction of LRS current reduces I_{ON}/I_{OFF}. *iii)* SLG avoids current overshoot during the set process, which

also reduces the maximum current during the reset transition (I_{RESET}): in the SLG-based RRAM, I_{RESET} was half CL, while in SLG-free, I_{RESET} was 2-3 times larger than CL (see Fig. 5b).

Ref. [98] fabricated a Pt/Ti/TiO_x/SLG RRAM and reported similar results as Ref. [217] (Fig. 5c). I_{ON}/I_{OFF} as well as both HRS and LRS currents were reduced. Therefore, from Refs. [98,217], SLG helps to stabilize RS at lower CLs, which reduces the reset current (probably due to the formation of narrower CFs) and the overall power consumption.

Ref.[55] also observed that lower CLs (10 μA) stabilize Pt/Ta/SLG/TaO_X/Pt RRAMs (Fig. 5d), producing an increase of the on the reset current and I_{ON}/I_{OFF} in the SLG-based cell (compared to SLG-free). These results are surprising because the CL used for the SLG-based cells was smaller, and it is usual for the reset to take place at currents similar to CL in all kinds of RRAMs (including ECMs, VCMs).[55] Indeed, Fig. 5d shows a current overshoot. We cannot tell how reproducible these observations are because, unlike Ref. [217], Ref. [55] did not include the evolution with the number of cycles. On the other hand, Ref.[217] observed reset currents smaller than CL in SLG-based devices. More work is thus necessary to confirm these observations.

3.5. Suppression of surface effects

Most devices based on TMOs are influenced by surface effects,[220] including surface band bending,[221] chemisorption/photodesorption,[222] and surface roughness.[223] The barrier for species diffusion provided by SLG was used by several groups. *E.g.*, Ref. [74] inserted SLG into an ITO/ZnO/ITO stack to explore the device performance variation under different atmospheres (see **Fig. 6**). O^{2-} chemisorption happened at the top surface of the MIM structures (in contact with the environment),

resulting in defects associated to the oxygen partial pressure. Due to oxygen ion chemisorption, the partial pressure of oxygen can influence the TMOs electrical properties, as more O_2 molecules are chemisorbed with increased partial pressure.[224-227] O_2 molecules are absorbed at the TMO surface defects, [224] such as oxygen vacancies,[228] acting as electron acceptors to form chemisorbed oxygen ions, which will contribute to decrease the conductivity of metal oxide. However, the introduction of SLG (i. e. forming an ITO/SLG/ZnO/ITO structure) protects the ZnO film from chemisorption of O_2 molecules, avoiding the surface effect. The effect of oxygen ions chemisorption on the switching properties of RRAMs was analyzed in Ref.[74] by comparing the resistance in HRS and LRS with and without SLG electrodes under various ambient conditions. Without SLG, HRS shifts to a higher resistance as it can interact with the atmospheric O_2,[224] because of the oxygen ions chemisorbed induce lower conductivity near the ZnO surface.[224,226] As the oxygen ions concentration increases, the surface band bending effect is more pronounced. However, with the SLG introduction at the ITO/ZnO interface the variation of HRS resistance is suppressed,[74] and it almost completely decouples the average variation of the HRS resistance from atmospheric conditions.[74] This improves device reliability, such as endurance > 10^2 cycles and retention time > 10^4 s.

3.6. Functionalization of graphene electrodes

Different functionalization strategies can be followed to achieve specific performances. E.g., SLG can be used as blocking interfacial layer to avoid metal/insulator interactions.[229] If SLG is intentionally patterned with selected amounts of holes or defects, the properties of the cell at those locations can be modified, leading to specific local phenomena, like local (instead distributed) O-vacancies scavenging.

Ref.[170] functionalized the SLG in a MGIM structure by using controlled Ar^+ ion-assisted bombardment, which generated different amounts of defects, depending on the bombardment energy. [230] By means of CAFM Ref. [170] showed that the leakage current in functionalized samples was much more confined than in pristine ones (see **Fig. 7**), probably due to the larger conductivity of the SLG-free locations (i.e. the holes patterned in SLG). MGIM devices with Ar^+ ion bombarded SLG had smaller variability than those without in the set and reset voltages, and more stable currents in each state.[170] This strategy was further studied in Ref.[171] by tuning ionic transport in Pd/Ta/SLG/Ta_2O_5/Pd RRAMs using SLG with engineered nanopores. SLG was grown by CVD on Cu and transferred with the assistance of a polymer scaffold.[165-167] The migration of oxygen ions in the device was controlled by opening some nanopores in SLG, which allowed to tune the properties of the devices.[171] However, since the nanopores are patterned with e-beam lithography, the process is less scalable than that in Ref.[170], which used ion-assisted-reaction treatment after transfer of MLG to etch residues as well as induce defects in SLG. In all, it was demonstrated that inserting a functionalized SLG in the structure of RRAM devices is a good approach to tune their properties.

Ref.[231] reversed the manufacturing order of the RRAM stack (from MLG/TaO_y/Ta_2O_{5-x}/MLG to MLG/Ta_2O_{5-x}/TaO_y/MLG). In this case, the conventional linear bipolar RS became highly non-linear due to the bottom MLG electrode being oxidized at 400ºC in an Ar/O_2 plasma during the reactive sputtering deposition of TaO_y. Due to the low currents driven by these devices (0.5 mA at 8 V), they show promising application as threshold switching and/or selector elements.

Another potential advantage of SLG electrode engineering is that the Fermi energy can be controlled, which is not possible in standard MIM structures. Using this

approach, Ref.[98] engineered the tunnelling barrier width and height at the interface of a Pt/Ti/TiO_2/SLG/Pt RRAM device, resulting in three orders of magnitude reduction of the switching power (from 10^{-5} W to 10^{-2} W).

3.7. Integration

One advantage when building NVMs using simple MIM structures is the potential for stackability and integration. One common approach [113, 232-233] consists in fabricating a nanostructured material with alternate metallic and insulating films. Then, a vertical aperture (hole) is patterned and the RS media is deposited. [113, 232-233] Finally, the rest of the hole is filled with another metal, leading to vertically aligned MIM cells in which the vertical electrode serves as common electrode, and each horizontal metallic film is the specific electrode of each (independent) MIM cell.[113,232] In this structure the thickness of each insulating film should be high enough to avoid cross-talk noise from cell-to-cell, therefore it cannot be reduced below a safe value (in the case of SiO_2~6 nm). [113] On the contrary, the thickness of the metal should be low enough to ensure good in-plane conductivity. SLG is thus a promising building block because: *i)* it is only 0.34 nm thick [113] and its in-plane conductivity is excellent (~3,000 $Wm^{-1}K^{-1}$); [234] and *ii)* the lateral connection between SLG and the RS media provides a lower contact resistance (compared to metals). Ref. [235] used FETs with metallic electrodes that contacted the SLG channel laterally, and observed a mobility of 140,000 cm^2/Vs, which is much higher than that of similar devices in which the SLG channel is connected vertically (40,000 cm^2/Vs), [236] and it is very close to the phonon limited model.[235] The reason is that the in-plane bonding is covalent, while metallic electrodes deposited on top of SLG rely on weaker Van der Waals interactions. A similar methodology can be used in RRAMs, employing SLG as planar electrode contacted

from the side (see **Fig. 8**).[113] Using this principle, Ref. [233] fabricated RRAM devices with $I_{ON}/I_{OFF} > 80$, low reset currents ~ 20 μA and low set/reset voltages (2 to 4 V).

Ref.[186] used a similar structure consisting of SLG as edge electrode to investigate the scaling limit of RRAM integration. In this case, the RS medium was a superstructure made of Ta_2O_{5-x}/TaO_y and, as in Ref. [233], SLG was grown by CVD and transferred on SiO_2 by an electrochemical approach.[237] The Pt column and SLG serve as pillar and edge electrodes respectively. As a result, SLG edge electrodes allowed a larger density of three dimensional RRAM integration.

4. Graphene oxide based switching media for RRAM

Even though the electrodes are a crucial elements defining the performance of RRAMs, the switching medium is the dominant one. [34] Apart from TMOs, a wide variety of materials have been proposed as switching media in RRAMs, including organic materials,[238] polymers,[239] perovskites[240], GRMs[241] and amorphous carbons. [84-89] Mixture/alloys of some of them, such as polymers with high density of graphene flakes[195] or organic polymers,[239] were also used.

GO and reduced GO (RGO) have been widely investigated for RS applications. [132-133, 241-253] GO films consisting of interconnected flakes are typically produced by LPE and spin coated on the surface of a substrates (which serves as top electrode), with subsequent deposition of top contacts on the GO surface [254] (see **Figs. 9** and **10)**. This contrasts with the atomically flat CVD-SLGs, and could have implications in terms of device-to-device variability.

Ref.[241] prepared a GO compound by Hummers method[255] and the resulting product was transferred onto $Pt/Ti/SiO_2/Si$ substrates, followed by top Cu electrodes evaporation. The resulting Cu/GO/Pt RRAMs contained a 30 nm thick GO film (see

Fig. 10), which showed I_{ON}/I_{OFF}>10, long retention times > 10^4 s, and low switching threshold < 1 V. The ability of GO to changes its electrical resistance when subjected to voltage stresses was later confirmed by in Al/GO/ITO cells.[249,256-257] Refs. [126, 258-262] combined a GO active layer with diverse electrode metals (Pt, Au, Al), which allowed tuning the RS characteristics of the devices. [126, 258-262]

Two competing hypothesis have been proposed to interpret the bipolar switching observed in GO films.[242,263] The first [242,263] resembles that of ECM cells using active metallic electrodes, in which metallic ions can diffuse from the electrodes towards the GO layer, leading to the formation/dissolution of a CF. The independence of the LRS resistance with temperature and the proportionality of the currents to the electric field support this mechanism.[242,263] An X-ray photoelectron spectroscopy (XPS) study of an Al/GO/ITO stack, detected Al atoms along the GO film when the device was working in LRS, pointing to mass transfer during the cyclic switching.[249] The second [241] is similar to that of homogenous VCM for inorganic materials, and suggests that absorption and desorption of oxygen functional groups could induce RS in the GO film.[264] In most cases, GO is associated to various oxygen groups, such as carboxyl,[265] hydroxyl, and epoxide, with their oxygen ions usually contributing to form the conduction path.[264-265] Two states sp^3 and sp^2 exist in these oxygen groups, the latter has larger conductivity due to the introduction of π-electrons from the removed oxygen groups. [264] The change of the oxygen bonding state in the GO film usually causes a variation of the leakage currents. [241] This interpretation received partial support from e-beam-induced current profile at the GO/metal interface and XPS depth profiles of oxygen and metals in HRS and LRS, which displayed distinct oxygen bonding near the interface.[126,266] However, the spatial distribution of the oxygen functional groups can vary in each resistive state. Furthermore, the experiments on

devices with different sizes indicate that the current leakage is proportional to the cell size.[105] Therefore, both results suggest that oxygen migration plays a dominant role in the switching of GO-based RRAMs.[241]

Ref.[267] observed different switching polarities, switching modes or the absence of them depending on the active metallic electrode used (Al, Cu, Ni, Ti). The switching directions are characterized by the different area, field and temperature dependences between them. Except for Ni electrodes (which did not show RS),[267] all the other electrodes (Al, Cu and Ti) showed bipolar switching under positive set (applied at the top electrode, bottom grounded).[267] Ti showed additional negative setting bipolar switching under negative set, and Al showed additional unipolar switching.[267] The bipolar RS under negative set might be related to the absorption/release of oxygen based functional groups, [241,268] while the bipolar RS under positive set may be associated to metallic ions diffusion.

The main performances shown by GO based RRAMs are compared in Table 3. The highest I_{ON}/I_{OFF} was achieved in ITO/GO/Ag [242] and p-Si/GO/Ag [247] structures. The use of Ag electrodes seems to provide the lowest switching voltages[133,153,242,245], but this contrasts Ref.[251], which shows operating voltages ~ 6.7V (the thickness of the GO film in Ref.[251] was ~15 nm, while in Refs. [133, 242] was not indicated). By comparing the rows 2 to 5 in Table 3,[248] it can be concluded that Cu electrodes provide higher I_{ON}/I_{OFF} than Ti, Ag and Au, probably due to the higher diffusivity of Cu atoms in the GO film, which may result in a more effective CF disruption during the reset process. It would be interesting to try ITO/GO/Cu and p-Si/GO/Ag RRAM structures. The ITO/GO/Al RRAMs from Ref. [249] show retention times > 10^7, but they are still insufficient for RRAM technology (see Table 1).[2] By comparing the ITO/GO/Al RRAMs from Ref.[249] with the ITO/GO/Ag from Ref. [242] it looks like Ag electrodes

cannot provide long retention (the values are 10^7 vs. 10^3), which is consistent with the lower operation voltages for Ag electrodes. [133,153,242,245] In any case, the long retention observed in Ref. [249] requires further corroboration (as well as the high operating voltages observed in Ref. [251]). The use of semiconductor electrodes in RRAMs, e.g. Si/GO/Al [250], Ge/GO/Al [250] and p-Si/GO/AG [247] show (unwanted) high operation voltages of -5.5V, -8.7V and 3.5V (respectively). While Si/GO/Al [250], Ge/GO/Al [250] show low I_{ON}/I_{OFF}<120, p-Si/GO/AG [247] reached 10^4. Further confirmation of the results in Ref.[247] is necessary. It is very striking that, despite all papers using spin coating resulted in thick >10 nm layers,[241, 245, 249, 250] the endurance for all RRAMs in Table 3 is just ~100 cycles. This value, which may be related to the large amount of defects (missing bonds) in the GO film,[269] is very far from the technology requirements for NVMs (10^9 cycles, see Table 1).[2] Similarly, despite all papers in Table 3 claiming that GO may be interesting for future nano RRAM devices, the RRAM sizes was > 7500 μm^2, and we are not aware of any CAFM-based RS study (like those compiled in Ref. [35]) in GO films. The data in Table 3 needs to be corroborated in smaller MIM cells.

The endurance can be enhanced by using RGO instead GO, as it can be observed by comparing Tables 3-4. Ref. [262] reported unipolar RS in ITO/RGO/ITO cells (5 μm in diameter), with endurance >10^5 cycles. The replacement of one of the ITO electrodes by Au [270] did not alter the operation voltage (2V) and retention time (10^5), indicating that in these structures the RGO (not the electrode) plays a dominant role in the charge transport. [270] The use of one Al electrode in conjunction with the RGO/TIO stack does not significantly alters the switching time [260] (compared to ITO/RGO/ITO)[262] even in much larger cells (~3 mm in diameter). When both electrodes are made of Al [271-272] the devices showed much lower I_{ON}/I_{OFF} < 100. This observation correlates with a reduction

of the operating voltages (~ 0.6V).[271-272] The use of Pt electrodes shows high operation voltages < 1.9V and high I_{ON}/I_{OFF},[273] similar to those of Au electrodes. This is reasonable because both Au and Pt are noble metals with low reactivity with the species in the GO film. In agreement with these observations, RGO-based RRAMs using Al electrodes showed the smallest retention times. [260, 34271, 374] A device with Ag electrodes showed the lowest I_{ON}/I_{OFF} (10) and endurance (100). [254]

GO and RGO can be combined with additional layers with the aim of further improving the performance of RRAMs.[194,264,275-278]. Prototype RRAM cells combining ZnO-graphene quantum dots (GQDs),[194] metallic (Ni[278], Au[243]) nanoparticles and nanocrystalline cellulose/GO[277] have been reported. Ref.[194] introduced ZnO–GQDs as active components and demonstrated a solution-processed organic NVM array with one diode one resistor (1D1R) architecture. The switching mechanism of the ZnO–GQDs devices was governed by thermally activated transport before the turn-on process.[194] The 1D1R cell showed typical unipolar switching and with low cross-talk noise. An analogous architecture of ZnO nanorods (ZnONRs) with GO displayed a significant reduction of the operating voltages (2.1 V) compared to the cell without ZnONRs (3.9V), indicating enhanced concentration of oxygen vacancies in the GO due to the incorporation of ZnONRs.[246] Ref.[278] used Ni-incorporated GO to fabricate RRAM devices with endurance >100 cycles, and Ref.[243] combined GO with Au nanoparticles, which lead to bipolar RS with retention times~10^4 s. [243]

The combination of GO with polymers such as poly (N-vinylcarbazole) derived GO (GO-PVK),[275] triphenylamine-based polyazomethine (TPAPAM),[274] showed typical bistable electrical conductivity and nonvolatile rewritable memory effects, with a turn-on voltage~ -1 V and I_{ON}/I_{OFF} > 10^3. Ref.[264] presented a RRAM-based on solution-processed GO/$Pr_{0.7}Ca_{0.3}MnO_3$ forming a cell of Pt/GO/PCMO/Pt. In this

structure, two active layers are necessary because GO or PCMO independently sandwiched by metal electrodes cannot reach stable RS. E.g., the Pt/PCMO/Pt control sample showed no RS, [264] due to the almost Ohmic contact between each layer, and the *I-V* characteristics of single Pt/GO/Pt device displayed an irreversible BD. However, the device with two active layers exhibited intrinsic and reversible bipolar RS, along with the conduction mechanisms associated to oxygen ions movement between the two active layers (see **Fig. 11**). Three different phases can be detected from *I-V* characteristics collected in these devices: *i)* An initial linear behaviour at low voltages. *ii)* A sudden current increase that switches the device to LRS, probably related to the movement of oxygen ions from the GO towards the PCMO surface, which contains large amounts of oxygen vacancies compared to the bulk region. And *iii)* the resistance of the PCMO layer is decreased by reducing the oxygen vacancy concentration, inducing the reset and transition back to HRS. Therefore, the electrical pulses can cyclically induce HRS to LRS transitions, and *vice versa*.

Refs. [243, 258] reported that GO can also result in multiple stable resistive states when incorporating either polyimide [258] The presence of more than one resistive state allows for a higher information storage density as, instead of bits, multiple digits can be stored. Up to four differentiated levels and retention times of at least 10^4 s have been achieved. [243] The performances of RRAMs using GO, RGO-polymer and mixed structures as RS media are summarized in Table 5. Outstanding performance in terms of endurance (10^8 cycles) is achieved in Refs. [275-276] using GO-polymer composites sandwiched by ITO-Al electrodes, which approach but not fit the NVM technology requirement (10^9). These two cells [275-276] also show high retention times>10^4s and I_{ON}/I_{OFF}~10^3, being only surpassed by the RGO/P3HT:PCBM/Al structures shown in Ref. [279] (10^4-10^5).

GO can also provide flexibility and transparency to the devices. E.g., ITO/GO/Ag were reported as RRAMs with I_{ON}/I_{OFF} ~ 10^3 and stable retention characteristics for > 10^3 s within 1000 cycles for r_b > 4 mm [249]. Ref. [262] fabricated RGO-based RRAMs by dip-coating, and obtained ~80% transparency from 425 to 900nm. These devices exhibited unipolar RS characteristics with I_{ON}/I_{OFF} >10^5, endurance ~10^5 cycles for each state, retention times >10^5 s and multilevel capability. The performance of flexible RRAMs using GO and RGO as RS media is summarized in Table 6. Outstanding performance (I_{ON}/I_{OFF}>10^3, retention >10^5s and endurance >10^3 cycles) was achieved in PEN/Ti/Pt/GO/Ti/Pt RRAMs,[280] with MIM cells ~100 nm × 100 nm, making these values more reliable. This is an important step towards enabling future transparent device applications based on GO and its derivatives.

5. Amorphous carbon as switching media for RRAM

Carbon is a very versatile element that can crystallize in forms of diamond, where it is fully sp^3 bonded, or graphite, where it is fully sp^2 bonded. Non-crystalline carbons are referred to as amorphous carbons. When the sp^3 fraction is higher than 50%, the amorphous carbon is called tetrahedral-amorphous carbon, ta-C. [281-284].

Amorphous carbons can change resistance by applying unipolar electrical pulses or voltage sweeps. RS in amorphous carbons has led to their addition to the selection of emerging memory technologies in the 2014 ITRS. [2] The switching mechanism, however, is still under debate. Several mechanisms have been put forward, such as sp^2 clustering [86, 285], sp^2 filament formation [286-289], metal filament formation [85,290] and electron trapping/detrapping [291].

In 1972 Ref.[292] first reported RS in 10nm thick evaporated a-C films sandwiched between Al electrodes, reporting 100,000 switching cycles. Ref. [292] found

that a forming step is needed to create a CF and activate RS. Switching only occurred by applying a positive voltage to the bottom Al electrode, while opposite polarity was needed for the RESET [292]. RS was attributed to metal filament formation, since Al is a diffusive metal and amorphous carbon produced by evaporation has usually very low sp^3 content and switching in sp^2 rich amorphous carbon has been found not to be reversible [285].

Non-volatile RS in doped amorphous carbon films was demonstrated by several groups. [84-89,293-300]. This includes RS in nitrogen [88-89,295-296], hydrogen [84-87], oxygen [294, 301], silicon [302], Co[297] and Cu [298-300] incorporated amorphous carbon films. Table 8 summarizes the literature RS data in doped amorphous carbons.

Refs.[88-89] reported a reversible NVM effect in nitrogen doped tetrahedral amorphous carbon, ta-C:N, with write times down to 100 μs.[90] They attributed the switching to the promotion of electrons from acceptor states in the gap to higher donor states. However, the LRS retention was poor, only one year,[90] too short for commercial applications. Ref.[295] prepared nanoporous nitrogen doped amorphous carbon and studied a Pt/C:N/Cu device structure. Set and reset occurred at opposite voltage polarities.[295] Decreasing the amount of nitrogen led to a reduction of switching voltages down to +0.6V for set and -0.5V for reset. [295] Over 1000 switching cycles and a retention > 80 days at room temperature were reported, still not good enough to meet industry requirements.[295] The switching mechanism was attributed to the formation and rupture of Cu filaments.[295] Ref.[296] reported the effect of nitrogen implantation on RS of amorphous carbon to analyze the role of sp^2 filamentation and clustering. Nitrogen implantation made the films more conductive with an increase in sp^2 bonding and clustering, facilitating the SET process.[296]

Several groups reported reversible, non-volatile switching in hydrogenated

amorphous carbon, a-C:H, [85-88], with the results summarized in Table 7. RESET within 30ns and SET in ~30ns were reported,[86] long data retention >10^5s,[85] 10^7 switching cycles[87] and I_{ON}/I_{OFF} ~10^3.[86] The RS mechanism was attributed to different processes: Ref.[85] assigned RS in Pt/a-C:H/metal structures, with the metal top electrode being Cu, Ag or Au, to the formation and rupture of metal filaments, due to diffusion of the top electrode metal into the a-C:H film.[85] Ref.[86] studied RS in a-C:H with TiN as bottom and Cu, Pt or W as top electrodes, and assigned RS to thermally induced conductive sp^2 clusters filament formation.[86] Ref.[87] attributed the switching to a sp^2 carbon CF formation in a TiN/a-C:H/Pt structure. RESET was achieved by applying the opposite voltage polarity to the bottom TiN electrode and attributed to hydrogen atoms pulled from the Pt top electrode and absorbed by double bonds in sp^2 carbon.[87]

A limiting factor in a-C:H RS is the need of a forming step, where the material needs to be biased at the breakdown electric field.[303] The breakdown results from a capacitive discharge current, which can be 10-20mA[86,303] and occurs within a few ns.[86,303] Therefore, an on-chip resistor or transistor is needed to limit the current during forming.[86,303] Due to the high current density during the forming step, metals from electrodes might diffuse into the carbon, if the forming is done in a dc-sweep, instead of an energy limiting short pulse.[85,287,295, 303]

The influence of other dopants, such as Co and Cu, was studied by Refs.[297-300], see Table 8. Ref.[297] studied RS in Co doped amorphous carbon. They observed non-volatile, bipolar and reversible RS with I_{ON}/I_{OFF} ~25, but good retention >10^5s at room temperature.[297] RS was attributed to a filament formed by Co ions created by an electrochemical reaction, migrating toward the top Al electrode through defects in the a-C film, forming a conductive path between top and bottom electrode.[297] Refs.[298-300]

investigated RS in Cu doped carbon. They got I_{ON}/I_{OFF}~10^2 and retention of 10^4 s at 85°C and >10^3 switching cycles.[298] Ref.[300] used a slightly different device configuration with both, top and bottom electrodes made of Pt. A forming step was needed. Subsequent set and reset processes could be achieved at ~+0.7V and -0.5V.[300] RS was attributed to the formation and rupture of Cu filaments.[298-300]

Ref.[294] prepared oxygenated amorphous carbon, a-CO_x, by physical vapour deposition. Ref.[294] reported switching times~50ns for SET and~10ns for RESET, with opposite voltage polarity needed.[294] Ref.[294] measured cycling endurance >10^4 in devices with W as bottom and Pt, Ti or W as top electrodes,[294] with I_{ON}/I_{OFF} ~ 5x10^2 during retention measurements up to 10^4s at 85°C. The RS mechanism was attributed to an electrochemical redox reaction leading to the formation of a conductive carbon filament.[294] The choice of metal electrode material was crucial for the reset process, with strong dependence on the electron affinity of the metal electrode.[294] To make the reduction reversible, two electrode materials were needed to store and release oxygen. One with similar electron affinity to carbon, such as W, and the other with higher electron affinity, such as Pt.[294]

RS in amorphous carbons with different sp^2/sp^3 ratio was reported by several groups.[285,304-312] RS in sp^2 rich a-C was studied in a Si/TiN/a-C devices, using a CAFM as top contact.[282] The key parameters of RS devices based on pure amorphous carbon are reported in Table 9. RS was assigned to an electro- thermally induced (Joule heating) increase in the sp^2 cluster size and was non-reversible.[285] RS in a-C was shown to be polarity independent.[304-307] Ref.[306] studied the influence of the top metal electrode material on RS, and assigned this to metal filamentation in devices with Cu top electrodes. Pt, W and Ni top electrodes did not show switching.[306] This was attributed to the less diffusive nature of those metals.[306] Data retention>10^5s,[304] low switching

voltage of 2V[306] within pulses of 1μs,[306] I_{ON}/I_{OFF} ~70,[305] endurance ~110[305] and device structures down to 50x50μm^2 [306] were demonstrated.

I_{ON}/I_{OFF} as well as endurance are the main challenges faced by RRAMs based on a-C. The issue of a low I_{ON}/I_{OFF} can be overcome by using ta-C. Ref.[308] demonstrated high I_{ON}/I_{OFF} in Pt/ta-C/(SLG)/Au devices. Devices with an interfacial SLG reached I_{ON}/I_{OFF}~4x10^5, while maintaining low switching power density of 14μW/μm^2.[308] This was attributed to the reduction of leakage currents due to the low SLG density of states near the Dirac point.[308] Refs.[288-289] explained the switching in terms of nanoscale sp^2 filament formation and rupture through field-induced dielectric breakdown and thermal fuse effect, i.e. an electro-thermally driven set process and a thermally driven reset process. Low switching voltages of 0.4V for reset within 10ns and 1.2V for set within 50ns,[288] 10^{13} read cycles at 75°C,[286] >10^6 s retention [290] with device sizes of 50nm diameter [289] and 10^3 switching cycles [288] were also demonstrated. The presence of multiple resistive states was reported by Ref.[308]. Multilevel storage is of particular interest as it allows to store more than one bit per cell, while the memristive behaviour can be exploited to provide a range of signal processing/computing-type operations, such as implementing logic, providing synaptic and neuron-like mimics, i.e. circuits that simulate brain-like neurological functions, and performing analogue signal processing functions, paving the way for non-von-Neumann computer architectures, in which processing and non-volatile storage are carried out simultaneously.[313-314]

Endurance is one of the major challenges for a-C based switching devices. A comparative study by Ref.[301] of RA in ta-C and a-CO_x with Pt bottom electrodes and W top electrodes suggested that by incorporating oxygen the endurance could be enhanced to 40000, but at the expense of bipolar operation.[301] In ta-C devices, SET and RESET were achieved with pulses of 50 and 4ns and switch energies of 15 and 3pJ,

while a-CO_x could be set and reset with 40 and 4ns pulses with switch energy of 2 and 1pJ, respectively.[301] Both, ta-C and a-CO_x showed good data retention of 10^4s at 85°C.[294, 301]

Refs.[301-302,311-312] theoretically studied the switching mechanism in amorphous carbons, and assigned RS to heat driven sp^2 clustering and filament formation.

Ref.[303] pointed out that one of the biggest advantages of carbon based memory devices might be the high temperature retention~250°C, making them attractive for automotive and harsh conditions.[303] Another advantage of carbon based memories is that devices do not rely on rare mineral extraction, with easier disposal/recycling, and low total energy production compared to other electronics materials.[280]

6. Layered materials

Non-carbon based LMs have also been introduced into the structure of RRAMs, manly TMDs (like MoS_2 [315-316] and $MoSe_2$[317]) and *h*-BN.[163] Ref. [318] reported a RRAM prototype using BP flakes.

TMDs are naturally semiconducting materials,[319] thus they are not ideally suited for RRAMs. For this reason, these materials need to be functionalized in order to form an insulating layer.[319] Ref. [320] suggested to combine TMDs with an insulator (such as polymers) whereby the TMD would act as dopant of the insulating layer. In Ref.[320] a stack of RGO/MoS_2-PVP/Al in which the PVP (polyvinylpyrrolidone), typically used to assist the exfoliation of MoS_2, became the dielectric RS-driving layer. The devices were fabricated using spin coating of the MoS_2-PVP solution on the RGO film, resulting on a thickness of 70 nm, and large 0.2×0.3 mm^2 electrodes were

thermally evaporated. The RRAM devices show I_{ON}/I_{OFF} ~ 10^2. Ref. [320] claimed the switching as due to charge trap and de-trap of the MoS_2 embedded in the PVP. However, Refs.[321-322] reported RS also in structures with pure PVP as active layers, while Ref.[273] detected RS in RGO. We note that Ref. [320] did not provide temperature nor area analyses, which makes it difficult to discern if the RS in these devices is a local or distributed phenomenon. Therefore, the ability of MoS_2 to drive the RS is questionable.

Similar studies were developed by Ref.[323] in a PET/Al/PMMA/MoS_2/PMMA/Al stack and by Ref.[324] for Au/ MoS_2-PMMA/SLG. These achieved I_{ON}/I_{OFF} ~10^4 and 2.5×10^3 (respectively). However the need for a TMD to be combined with PMMA is doubtful. Ref.[325] demonstrated that MoS_2-free Ag/PMMA/ITO devices can also achieve reproducible RS (I_{ON}/I_{OFF} ~10^2), which is driven by the penetration of metallic ions into the polymer, leading to a reversible CF though it. The combination of MoS_2 and GO resulted on a similar I_{ON}/I_{OFF} ~10^2 for the RRAM device.[326] Ref.[327] produced printable RRAM memories with tuneable performances using Ag/MoS_2-MoO_x/Ag stacks, with I_{ON}/I_{OFF} >10^6, retention times >8000s, and non RS degradation after bending>10^4 times. As in Refs.[324,326], the RS in Ref. [320] does not seem to be attributable to the MoS_2 sheets, which served to homogenize the interface between the MoOx and Ag bottom electrode. A different approach was reported in Ref.[328], which used MoS_2 flakes, also giving RS. In this case, the resistance changes were attributed to tunnelling across junction barriers. Very similar devices, but using $MoSe_2$ nano-islands, were studied in Ref. [317], which showed I_{ON}/I_{OFF}~12 and low currents (>1μA) in LRS.

RS driven by MoS_2 was reported by Refs.[315-316] Ref.[317] used three-terminal horizontal devices similar to FETs (see **Figs. 12a** and 12b), with a grain boundary (GB) in the MoS_2 extending in the channel. Ref. [320] considered GB different configurations,

including parallel and perpendicular to the channel, as well as intersecting. In all cases, $I_{ON}/I_{OFF} > 10^2$ was achieved. RS in these devices was assigned to the motion of S vacancies in the MoS_2, which tend to accumulate at the GBs.[320] However, the reproducibility of this phenomenon was not firmly established, as Ref. [315] reported only 15 cycles. On the other hand, Ref.[316] compared two vertical Ag/MoS_2/Ag devices using a 550 nm MoS_2 film formed by MoS_2 flakes dispersed in propanol solvent and spin-coated on a Ag foil, followed by a thermal treatment at 130ºC for 12h and 0.1 mm^2 top electrode deposition using Ag paste (Figs. 12c and 12d). The differences between the two devices was the MoS_2 phase, in one case 1T flakes, and in the other 2H bulk. Despite the methodologies not being ideal for scaling and integration (deposition of electrodes by Ag paint using a shadow mask is to be avoided because it can lead to contaminants at the interface, inhomogeneous shapes and cracks in the 2D material) the devices using 1T-MoS_2 showed good RS behaviour with $I_{ON}/I_{OFF} > 10^3$ during 100 cycles. Ref. [316] assigned the RS to the migration of Mo and S ions under electrical field. Ref. [316] also included a modification of this device using Ag/MoS_2/Ag/MoS_2/Ag vertical structures, showing the possibility reducing the current at low voltages (<0.2 V) by negative differential resistance, which may be useful to avoid sneak path current in crossbar arrays. Nevertheless, none of the MoS_2-based works to date presents a conclusive memristive analysis. E.g. Ref. [316] claims 1000 cycles, but no variability analyses (like e.g. those in Refs. [315-317, 324]) are presented (just 3 *I-V* curves are displayed). More information on the different TMDs-based RRAMs is in Table 10, including dependence on critical parameters, such as device area, working temperature, top electrode material and current limitations (among others). The RS parameters are still far from those reported for state-of-the-art TMO-based RRAM memories (see Table 1). [2, 31-33]

The use of *h*-BN in RRAM is even more incipient. In principle, as BN is an insulator,[163] if a reversible CF/BD can be induced through it, the RS behaviour should be more accentuated (larger I_{ON}/I_{OFF}) due to the larger resistivity in HRS (the constriction would be more insulating than in semiconducting materials). Nevertheless, this is in principle not an easy task, as the BD may become irreversible depending on the atomic structure of the *h*-BN stack. One should clearly distinguish between research articles using layered *h*-BN[163] (see **Figs. 13c** and 13d), and those in which amorphous BN was used (Figs. 13a and 13b).[329] Ref.[329] claimed the fabrication of RRAMs using multilayer *h*-BN stacks, but the layered nature of the film is not supported by the cross-sectional TEM images, and the layer looks more like an amorphous BN film (see Figs. 13a and 13c). This is very important because the amorphous BN film may not hold the properties of the *h*-BN stack, such as transparency, [330] flexibility, [331] high thermal conductivity [332] and high chemical stability [333]. Ref. [316] fabricated a family of RRAMs using *h*-BN as RS medium. By tuning the *h*-BN stack thickness and the *h*-BN domain size Ref. [163] achieved forming-free operation, low switching voltages down to 0.5 V, high I_{ON}/I_{OFF} up to 10^6, retention times > 10 hours and low device-to-device variability (i.e. deviations of V_{SET}/V_{RESET} <10%). In Ref. [163] the RS was attributed to the migration of B atoms towards the electrodes, as well as metallic ions penetration into the *h*-BN stack to form and disrupt one/few CFs. These atomic diffusions are more abundant at GBs, which are defect-rich locations (missing bonds, missing atoms, pentagonal/heptagonal lattices)[334] that can favour atomic rearrangements at lower potentials (compared to the grains), leading to a softer BD that may be easier to recover.[335] The formation of B-vacancies at the GBs of polycrystalline *h*-BN stacks (see Fig. 13c) presents an interesting parallelism to O-vacancies at the GBs of polycrystalline TMOs. [335] The key role of the GBs in the RS is supported by the fact

that the BD process in single crystalline *h*-BN flakes is an irreversible phenomenon that leads to the removal of the material,[336] with the formation of holes during a characteristic layer-by-layer BD process. Therefore, it is unlikely that a perfect single crystalline *h*-BN would offer RS capabilities. Ref. [107] investigated a RRAM comprising a monolayer CVD-grown *h*-BN flake inserted between the top electrode and the dielectric of an Al/WO_3/Al cell, but the performance was worse than the *h*-BN free counterpart ($I_{ON}/I_{OFF} < 10$). Probably the reason is it is difficult to create CFs in *h*-BN/WO_3 superstructures, i.e. the CF is only created at large electrical fields that produce the irreversible BD in the *h*-BN/WO_3 stack. Ref. [337] reported indications of RS in layered Ti/*h*-BN/Cu stacks (Fig. 13c). The devices exploited the Cu substrate used to grow the *h*-BN as bottom electrode, avoiding the need for transfer.[316] When applying constant voltage stresses (CVS) at 2.5 V to the devices, the current vs. time (*I-t*) curves show sudden changes of the electronic resistance (up to 10^3) similar to unipolar RS characteristics.[337] A detailed comparison of the RS capabilities of *h*-BN-based devices in literature is presented in Table 11. Ref. [338] also observed unipolar RS transitions in planar nanogap-based *h*-BN obtained by MC. However, thus far, the use of planar structures in RRAM technology is very limited due to the difficulty to control the rupture kinetics of the nanogaps, which may result in a poor RS endurance and prohibitive device-to-device variability. We note that statistical information of the RS in planar devices made of any GRM has not yet been reported. Moreover, MC is not an scalable technique. Ref. [337] reported layer-by-layer BD at the grains by means of CAFM, while at the same time measuring reproducible conductivity changes at the device level, which may be related to the presence of GBs. As the use of LM-dielectrics provides a flatter interface to graphene and TMDs than high-k dielectrics, [179-180] RS applications of *h*-BN should be deeper investigated.

BP is a layered semiconductor prone to degradation when exposed to atmosphere.[339] The degradation of the surface is generated by the insertion of oxygen groups, leading to a PO_X structure.[339-340] This layer provides RS capability, as reported by Ref.[318]. Ref.[318] exfoliated BP using both γ-butyrolactone and isopropanol and the devices were fabricated by spin-coating on a ITO/PET flexible and transparent substrate, followed by top circular (500 μm in diameter) Ag electrode deposition by magnetron sputtering using a shadow mask. Ref. [318] observed that, after some days/months of exposure to atmosphere, reproducible RS with I_{ON}/I_{OFF} up to 10^3-10^4 can be achieved (**Fig. 14**). Ref. [318] attributed this to the formation of Ag conductive filaments across the oxidized and insulating PO_X superficial layer. However, Ref. [318], was just a proof-of-concept, lacking important RRAM parameters, specially variability. Ref.[119] reported the observation of RS in (PET)/Au/BPQD-PVP/Ag structures, with I_{ON}/I_{OFF} >10^4 and endurance >1100 cycles. Both BP-based RRAM devices (in Refs. [119,318]) were fabricated by LPE and spin coating and showed flexible capability. The characteristics of these two prototypes are summarized in Table 12. Unfortunately, none of these works show endurance analyses, they just concentrate on the proof-of-concept and I_{ON}/I_{OFF} ratio, which makes it difficult to know the real usefulness of this material in RRAMs.

7. Discussion, challenges and prospects

The most advanced RRAMs use MIM structures formed by metallic electrodes (Ti, Au, Ag, Cu, Ni, Pt) coupled with TMOs (HfO_2,[39-42] Al_2O_3,[43-46] TiO_2 [47-50] and TaO_X).[51-52] RS in metal/TMO/metal structures was first observed in 1962,[341] and RS-based memories were proposed in 1967. [342] After more than 50 years of research, devices with high operation speeds (~ 300 ps/transition),[32,44-45,60] low power

consumption (~0.1 pJ/transition),[32,44] good endurance (above 10^{12} cycles),[33,111,346-347,364] long data retention times (above 10 years),[46,364] small size (down to 10 nm × 10 nm),[31,296] and high integration capacity (> 1 × 10^{11} bits/cm^2) [2] have been developed. GRMs were firstly introduced in the structure of RRAMs in 2008, [103] and in less than a decade the performance of some GRM-based RRAMs prototypes have fit some of the NVM technology requirements (low operation voltages <1V,[163,251] high switching speeds down to 1 ns, [286,273,280] endurance >10^9 cycles, [286] and small cell size (8.5 nm^2). [296]

Table 1 compares the best performances reported for TMO-based and GRM-based RRAM devices. These are similar for both types of RRAMs, and in one case (endurance) one GRM-based RRAM achieved record values. Several GRM-based RRAMs showed low (< 1V) operating voltages, [163,248,253] and acceptable switching speeds. [286,273,280] In contrast, the number of TMO-based RRAMs that fit at least one technology requirement is much larger (Table 1 only displays few of them). Therefore, more work in the direction of GRMs-based RRAMs is necessary.

7.1. Fabrication

The fabrication methods used for GRMs-based RRAMs should be improved. E.g., one of the best endurances reported for RRAMs using non-carbon GRMs (10^3 cycles in Ag/MoS_2/Ag)[316] was observed using Ag foils as bottom electrode, and top electrodes deposited with Ag paint and MIM cell sizes ~0.1 mm^2. None of these processes/parameters are compatible with industry, and the knowledge extracted from such works may not be applicable to real ultra scaled (state-of-the-art) RRAMs. Future work in GRMs-based RRAMs should concentrate on the use of industry-compatible methodologies (i.e. for the deposition of electrodes evaporation/ and/or sputtering are

preferred) and smaller device sizes (so that the conclusions extracted can be applicable to nanosized devices).

Furthermore, in most works using transferred SLG as interface electrode (see, e.g, Table 2) the device size is very large (>8000 μm^2). Under such large areas, it is common that SLG layers show cracks, especially after the transfer. [168-169] As the transversal electrical resistance of the MGI junction (non cracked region) is larger than that of the MI one (at the cracked region),[170-171] and because the forming/BD is a stochastic process that always takes place at the electrically weakest location of the area under stress (less insulating),[343-344] CFs in these devices are more prone to be formed at SLG cracked locations (e.i. MIM, instead MGIM). Moreover, as the currents measured through the devices (specially in LRS) are mainly driven by the CFs, the *I-V* characteristics of many RRAMs using transferred SLG may refer to these nanosized MI junctions, and they may not be representative of the MGI structures under study. Ref.[217] reported that the insertion of SLG electrodes in TMO-based RRAMs reduces I_{HRS} 1-3 orders of magnitude due to an increase of the out-of-plane resistance (non-cracked regions). Since the endurance and retention time is related to the CF properties, the presence of cracks should have a major influence. Future works using transferred SLG should prove that no cracks are present. One route could be to reduce the device area, which lessens the probability of finding a crack. Another option is to use MLG, which presents less cracks and is more resistant to mechanical fractures during transfer. [163]

Many GRMs-based RRAMs works based on polymer-scaffold-assisted transfer did not evaluate the presence of residues on the GRM surface after polymer removal. These may result in an effective reduction of the device size, given their high thickness >10 nm and insulating nature.[345] This process is random, but can be reduced

by using better cleaning processes,[172] which may device-to-device variability problems.[135-137] Future works should include nanoscale surface characterization techniques, such as topographic AFM maps. Including annealing treatments after the transfer to remove rests of polymer may be an option.

Therefore, GRM transfer should be avoided when possible, not only due to device performance concerns, but also because it slows down the fabrication process (making it more expensive). The ideal solution would be to develop transfer-free processes, but the direct growth of GRMs on TMOs is a longer term goal. The use of insulating LMs as RS medium is preferred because, first, they do not need transfer,[163] and second, the absence of cracks can be corroborated by the observation of a forming and/or set process.[329] Present works on CVD-grown *h*-BN reported transfer-free RRAM devices,[163,329] but they still used metallic foils. The direct growth of GRMs by CVD (or any other scalable technique) on metal coated flat wafers is highly desired. Another option is to use LPE GRM insulators that can be spin coated on arbitrary substrates, but that may present variability concerns given their large roughness (typically ~ 20 nm)[134], much larger than flat GRMs prepared by CVD (graphene, *h*-BN). The use of coating methods that reduce the roughness below 1 nm is necessary. Note that the roughness of TMOs for RRAM (usually grown by ALD) is ~ 0.2 nm. [35,62,135]

7.2. Characterization

Many papers on GRMs-based RRAMs only focused on RS proof-of-concept, showing acceptable >10^2 I_{ON}/I_{OFF} in very large >1 mm^2 devices. [196, 316] Information on the number of devices tested in each work and variability analyses is missing. Usually the reports do not concentrate on the study of the technology requirements (note that

high I_{ON}/I_{OFF} is not a technology requirement, i.e. just one order of magnitude is enough to reliably distinguish HRS and LRS).[2] E.g., we did not find any GRM-based RRAM report giving the power consumption in units of Energy (e.g. Joules) per transition, which are the values demanded by the industry[2]. Similarly, most GRMs-based RRAMs works do not focus enough on the switching times (e.g. detailed zoomed in plots at the set/reset transition are often missing). Sometimes, endurance and retention plots are shown, but the values ($<10^3$ cycles [351] and $>10^7$s [249], respectively) are still insufficient to meet the industry requirements.[2] The only paper showing excellent switching times and power consumption (Ref. [286] Table 1) comes from industry. Future works should study several device parameters, such as RS medium thickness, electrode material and current limitation, as well as provide information on endurance, retention, temperature, variability analyses performed with probestation, modelling and CAFM. The use of CAFM to demonstrate the switching between HRS and LRS in some GRMs-based reports is very deficient, as no statistical analyses of the CF current/size of the CFs is provided. The methods for a correct characterization of RS using CAFM are described in Ref. [35]. Similarly, the structure of LMs-based RS is often not well supported, as explained in Fig. 13. Furthermore, the type of electrical stresses applied to most of the devices (*I-V* curves) are suitable only for proof-of-concept, but real devices work under fast (<10ns) voltage pulses.[34]

Many GRMs-based RRAM reports do not present variability analyses (just typical values are shown), which raises concerns on the reliability and reproducibility of the results. Device-to-device variability was rarely reported (see e.g. Refs. [163]). In the future, more information about the dispersion of V_{SET} and V_{RESET} in groups of more than 20 devices is needed. The inclusion of atomistic simulations and physical modelling to further complement the experimental observations is also necessary. For

example, the QPC model,[210] one of the most widespread for studying the different conductance levels in HRS and LRS in RRAMs, [205-206] has been used in very few GRMs-based devices.[163,308]

7.3. Technology viability

The number of TMO-based RRAMs reporting performances above the technology requirements is much larger than for GRM-based ones. For this reason, TMO-based RRAMs are more reliable and (still) superior to GRM-based RRAMs. Moreover, as for TMO-based RRAMs, there is still not a GRM-based RRAM fitting all technology requirements simultaneously, indicating that more research is required. Nevertheless, the faster optimization speed of GRM-based RRAMs as well as the superior electronic,[76] physical,[77] chemical,[78] mechanical,[79] optical,[80] magnetic[81] and thermal[82] properties.[83] of GRMs (compared to TMOs) are strong arguments to further explore this technology.

7. Conclusions

GRMs have been introduced in the structure of RRAMs with the objectives of *i)* enhancing their performance as NVM (endurance, retention, switching time, power consumption, operation voltages) and *ii)* provide additional capabilities (flexibility, transparency, high chemical stability, thermal heat dissipation). On one hand, graphene can be used as electrode to provide flexibility and transparency to the devices, and/or as a interface layer between the electrode and the RS medium to reduce the cycle-to-cycle variability by avoiding atomic diffusion between the electrode and insulator, reduce the power consumption due to its high out-of-plane contact resistance (compared to metallic electrodes), suppress surface effects by avoiding chemisorption and/or photodesorption and surface band bending, allow tuning the properties of the devices

by functionalization, and reducing the thickness of the electrodes and improving the three dimensional stackability. On the other hand, GO, a-C, TMDs, *h*-BN and BP can be used as active RS medium to induce the resistivity changes either by migration of intrinsic species (such as oxygen in GO and sulfur in MoS_2) or by penetration of metallic ions from adjacent electrodes. Graphene is usually produced by CVD and inserted in the RRAMs by polymer-assisted transfer. When using *h*-BN as RS medium, the standard transfer can be avoided, and the catalyst substrate for CVD growth can be used as bottom electrode. GO and BP are usually produced by LPE and spin coated on conductive wafer, which serves as bottom electrode. TMDs have been inserted in RRAMs either by CVD plus transfer and LPE plus spin coating. In all cases, top electrodes can be easily evaporated on top using an evaporator/ sputtering coupled with an standard photolithography step.

GRMs-based RRAMs have shown reproducible unipolar and bipolar RS with high $I_{ON}/I_{OFF}>10^5$, low operating voltages <1V and fast switching times (<30 ns). In most reports the switching is attributed to the formation/disruption of CFs in the RS medium, and the atomic rearrangements in each state transition are related to the movement of intrinsic species and/or penetration of metallic ions from adjacent layers, showing parallelism with TMO-based RRAMs. GRMs have also been mixed/embedded with polymers, nanoparticles, nanorods and quantum dots in order to enhance the performance (mainly retention and endurance) of the devices, but in many cases it is unclear the real need/usefulness of the GRMs for the RRAM device. Despite all efforts, NVMs technological requirements like endurance $>10^9$ cycles and data retention >10 years still remain a challenge. Only one report using a-C as dielectric demonstrated excellent endurance above 10^9 cycles, and we are not aware of any GRMs-based RRAM showing retention times > 10 years. From the point of view of

flexibility, GRMs-based RRAMs showed the ability to hold RS under more than >10^5 bending stresses with radius down to few mm (no technological requirements in this sense have been established). Moreover, GRMs-based RRAMs with transparencies >92% have been reported. The benefits of other GRMs properties (such as high chemical stability and thermal heat dissipation) on the performance of RRAMs have not been discussed.

Most of RS studies in GRMs concentrated on poof-of-concept demonstrations using large area (>2000 μm^2) devices, which makes difficult to extrapolate to real ultra-scaled RRAMs. Future GRMs-based studies should use smaller (<1μm^2) sizes, focus on demonstrating performances (i.e. endurance, retention, switching time and power consumption) above the NVM technology requirements, and include reliability and variability analyses. The use of atomistic simulations and physical modelling to support/explain the experimental observations is also necessary.

Nevertheless, the fact that GRMs-based devices already fit some NVM technology requirements (operating voltages, endurance and switching times) makes this field worth of further investigation.

Acknowledgements

We acknowledge support from the Young 1000 Global Talent Recruitment Program of the Ministry of Education of China, the National Natural Science Foundation of China (grants no. 61502326, 41550110223), the Jiangsu Government (grant no. BK20150343), the Ministry of Finance of China (grant no. SX21400213), the Young 973 National Program of the Chinese Ministry of Science and Technology (grant no. 2015CB932700), the Collaborative Innovation Center of Suzhou Nano

Science & Technology, the Jiangsu Key Laboratory for Carbon-Based Functional Materials & Devices, the Priority Academic Program Development of Jiangsu Higher Education Institutions, the National Natural Science Foundation of China under Grant Nos. 61521064, 61322408, 61422407, the Beijing Training Project for the Leading Talents in S&T under Grant No. ljrc201508, the Opening Project of Key Laboratory of Microelectronic Devices & Integrated Technology, Institute of Microelectronics, Chinese Academy of Sciences, the EU Graphene Flagship, FP7 Grant CARERAMM, ERC Grants Hetero2D and Highgraink, EPSRC Grants EP/K01711X/1, EP/K017144/1, EP/N010345/1, EP/M507799/1, EP/L016087/1, EP/M013243/1. All the members of Prof. Lanza group are acknowledged for literature review.

References

[1] A. Chen, *Solid-State Electron. 2016*, DOI: 10.1016/j.sse.2016.07.006.

[2] International Technology Roadmap for Semiconductors, 2013 Edition, Process Integration, Devices, and Structures section (last accessed online February 11th 2015, website: www.itrs.net).

[3] D. Kumar, *Preprints* **2016**, DOI: 10.20944/preprints201607.0093.v1

[4] http://www.statisticbrain.com/average-cost-of-hard-drive-storage/

[5] Web-Feet Research: http://www.webfeetresearch.com (Accessed: May 8th of 2016).

[6] D. Kahng, S. M. Sze, *Bell Syst. Tech. J.* **1967**, *46*, 1288.

[7] "IBM Reports Advance in Shrinking Chip Circuitry". *The Wall Street Journal. July 9, **2015***. Retrieved July 9, 2015.

[8] Equipment and Tool Institute, http://eti-home.org/Newsletter-V02/The-Bus-is-

Full.html, 2010.

[9] S. Okhonin, M. Nagoga, E. Carman, R. Beffa, E. Faraoni in IEEE Int. Electron *Dev. Meeting*, Washington, DC, USA, 10-12 December, **2007**.

[10] C. Navarro, M. Bawedin, F. Andrieu, S. Cristoloveanu, *IEEE Electron Device Lett*. **2015**, *36*, 5.

[11] T. Atsumi, S. Nagatsuka, H. Inoue, T. Onuki, T. Saito, Y. Ieda, Y. Okazaki, A. Isobe, Y. Shionoiri, K. Kato, T. Okuda, J. Koyama, S. Yamazaki, 4th IEEE Int. Memory Workshop, **2012**, 99.

[12] Y. Li, Y. Z. Wang, Q. Cui, *J. Renewable Sustainable Energy* **2016**, *8*, 015901.

[13] C. T. Chu, Y. K. Wang, P. K. Liao, 5th International Symposium on Next-Generation Electronics (ISNE), 4-6 May, **2016**.

[14] Authenticating ferroelectric random access memory (F-RAM) device and method US 9330251 B1, May 3, **2016.**

[15] Z. Xu, B. Liu, Y. F. Chen, Z. H. Zhang, D. Gao, H. Wang, Z. T. Song, C. Z. Wang, J. D. Ren, N. F. Zhu, Y. H. Xiang, Y. P. Zhan, S. L. Feng, *Solid-State Electron*. **2016**, *116*, 119.

[16] P. M. Palangappa, J. Y. Li, K. Mohanram, *IEEE Transactions on Computers* **2016**, *65*, 1025.

[17] P. K. Amiri, K. L. Wang, *Proc. 6th IEEE Int. Memory Workshop*, **2014**, *10*.

[18] Utilization of the anomalous hall effect or polarized spin hall effect for MRAM application, US 9269415 B1, **2016**.

[19] A. Calderoni, S. Sills, N. Ramaswamy, *Proc. 6th IEEE Int. Memory Workshop*, **2014,** *5.*

[20] W. J. Ma, *Electron. Lett*. **2016**, *52*, 9.

[21] A. Belmonte, A. Fantini, A. Redolfi, M. Houssa, M. Jurczak, L. Goux, *Solid-*

State Electron. **2016**, *125*, 189.

[22] N. Gonzales, J. Dinh, D. Lewis, N. Gilbert, B. Pedersen, D. Kamalanathan, J. R. Jameson, S. Hollmer, *Memory Workshop (IMW)*, **2016** IEEE 8th Internationl.

[23] L. Li, D. Z. Wen, *Organic Electron*. **2016**, *34*, 12.

[24] S. Y. Ning, T. O. Iwasaki, S. Hachiya, G. Rosendale, M. Manning, D. Viviani, T. Rueckes, K. Takeuchi, *Jpn. J. Appl. Phys*. **2016**, *55*, 04EE01.

[25] W. Zhao, E. Belhaire, C. Chappert, P. Mazoyer, *ACM Trans. Embedded Comput. Syst.* **2009**, *9*, 1.

[26] J. J. Nowak, R. P. Robertazzi, J. Z. Sun, G. Hu, J. H. Park, J. Lee, A. J. Annunziata, G. P. Lauer, R. Kothandaraman, E. J. O'Sullivan, P. L. Trouilloud, Y. Kim, D. C. Worledge, *IEEE MAGNETICS LETTERS*, **2016**, *7.*

[27] Z. Liu, A. A. Yasseri, J. S. Lindsey, D. F. Bocian, *Science* **2003**, *302*, 1543.

[28] W. G. Kuhr, A. R. Gallo, R. W. Manning, C. W. Rhodine, *MRS Bulletin*, **2004**, *29*, 805.

[29] L. Cario, C. Vaju, B. Corraze, V. Guiot, E. Janod, *Adv. Mater*. **2010**, *22*, 5193.

[30] J. Tranchant, E. Janod, L. Cario, B. Corraze, E. Souchier, J. L. Leclercq, P. Cremillieu, P. Moreau, M. P. Besland, *Thin Solid Films* **2013**, *533*, 61.

[31] B. Govoreanu, G. S. Kar, Y. Y. Chen, V. Paraschiv, A. Fantini, I. P. Radu, L. Goux, S. Clima, R. Degraeve, N. Jossart, In *IEEE Int. Electron Dev. Meeting*, Washington, DC, USA, 5-7 December, **2011**.

[32] H. Y. Lee, Y. S. Chen, P. S. Chen, P. Y. Gu, Y. Y. Hsu, S. M. Wang, W. H. Liu, C. H. Tsai, S. S. Sheu, P. C. Chiang, W. P. Lin, C. H. Lin, W. S. Chen, F. T. Chen, C. H. Lien, and M.-J. Tsai, In *IEEE Int. Electron Dev. Meeting*, San Francisco, CA, USA, 6-8 December, **2010**.

[33] M. J. Lee, C. B. Lee, D. S. Lee, S. R. Lee, M. Chang, J. H. Hur, Y. B. Kim, C.

J. Kim, D. H. Seo, S. Seo, U. I. Chung, I. K. Yoo, K. Kim, *Nat. Mater.* **2011**, *10*, 625.

[34] R. Waser, D. Ielmini, H. Akinaga, H. Shima, H.-S. P. Wong, J. J. Yang, S. Yu, in Resistive Switching: From Fundamentals of Nanoionic Redox Processes to Memristive Device Applications, Vol. 1 (Eds: D. Lelmini, R. Waser), Wiley-VCH, Berlin, **2016**, p. 1.

[35] M. Lanza, *Materials* **2014**, *7*, 2155.

[36] E. Gale, *Semicond. Sci. Technol*. **2014**, *29*, 10.

[37] K. Tsunoda, Y. Fukuzumi, J. R. Jameson, Z. Wang, P. B. Griffin, Y. Nishi, *Appl. Phys. Lett.* **2007**, *90*, 113501.

[38] A. Sawa, *Mater. Today* **2008**, *11*, 28.

[39] S. B. Long, L. Perniola, C. Cagli, J. Buckley, X. J. Lian, E. Miranda, F. Pan, M. Liu, J. Sune, *Sci. Rep.* **2013**, *3*, 2929.

[40] X. Wu, S. Mei, M. Bosman, N. Raghavan, X. X. Zhang, D. Y. Cha, K. Li, K. L. Pey, *Adv. Electro. Mater.* **2015**, *1*, 1500130.

[41] U. Chand, K. C. Huang, C. Y. Huang, C. H. Ho, C. H. Lin, T. Y. Tseng, *J. Appl. Phys*. **2015**, *117*, 184105.

[42] D. Duncan, B. Magyari-Kope, Y. Nishi, *Appl. Phys. Lett.* **2016**, *108*, 043501.

[43] B. Sarkar, B. Lee, V. Misra, *Semiconductor Sci. Technol.* **2015**, *30*, 105014.

[44] C. Ahn, Z. Jiang, C. S. Lee, H. Y. Chen, J. Liang, L. S. Liyanage, H. S. P. Wong, *IEEE Trans. Electron Devices* **2015**, *62*, 2197.

[45] J. Zhou, F. Cai, Q. Wang, B. Chen, S. Gaba, W. D. Lu, *IEEE Trans. Electron Devices* **2016**, *37*, 404.

[46] L. G. Wang, X. Qian, Y. Q. Cao, Z. Y. Cao, G. Y. Fang, A. D. Li, D. Wu, *Nano Research Lett.* **2015**, *10*, 135.

[47] H. Y. Jeong, S. K. Kim, J. Y. Lee, S. Y. Choi, *J. Electrochem. Soc.* **2011**, *158*, 979.

[48] J. Shim, I. Kim, K. P. Biju, M. Jo, J. Park, J. Lee, S. Jung, W. Lee, S. Kim, S. Park, H. Hwang, *J. Appl. Phys.* **2011**, *109*, 033712.

[49] J. J. Huang, C. W. Kuo, W. C. Chang, T. H. Hou, *Appl. Phys. Lett.* **2010**, *96*, 262901.

[50] H. Y. Jeong, Y. I. Kim, J. Y. Lee, S. Y. Choi, *Nanotechnology* **2010**, *21*, 115203.

[51] M. X. Yu, Y. M. Cai, Z. W. Wang, Y. C. Fang, Y. F. Liu, Z. Z. Yu, Y. Pan, Z. X. Zhang, J. Tan, X. Yang, M. Li, R. Huang, *Sci. Rep.* **2016**, *6*, 21020.

[52] Y. D. Zhao, P. Huang, Z. Chen, C. Liu, H. T. Li, W. J. Ma, B. Gao, X. Y. Liu, J. F. Kang, in *IEEE Silicon Nanoelectronics Worshop*, Kyoto, Japan, 14-15 June **2015**.

[53] B. Gao, W. Y. Chang, B. Sun, H. W. Zhang, L. F. Liu, X. Y. Liu, R. Q. Han, T. B. Wu, J. F. Kang, in *Int. Symp. VLSI Technol., Syst., Appl.*, Hsinchu, China, 26-28 April **2010**.

[54] G. Bersuker, D. C. Gilmer, D. Veksler, P. Kirsch, L. Vandelli, A. Padovani, L. Larcher, K. McKenna, A. Shluger, V. Iglesias, M. Porti, M. Nafria, *J. Appl. Phys.* **2011**, *110*, 124518.

[55] M. Lubben, P. Karakolis, V. I. Sougleridis, P. Normand, P. Dimitrakis, I. Valov, *Adv. Mater*. **2015**, *27*, 6202.

[56] R. Waser, R. Dittmann, G. Staikov, K. Szot, *Adv. Mater.* **2009**, *21*, 2632.

[57] T. Hino, T. Hasegawa, K. Terabe, T. Tsuruoka, A. Nayak, T. Ohno, M. Aono, *Sci. Technol. Adv. Mater.* **2011**, *12*, 013003.

[58] U. Russo, D. Ielmini, A. L. Lacaita, M. N. Kozicki, *IEEE Trans. Electron Devices* **2009**, *56*, 5.

[59] I. Valov, R. Waser, J. R. Jameson, M. N. Kozicki, *Nanotechnology* **2011**, *22*, 254003.

[60] N. Xu, L. F. Liu, X. Sun, C. Chen, Y. Wang, D. D. Han, X.Y. Liu, R.Q. Han, J. F. Kang, B. Yu, *Semicond. Sci. Technol.* **2008**, *23*, 075019.

[61] B. Gao, W.Y. Chang, B. Sun, H. W. Zhang, L. F. Liu, X. Y. Liu, R. Q. Han, T. B. Wu, J. F. Kang, In *International Symposium on VLSI Technology Systems and Applications*, Taiwan, China, 26-28 Apirl **2010**.

[62] M. Lanza, G. Bersuker, M. Porti, E. Miranda, M. Nafría, X. Aymerich, *Appl. Phys. Lett.* **2012**, *101*, 193502.

[63] R. Annunziata, P. Zuliani, M. Borghi, G. De Sandre, L. Scotti, C. Prelini, M. Tosi, I. Tortorelli, F. Pellizzer, in *IEEE Int. Electron Dev. Meeting*, Baltimore, MD, USA, 7-9 December, **2009**.

[64] K. Tsuchida, T. Inaba, K. Fujita, Y. Ueda, T. Shimizu, Y. Asao, T. Kajiyama, M. Iwayama, K. Sugiura, S. Ikegawa, T. Kishi, T. Kai, M. Amano, N. Shimomura, H. Yoda, Y. Watanabe, in *IEEE Int. Solid-State Circuits Conference Digest of Technical Papers*, San, Francisco, CA, USA, 7-11 February **2010**.

[65] H. Y. Lee, P. S. Chen, T. Y. Wu, Y. S. Chen, C. C. Wang, P. J. Tzeng, C. H. Lin, F. Chen, C. H. Lien, M. J. Tsai, in *IEEE Int. Electron Dev. Meeting*, San Francisco, CA, USA, 25-17 December, **2010**.

[66] Q. Luo, X. X. Xu, H. T. Liu, H. B. Lv, T. C. Gong, S. B. Long, Q. Liu, H. T. Sun, W. Banerjee, L. Li, J. F. Gao, N. D. Lu, S. S. Chung, J. Li, M. Liu, in *IEEE Int. Electron Dev. Meeting*, Washington, Dc, USA, 7-9 December, **2015**.

[67] T. Breuer, A. Siemon, E. Linn, S. Menzel, R. Waser, V. Rana, *Adv. Electron. Mater.* **2015**, *1*, 1500138.

[68] The Crossbar RRAM Advantage: Simply Fast, Simply Scalable, Simply Reliable: http://crossbar-inc.com/technology/rram-advantages/ (Accessed: August 25th of 2016)

[69] Y. Sakotsubo, S. Sagamihara, M. Terai, S. Kotsuji, Y. Saito, M. Tada, Y. Yabe, H. Hada, VLSI Technology (VLSIT), Honolulu, Hawaii, USA, 15-17 June **2010**.

[70] T. Yamamoto, T. Kubo, T. Sukegawa, E. Takii, Y. Shimamune, N. Tamura, T. Sakoda M. Nakamura, H. Ohta, T. Miyashita, H. Kurata, S. Satoh, M. Kase, T. Sugii, IEEE International Electron Devices Meeting, Washington DC, USA, 10-12 December **2007**.

[71] Website of Panasonic: (Microcontrollers) https://na.industrial.panasonic.com /products/semiconductors/microcontrollers/8-bit-low-power-microcomputers-mn101l-series.

[72] Website of Adesto Technologies: http://www.adestotech.com/products/mavriq/

[73] Website of Nantero: http://nantero.com/technology/

[74] P. K. Yang, W. Y. Chang, P. Y. Teng, S. F. Jeng, S. J. Lin, P. W. Chiu, J. H. He, in *Proceedings of the IEEE* **2013**, *101*, 1732.

[75] Y. Ji, S. Lee, B. Cho, S. Song, T. Lee, *ACS Nano* **2011**, *5*, 5995.

[76] A. H. C. Neto, F. Guinea, N. M. R. Peres, K. S. Novoselov, A. K. Geim, *Rev. Mod. Phys.* **2009**, *81*, 109.

[77] E. Stolyarova, D. Stolyarov, K. Bolotin, S. Ryu, L. Liu, K.T. Rim,M. Klima,M. Hybertsen, I. Pogorelsky, I. Pavlishin, K. Kusche, J. Hone, P. Kim, H.L. Stormer, V. Yakimenko, G. Flynn, *Nano Lett.* **2009**, *9*, 332.

[78] S. Chen, L. Brown, M. Levendorf, W. Cai, S.-Y. Ju, J. Edgeworth, X. Li, C. W. Magnuson, A. Velamakanni, R. D. Piner, J. Kang, J. Park, R. S. Ruoff, *ACS Nano* **2011**, *5*, 1321.

[79] C. Lee, X. Wei, J. W. Kysar, J. Hone, *Science* **2008**, *321*, 385.

[80] F. Bonaccorso, Z. Sun, T. Hasan, A. C. Ferrari, *Nat. Photonics* **2010**, *4*, 611.

[81] N. Tombros, C. Jozsa, M. Popinciuc, H. T. Jonkman, B. J. van Wees, *Nature* **2007**, *448*, 571.

[82] A. Balandin, S. Ghosh, W. Bao, I. Calizo, D. Teweldebrhan, F. Miao, C. N. Lau, *Nano Lett*. **2008**, *8*, 902.

[83] A.C. Ferrari et al. *Nanoscale* **2015**, *7*, 4598.

[84] R. U. A. Khan, S. R. P. Silva, *Diamond Relat. Mater.* **2001**, *10*, 1036.

[85] F. Zhuge, W. Dai, C. L. He, A. Y. Wang, Y. W. Liu, M. Li, Y. H. Wu, P. Cui, R. W. Li, *Appl. Phys. Lett.* **2010**, *96*, 163505.

[86] L. Dellmann, A. Sebastian, P. Jonnalagadda, C. A. Santini, W. W. Koelmans, C. Rossel, E. Eleftheriou, *Proc. Eur Solid-state Device Res. Conf.* **2013**, 268.

[87] Y. J. Chen, H. L. Chen, T. F. Young, T. C. Chang, T. M. Tsai, K. C. Chang, R. Zhang, K. H. Chen, J. C. Lou, T. J. Chu, J. H. Chen, D. H. Bao, S. M. Sze, *Nanoscale Res. Lett.* **2014**, *9*, 52.

[88] E. G. Gerstner, D. R. McKenzie, *Diamond Relat. Mater.* **1998**, *7*, 1172.

[89] E. G. Gerstner, D. R. McKenzie, *J. Appl. Phys*. **1998**, *84*, 5647.

[90] F. Bonaccorso, A. Lombardo, T. Hasan, Z. Sun, L. Colombo, A. C. Ferrari, *Mater. Today* **2012**, *15*, 564.

[91] S. Jang, E. Hwang, J. H. Cho, *Nanoscale* **2014**, *6*, 15286.

[92] S. Jang, E. Hwang, J. H. Lee, H. S. Park, J. H. Cho, *Small* **2015**, *11*, 311.

[93] S. M. Kim, E. B. Song, S. Lee, J. Zhu, D. H. Seo, M. Mecklenburg, S. Seo, K. L. Wang, *ACS Nano* **2012**, *6*, 7879.

[94] S. Lee, E. B. Song, S. M. Kim, Y. Lee, D. H. Seo, S. Seo, K. L. Wang, *Appl. Phys. Lett.* **2012**, *101*, 1.

[95] Y. Park, S. Park, I. Jo, B. H. Hong, Y. Hong, *Org. Electron.* **2015**, *27*, 227.

[96] S. T. Han, Y. Zhou, Q. D. Yang, L. Zhou, L. B. Huang, Y. Yan, C. S. Lee, V. A. L. Roy, *ACS Nano* **2014**, *8*, 1923.

[97] Y. N. Kim, N. H. Lee, D. Y. Yun, T. W. Kim, *Org. Electron.* **2015**, *25*, 165.

[98] Y. Park, D. Gupta, C. Lee, Y. Hong, *Org. Electron.* **2012**, *13*, 2887.

[99] N. Zhan, M. Olmedo, G. P. Wang, J. L. Liu, *Appl. Phys. Lett.* **2011**, *99*, 113112.

[100] D. Selli, M. Baldoni, A. Sgamellotti, F. Mercuri, *Nanoscale* **2012**, *4*, 1350.

[101] A. Sinitskii, J. M. Tour, *ACS Nano* **2009**, *3*, 2760.

[102] X. M. Wang, W. G. Xie, J. Du, C. L. Wang, N. Zhao, J. B. Xu, *Adv. Mater.* **2012**, *19*, 2614.

[103] B. Standley, W. Z. Bao, H. Zhang, J. Bruck, C. N. Lau, M. Bockrath, *Nano Lett*. **2008**, *8*, 3345.

[104] Y. B. Li, A. Sinitskii, J. M. Tour, *Nat. Mater.* **2008**, *7*, 966.

[105] J. Yao, J. Lin, Y. H. Dai, G. Ruan, Z.Yan, L. Li, L. Zhong, D. Natelson, J. M. Tour, *Nat. Commun.* **2012**, *3*, 1101.

[106] K. S. Novoselov, A. K. Geim, S. V. Morozov, D. Jiang, Y. Zhang, S. V. Dubonos, I. V. Grigorieva, A. A. Firsov. *Science* **2004,** *306*, 666.

[107] J. Kim, D. Kim, Y. Jo, J. Han, H. Woo, H. Kim, K. K. Kim, J. P. Hong, H. Im, *Thin Solid Films* **2015**, *589*, 188.

[108] A. Asamitsu, Y. Tomioka, H. Kuwahara, Y. Tokura, *Nature* **1997**, *388*, 50–52.

[109] D. C. Kim, S. Seo, S. E. Ahn, D. S. Suh, M. J. Lee, B. H. Park, I. K. Yoo, I. G. Baek, H. J. Kim, E. K. Yim, J. E. Lee, S. O. Park, H. S. Kim, U-In Chung, J. T. Moon, B. I. Ryu, *Appl. Phys. Lett.* **2006**, *88*, 202102.

[110] B. J. Choi, D. S. Jeong, S. K. Kim, C. Rohde, S. Choi, J. H. Oh, H. J. Kim, C. S. Hwang, K. Szot, R. Waser, B. Reichenberg, S. Tiedke, *J. Appl. Phys.* **2005**,

98, 033715.

[111] I. G. Baek, M. S. Lee, S. Seo, M. J. Lee, D. H. Seo, D. S. Suh, J. C. Park, S.O. Park, H. S. Kim, I. K. Yoo, U. I. Chung, J. T. Moon, in *IEEE Int. Electron Dev. Meeting*, San Francisco, CA, USA , 13-15 December **2004**.

[112] D. S. Jeong, H. Schroeder, R. Waser, *Electrochem. Solid-State Lett.* **2007**, *10*, G51-G53.

[113] S. Lee, J. Sohn, Z. Jiang, H. Chen, H. S. Philip Wong, *Nat. Commun.* **2015**, *6*, 8407.

[114] C. A. Ross, H. I. Smith, T. Savas, M. Schattenburg, M. Farhoud, M. Hwang, M. Walsh, M. C. Abraham, R. J. Ram, *J. Vac. Sci. Technol. B* **1999**, *17*, 3168.

[115] Y. Ji, M. Choe, B. Cho, S. Song, J. Yoon, H. C. Ko, T. Lee, *Nanotechnology* **2012**, *23*, 105202.

[116] C. X. Wu, F. S. Li, T. L. Guo, *Appl. Phys. Lett.* **2014**, *104*, 183105.

[117] S. Ghosh, I. Calizo, D. Teweldebrhan, E. P. Pokatilov, D. L. Nika, A. A. Balandin, W. Bao, F. Miao, C. N. Lau, *Appl. Phys. Lett*. **2008**, *92*, 151911.

[118] Y. Chen, B. Zhang, G. Liu, X. D. Zhuang, E. T. Kang, *Chem. Soc. Rev*. **2012**, *41*, 4688.

[119] X. Zhang, H. Xie, Z. Liu, C. Tan, Z. Luo, H. Li, J. Lin, L. Sun, W. Chen, Z. Xu, Li.Xie, W. Huang, H. Zhang, *Angew. Chem. Int. Ed*. **2015**, *54*, 3653.

[120] Graphene-based MIM diode and associated methods, US 9202945 B2, **2015**.

[121] K. S. Novoselov, D. Jiang, F. Schedin, T. J. Booth, V. V. Khotkevich, S. V. Morozov, A. K. Geim, *Proc. Natl. Acad. Sci. U. S. A.* **2005**, *102*, 10451.

[122] G. L. Yua, R. Jalilb, B. Belleb, A. S. Mayorova, P. Blakeb, Fr. Schedinb, S. V. Morozovc, L. A. Ponomarenkoa, F. Chiappinid, S. Wiedmannd, Uli Zeitlerd, M. I. Katsnelsone, A. K. Geima, K. S. Novoselova, D. C. Eliasa, *PNAS*, **2013**, *110*,

3282.

[123] L. Britnell, R. V. Gorbachev, R. Jalil, B. D. Belle, F. Schedin, M. I. Katsnelson, L. Eaves, S. V. Morozov, A. S. Mayorov, N. M. R. Peres, A. H. C. Neto, J. Leist, A. K. Geim, L. A. Ponomarenko, and K. S. Novoselov, *Nano Lett.* **2012**, 12, 1707.

[124] Y. Hernandez, V. Nicolosi, M. Lotya, F. M. Blighe, Z. Sun, S. De, I. T. Mcgovern, B. Holland, M. Byrne, Y. K. Gunko, J. J. Boland, P. Niraj, G. Duesberg, S. Krishnamurthy, R. Goodhue, J. Hutchison, V. Scardaci, A. C. Ferrari, J. N. Coleman, *Nat. Nanotechnol.* **2008**, *3*, 563.

[125] X. S. Li, W. W. Cai, J. H. An, S. Y. Kim, J. Nah, D. X. Yang, R. Piner, A. Velamakanni, I. Jung, E. Tutuc, S. K. Banerjee, L. G. Colombo, R. S. Ruoff, *Science* **2009**, 324, 1312.

[126] H. Y. Jeong, J. Y. Kim, J. W. Kim, J. O. Hwang, J. E. Kim, J. Y. Lee, T. H. Yoon, B. J. Cho, S. O. Kim, R. S. Ruoff, S. Y. Choi, *Nano Lett.* **2010**, 10, 4381.

[127] S. Porro, E. Accornero, C. F. Pirri, C. Ricciardi, *Carbon* **2015**, *85*, 383.

[128] S. Seo, Y. H. Yoon, J. H. Lee, Y. H. Park, H. Y. Lee, *ACS Nano* **2013**, *7*, 3607.

[129] M. Lotya, Y. Hernandez, P. J. King, R. J. Smith, V. Nicolosi, L. S. Karlsson, F. M. Blighe, S. De, Z. Wang, I. T. McGovern, G. S. Duesberg, J. N. Coleman, *J. Am. Chem. Soc.* **2009**, *131*, 3611.

[130] J. N. Coleman et al. *Science*, **2011**, *311*, 568.

[131] S. C. Ray, S. K. Bhunia, A. Saha, N. R. Jana, *Microelectron. Eng.* **2015**, *146*, 48.

[132] I. Banerjee, P. Harris, A. Salimian, A. K. Ray, *IET Circuits, Devices & Systems*, **2015**, *9*, 428.

[133] S. Porro, C. Ricciardi, *RSC Adv.* **2015**, *5*, 6856.

[134] A. Matkovic, I. Milosevic, M. Milicevic, T. Tomasevic-Ilic, J. Pesic, M. Music, M. Spasenovic, D. Jovanovic, B. Vasic, C. Deeks, R. Panajotovic, M. R. Belic, R. Gajic, *2D Mater*. **2016**, *3*, 015002.

[135] M. Lanza, M. Porti, M. Nafría, G. Benstetter, W. Frammelsberger, H. Ranzinger, E. Lodermeier, G. Jaschke, *Microelectron. Reliab.* **2007**, *47*, 1424.

[136] J. Petry, W. Vandervorst, O. Richard, T. Conard, P. DeWolf, V. Kaushik, A. Delabie, S. V. Elshocht, Mater Res Soc Symp Proc, San Francisco, CA, USA, 13–16 April **2004**.

[137] M. Lanza, M. Porti, M. Nafría, X. Aymerich, G. Benstetter, E. Lodermeier, H. Ranzinger G. Jaschke, S. Teichert, L. Wilde, P. Michalowski, *IEEE Trans. Nanotechnol.* **2011**, *10*, 344.

[138] C. L. Tan, Z. D. Liu, W. Huang, H. Zhang, *Chem. Soc. Rev.* **2015**, *44*, 2615.

[139] L. Y. Niu, J. N. Coleman, H. Zhang, H. Shin, M. Chhowalla, Z. J. Zheng, *Small* **2016**, *12*, 272.

[140] J. Q. Liu, Z. Q. Lin, T. J. Liu, Z. Y. Yin, X. Z. Zhou, S. F. Chen, L. H. Xie, F. Boey, H. Zhang, W. Huang, *Small* **2010**, *6*, 1536.

[141] P. Blake, P. D. Brimicombe, R. R. Nair, T. J. Booth, D. Jiang, F. Schedin, L. A. Ponomarenko, S. V. Morozov, H. F. Gleeson, E. W. Hill,A. K. Geim, K. S. Novoselov, *Nano Lett*. **2008**, *8*, 1704.

[142] K. S. Kim, Y. Zhao, H. Jang, S. Y. Lee, J. M. Kime, K. S. Kim, J. H. Ahn, P. Kim, J. Y. Choi, B. H. Hong, *Nature*, **2009**, *457*, 706.

[143] J. Coraus, A. T. Ndiaye, M. Engler, C. Busse, D. Wall, N. Buckanie, F. J. M. Heringdorf, R. V. Gastel, B. Poelsema, T. Michely, *New J. Phys.* **2009**, *11*, 023006.

[144] Y. Z. Xue, B. Wu, Y. L. Guo, L. P. Huang, L. Jiang, J. Y. Chen, D. C. Geng, Y.

Q. Liu, W. P. Hu, G. Yu, *Nano Res.* **2011**, 4, 1208.

[145] Z. W. Peng, Z. Yan, Z. Z. Sun, J. M. Tour, *ACS Nano* **2011**, *5*, 8241.

[146] D. R. Lenski, M. S. Fuhrer, *J. Appl. Phys*. **2011**, *110*, 013720.

[147] T. Kato, R. Hatakeyama, *ACS Nano* **2012**, *6*, 8508.

[148] Y. J. Zhan, Z. Liu, S. Najmaei, P. M. Ajayan, J. Lou, *Small*, **2012**, 8, 966.

[149] S. F. Wu, C. M. Huang, G. Aivazian, J. S. Ross, D. H. Cobden, X. D. Xu, *ACS Nano*, **2013**, 7, 2768.

[150] K. K. Liu, W. J. Zhang, Y. H. Lee, Y. C. Lin, M. T. Chang, C. Su, C. S. Chang, H. Li, Y. M. Shi, H. Zhang, C. S. Lai, L. J. Li, *Nano Lett.* **2012**, 12, 1538.

[151] Y. H. Lee, X. Q. Zhang, W. J. Zhang, M. T. Chang, C. T. Lin, K. D. Chang, Y. C. Yu, J. T. W. Wang, C. S. Chang, L. J. Li, T. W. Lin, *Adv. Mater.* **2012**, 24, 2320.

[152] Y. F. Yu, C. Li, Y. Liu, L. Q. Su, Y. Zhang and L. Y. Cao, *Sci. Rep.* **2013**, 3, 1866.

[153] S. Kikkawa, R. Shimanouchi-Futagami, M. Koizumi, *Appl. Phys. A* **1989**, *49*, 105.

[154] E. S. Peters, C. J. Carmalt, I. P. Parkin, D. A. Tocher, *Eur. J. Inorg. Chem*. **2005**, *20*, 4179.

[155] C. Cong, J. Shang, X.Wu, B. C. Cao, N. Peimyoo, C. Y. Qiu, L. T. Sun, T. Yu, arXiv:1312.1418.

[156] J. Xia, X. Huang, L. Z. Liu, M. Wang, L. Wang, B. Huang, D. D. Zhu, J. J. Li, C. Z. Gu, X. M. Meng, *Nanoscale* **2014**, *6*, 8949.

[157] X. Wang, Y. Gong, G. Shi, W. L. Chow, K. Keyshar, G. L. Ye, R. Vajtai, J. Lou, Z. Liu, E. Ringe, B. K. Tay, P. M. Ajayan, *ACS Nano* **2014**, *8*, 5125.

[158] J. K. Huang, J. Pu, C. L. Hsu, M. H. Chiu, Z. Y. Juang, Y. H. Chang, W. H. Chang, Y. Iwasa, T. Takenobu, L. J. Li, *ACS Nano* **2013**, *8*, 923.

[159] L. Song, L. J. Ci, H. Lu, P. B. Sorokin, C. H. Jin, J. Ni, A. G. Kvashnin, D. G. Kvashnin, J. Lou, B. I. Yakobson, P. M. Ajayan, *Nano Lett.* **2010**, *10*, 3209.

[160] S. M. Kim, A. Hsu, M. H. Park, S. H. Chae, S. J. Yun, J. S. Lee, D. H. Cho, W. J. Fang, C. G. Lee, T. Palacios, M. Dresselhaus, K. K. Kim, Y. H. Lee, J. Kong, *Nat. Commun.* DOI: 10.1038/ncomms9662.

[161] Y. Gao, W. C. Ren, T. Ma, Z. B. Liu, Y. Zhang, W. B. Liu, L. P. Ma, X. L. Ma, H. M. Cheng, *ACS Nano* **2013**, *7*, 5199.

[162] J. B. Smith, D. Hagaman, H. F. Ji, *Nanotechnology* **2016**, *27*, 215602.

[163] Chengbin Pan, Yanfeng Ji, Na Xiao, Fei Hui, Kechao Tang, Yuzheng Guo, Xiaoming Xie, Francesco M. Puglisi, Luca Larcher, Enrique Miranda, Lanlan Jiang, Yuanyuan Shi, Ilia Valov, Paul C. McIntyre, Rainer Waser and Mario Lanza, Adv. Functional Mater. (submitted)

[164] M. Lanza, Y. Wang, T. Gao, A. Bayerl, M. Porti, M. Nafria, Y. B. Zhou, G. Y. Jin, Z. F. Liu, Y. F. zhang, D. P. Yu, H. L. Duan, *Nano Research* **2013**, 6, 485.

[165] J. W. Suk, A. Kitt, C. Magnuson, Y. F. Hao, S. Ahmed, J. An, A. K. Swan, B. B. Goldberg, R. S. Ruoff. *ACS Nano*, **2011**, 5, 6916.

[166] M. Lanza, A. Bayerl, T. Gao, M. Porti, M. Nafria, G. Y. Jing, Y. F. Zhang, Z. F. Liu, H. L. Duan. *Adv. Mate*r. **2013**, 25, 14401444.

[167] M. Lanza, T. Gao, Z. X. Yin, Y. F. Zhang, Z. F. Liu, Y. Z. Tong, Z. Y. Shen, H. L. Duan, *Nanoscale* **2013**, 5, 10816.

[168] X. S. Li, Y. W. Zhu, W. W. Cai, M. Borysiak, B. Y. Han, D. Chen, R. D. Piner, L. Colombo, R. S. Ruoff, *Nano Lett*. **2009**, *9*, 4359.

[169] L. B. Gao, G. X. Ni, Y. P. Liu, B. Liu, A. H. Castro Neto, K. P. Loh, *Nature* **2014**, *505*, 190.

[170] K. Lee, I. Hwang, S. Lee, S. Oh, D. Lee, C. K. Kim, Y. Nam, S. Hong, C. Yoon,

R. B. Morgan, H. Kim, S. Seo, D. H. Seo, S. Lee, B. H. Park, *Sci. Rep.* **2015**, *5*, 11279.

[171] J. H. Lee, C. Du, K. Sun, E. Kioupakis, W. D. Lu, *ACS Nano* **2016**, *10*, 3571.

[172] A. Pirkle, J. Chan, A. Venugopal, D. Hinojos, C. W. Magnuson, S. Mcdonnell, L. Colombo, E. M. Vogel, R. S. Ruoff, R. M. Wallace, *Appl. Phys. Lett.* **2011**, *99*, 122108.

[173] D. Y. Wang, I. S. Huang, P. H. Ho, S. S. Li, Y. C. Yeh, D. W. Wang, W. L. Chen, Y. Y. Lee, Y. M. Chang, C. C. Chen, C. T. Liang, C. W. Chen, *Adv. Mater.* **2013**, 25, 4521.

[174] A. P. Esser-Kahn, P. R. Thakre, H. Dong, J. F. Patrick, V. K. Vlasko-Vlasov, N. R. Sottos, J. S. Moore, S. R. White, *Adv. Mater.* **2011**, *23*, 3654.

[175] C. G. Willson, R. R. Dammel, A. Reiser, Emerging Lithographic Technologies Proc. SPIE **1997,** 28.

[176] P. Sutter, J. Lahiri, P. Zahl, B. Wang, E. Sutter, *Nano Lett.* **2013**, *13*, 276.

[177] W. Yang, G. R. Chen, Z. W. Shi, C. C. Liu, L. C. Zhang, G. B. Xie, M. Cheng, D. M. Wang, R. Yang, D. X. Shi, K. Watanabe, T. Taniguchi, Y. G. Yao, Y. B. Zhang, G. Y. Zhang, *Nat. Mater.* **2013**, *12*, 792.

[178] S. Ratha, C. S. Rout, Appl. *Mater. Interfaces* **2013**, *5*, 11427.

[179] X. R. Wang, S. M. Tabakman, H. J. Dai, *J. Am. Chem. Soc*. **2008**, 130, 8152.

[180] S. McDonnell, B. Brennan, A. Azcatl, N. Lu, H. Dong, C. Buie, J. Kim, C. L. Hinkle, M. J. Kim, R. M. Wallace, *ACS Nano* **2013**, 7, 10354.

[181] H. Y. Nan, Z. L. Wang, W. H. Wang, Z. Liang, Y. Lu, Q. Chen, D. W. He, P. H. Tan, F. Miao, X. R. Wang, J. L. Wang, Z. H. Ni, *ACS Nano* **2014**, 8, 5738.

[182] A. A. Demkov, O. F. Sankey, *Phys. Rev. Lett*. **1999**, 83, 2038.

[183] J. L. Alay, M. Hirose, *J. Appl. Phys*. **1997**, 81, 1606.

[184] B. Brar, G. D. Wilk, A. C. Seabaugh, *Appl. Phys. Lett*. **1996**, 69, 2728.

[185] B. Chakrabarti, T. Roy, E. M. Vogel, *IEEE Electron Dvice Letters*, **2014**, 35, 7.

[186] Y. Bai, H. Wu, K. Wang, R. Wu, L. Song, T. Li, J. Wang, Z. Yu, H. Qian. *Sci. Rep.* **2015**, *5*, 13785.

[187] G. Fisichella, G. Greco, F. Roccaforte, F. Giannazzo, *Nanoscale* **2014**, *6*, 8671.

[188] J. W. Seo, J.W. Park, K. S. Lim, J.H. Yang, S. J. Kang, *Appl. Phys. Lett.* **2008**, *93*, 223505.

[189] H. D. Kim, H. M. An, Y. Seo, T. G. Kim, *IEEE Electron Device Lett.* **2011**, *32*, 1125.

[190] K. C. Liu, W. H. Tzeng, K. M. Chang, Y. C. Chan, C. C. Kuo, *Microelectron. Eng.* **2011**, *88*, 1586.

[191] J. Lee, O. Kim, *Jpn. J. Appl. Phys.* **2011**, *50*, 06GF01.

[192] H. Zhao, H. Tu, F. Wei, J. Du, *IEEE Electron Devices Lett.* **2014**, *61*, 5.

[193] K. Zheng, X. W. Sun, J. L. Zhao, Y. Wang, H. Y. Yu, H. V. Demir, K. L. Teo, *IEEE Electron Devices Lett.* **2011**, *32*, 6.

[194] Y. S. Ji, S. A. Lee, A. N. Cha, M. Goh, S. Bae, S. Lee, D. I. Son, T. W. Kim. *Organic electron*. **2015**, *18*, 77.

[195] D. I. Son, T. W. Kim, J. H. Shim, J. H. Jung, D. U. Lee, J. M. Lee, W. I. Park, W. K. Choi, *Nano Lett.* **2010**, *10*, 2441.

[196] M. Qian, Y. Pan, F. Liu, M. Wang, H. Shen, D. He, B. Wang, Y. Shi, F. Miao, X. Wang, *Adv. Mater.* **2014**, *26*, 3275.

[197] H. Shima, F. Takano, H. Muramatsu, H. Akinaga, Y. Tamai, I. H. Inque, H. Takagi, *Appl. Phys. Lett.* **2008**, *93*, 113504.

[198] H. Shima, T. Nakano, H. Akinaga, *Appl. Phys. Lett.* **2010**, *96*, 192107.

[199] H. Lv, M. Wang, H. Wan, Y. Song, W. Luo, P. Zhou, T. Tang, Y. Lin, R. Huang,

S. Song, J. G. Wu, H. M. Wu, M. H. Chi, *Appl. Phys. Lett.* **2009**, *94*, 213502.

[200] C. Y. Lin, D. Y. Lee, S. Y. Wang, C. C. Lin, T. Y. Tseng, *Surface Coatings Technol.* **2008**, *203*, 628.

[201] T. N. Fang, S. Kaza, S. Haddad, A. Chen, Y. C. Wu, Z. Lan, S. Avanzino, D. Liao, C. Gopalan, S. Choi, S. Mahdavi, M. Buynoski, Y. Lin, C. Marrian, C. Bill, M. VanBuskirk, M. Taguchi, *Tech. Dig. Int. Electron Devices Meeting*, San Francisco, CA, USA, **2006**.

[202] C. B. Lee, B. S. Kang, A. Benayad, M. J. Lee, S. E. Ahn, K. H. Kim, G. Stefanovich, Y. Park, I. K. Yoo, *Appl. Phys. Lett.* **2008**, *93*, 042115.

[203] K. M. Kim, B. J. Choi, Y. C. Shin, S. Choi, and C. S. Hwang, *Appl. Phys. Lett.* **2007**, *91*, 012907.

[204] S. Seo, M. J. Lee, D. C. Kim, S. E. Ahn, B. -H. Park, Y. S. Kim, I. K. Yoo, I. S. Byun, I. R. Hwang, S. H. Kim, J. S. Kim, J. S. Choi, J. H. Lee, S. H. Jeon, S. H. Hong, B. H. Par. *Appl. Phys. Lett.* **2005**, *87*, 263507.

[205] X. Lian, X. Cartoixa, E. Miranda, L. Perniola, R. Rurali, S. Long, M. Liu, J. Sune, *J. Appl. Phys.* **2014**, *115*, 244507.

[206] X. Lian, M. Lanza, A. Rodríguez, E. Miranda, J. Suñé, in *IEEE Int. Conf. Solid-State Integr. Circuit Technol.*, Guilin, China, 28-31 October **2014**.

[207] S. B. Long, X. J. Lian, C. Cagli, X. Cartoix_a, R. Rurali, E. Miranda, D. Jim_enez, L. Perniola, M. Liu, J. Sune, *Appl. Phys. Lett.* **2013**, *102*, 183505.

[208] Y. C. Yang, W. Lu, *Nanoscale* **2013**, *5*, 10076.

[209] V. V. N. Obreja, C. Codreanu, D. Poenar, O. Buiu, *Microelectron. Reliab.* **2011**, 51, 536.

[210] M. Lanza, M. Porti, M. Nafría, X. Aymerich, E. Whittaker, B. Hamilton, *Microelectron. Reliab.* **2010**, *50*, 1312.

[211] S. H. Seo, J. S. Hwang, J. M. Yang, W. J. Hwang, J. Y. Song, W. J. Lee, *Thin Solid Films* **2013**, *546*, 14.

[212] S. S. Hwang, S. Y. Jung, Y. C. Joo, *J. Appl. Phys.* **2008**, *104*, 044511.

[213] N. Raghavan, K. L. Pey, K. Shubhakar, M. Bosman, *IEEE Electron Device Lett.* **2011**, *32*, 78.

[214] E. A. Miranda, C. Walczyk, C. Wenger, T. Schroeder, *IEEE Electron Device Lett.* **2010**, *31*, 609.

[215] J.S. Bunch, S.S. Verbridge, J.S. Alden, A.M. van der Zande, J.M. Parpia, H.G. Craighead, P.L. McEuen, *Nano Lett.* **2008**, *8*, 2458.

[216] J. B. Oostinga, H. B. Heersche, X. L. Liu, A. F. Morpurgo, L. M. K. Vandersypen, *Nat. Mater.* **2008**, *7*, 151.

[217] H. Tian, H. Y. Chen, B. Gao, S. M. Yu, J. L. Liang, Y. Yang, D. Xie, J. F. Kang, T. L. Ren, Y. G. Zhang, H. S. P. Wong. *Nano Lett.* **2013**, *13*, 651.

[218] N. T. Kirkland, T. Schiller, N. Medhekar, N. Birbilis, *Corros. Sci.* **2012**, *56*, 1.

[219] L. L. Zhang, R. Zhou, X. S. Zhao, *J. Mater. Chem.* **2010**, *20*, 5983.

[220] C. Y. Chen, J. R. D. Retamal, D. H. Lien, M. W. Chen, I. W. Wu, Y. Ding, Y. L. Chueh, C. I. Wu, J. H. He, *ACS Nano* **2012**, *6*, 9366.

[221] Q. H. Li, T. Gao, Y. G. Wang, T. H. Wang, Appl. *Phys. Lett.* **2005**, *86*, 123117.

[222] C. Y. Chen, C. A. Lin, J. H. He, *Nanotechnology* **2009**, *20*, 185605.

[223] W. K. Hong, G. Jo, S. S. Kwon, S. Song, T. Lee, *IEEE Trans. Electron Dev.* **2008**, *55*, 3020.

[224] J. H. He, C. H. Ho, C. Y. Chen, *Nanotechnology* **2009**, *20*, 065503.

[225] Z. Fan, D. Wang, P. C. Chang, W. Y. Tseng, J. G. Lu, *Appl. Phys. Lett.* **2004**, *85*, 5923.

[226] C. Y. Chen, M. W. Chen, J. J. Ke, C. A. Lin, J. R. D. Retamal, J. H. He, *Pure*

Appl. Chem. **2010**, *82*, 2055.

[227] M. W. Chen, J. R. D. Retamal, C. Y. Chen, J. H. He, *IEEE Electron Dev. Lett.* **2012**, *33*, 411.

[228] V. E. Henrich, P. A. Cox, Surface Science of Metal Oxides, Cambridge University Press, Cambridge, UK, **1994**.

[229] H. Jeon, J. Park, W. Jang, H. Kim, S. Ahn, K.-J. Jeon, H. Seo, H. Jeon, *Carbon* **2014**, *75*, 209.

[230] L. G. Cançado, A. Jorio, E. M. Ferreira, F. Stavale, C. A. Achete, R. B. Capaz, M. V. O. Moutinho, A. Lombardo, T. S. Kulmala, Ferrari, A. C. *Nano Lett.* **2011**, *11*, 3190.

[231] Y. C. Yang, J. Lee, S. Lee, C. H. Liu, Z. H. Zhong, W. Lu, *Adv. Mater.* **2014**, *26*, 3693.

[232] S. Yu, H. Y. Chen, B. Gao, J. Kang, H. S. P. Wong, *ACS Nano* **2013**, *7*, 2320.

[233] J. Sohn, S. Lee, Z. Jiang, H. Y. Chen, H. S. P. Wong, in *IEEE int. Electron Dev. Meeting (IEDM)*, San Francisco, CA, USA, 15-17 Dec. **2014**.

[234] S. Stankovich, D. A. Dikin, G. H. B. Dommett, K. M. Kohlhaas, E. J. Zimney, E. A. Stach, R. D. Piner, S. T. Nguyen, R. S. Ruoff, *Nature*, **2006**, *442*, 282.

[235] L. Wang, I. Meric, P. Y. Huang, Q. Gao, Y. Gao, H. Tran, T. Taniguchi, K. Watanabe, L. M. Campos, D. A. Muller, J. Guo, P. Kim, J. Hone, K. L. Shepard, C. R. Dean, *Science* **2013**, *342*, 614.

[236] J. H. Chen, C. Jang, S. D. Xiao, M. Ishigami, M. S. Fuhrer, *Nat. Nanotechnol.* **2008**, *3*, 206.

[237] L. Gao, W. Ren, H. Xu, L. Jin, Z. Wang, T. Ma, L. P. Ma, Z. Zhang, Q. Fu, L. M. Peng, X. Bao, H. M. Cheng, *Nat. Commun.* **2012**, *3*, 699.

[238] D. R. Stewart, D. A. A. Ohlberg, P. A. Beck, Y. Chen, R. S. Williams, J. O.

Jeppesen, *Nano Lett.* **2004**, *4*, 133.

[239] Y. Yang, J. Y. Ouyang, L. P. Ma, R. J. H. Tseng, C. W. Chu, *Adv. Funct. Mater*. **2006**, *16*, 1001.

[240] C. C. Lin, B. C. Tu, C. C. Lin, C. H. Lin, T. Y. Tseng, IEEE Electron Device Lett. **2006**, *27*, 725.

[241] C. L. He, F. Zhuge, X. F. Zhou, M. Li, G. C. Zhou, Y. W. Liu, J. Z. Wang, B. Chen, W. J. Su, Z. P. Liu, Y. H. Wu, P. Cui, R. W. Li, *Applied Physics Letters* **2009**, 95, 232101.

[242] M. D. Yi, Y. Cao, H. F. Ling, Z. Z. Du, L. Y. Wang, T. Yang, Q. L. Fan, L. H. Xie, W. Huang, *Nanotechnology* **2014**, *25*, 185202.

[243] D. Y. Yun, T. W. Kim, *Carbon* **2015**, *88*, 26.

[244] D. H. Yoo, T. V. Cuong, S. H. Hahn, *Current Appl. Phys*. **2014**, *14*, 1301.

[245] F. Zhuge, B. Hu, C. He, X. Zhou, Z. Liu, R. W. Li, *Carbon* **2011**, *49*, 3796.

[246] G. Khurana, P. Misra, N. Kumar, R. S. Katiyar, *J. Phys. Chem. C* **2014**, *118*, 21357.

[247] P. Hazra, A. N. Resmi, K. B. Jinesh, *Appl. Phys. Lett.* **2016**, *108*, 153503.

[248] S. K. Hong, J. E. Kim, S. O. Kim, B. J. Cho, *J. Appl. Phys.* **2011**, *110*, 044506.

[249]s. L. Hong, J. E. Kim, S. O. Kim, S. Y. Choi, B. J. Cho, *IEEE Electron Device Lett.* **2010**, *31*, 1005.

[250] S. M. Jilani, T. D. Gamot, P. Banerji, S. Chakraborty, *Carbon* **2013**, *64*, 187.

[251] G. Venugopal, S. J. Kim, *J. Nanosci. Nanotechnol.* **2012**, *12*, 8522.

[252] G. Khurana, P. Misra, R. S. Katiyar, *Appl. Phys. Lett.* **2013**, *114*, 124508.

[253] G. N. Panin, O. O. Kapitanova, S. W. Lee, A. N. Baranov, and T. W. Kang, *Jpn J. Appl. Phys.* **2011**, *50*, 070110.

[254] H. Tian, H.Y. Chen, T. L. Ren, C. Li, Q. T. Xue, M. A. Mohammad, C. Wu, Y.

Yang, H.S. Philip Wong, *Nano Lett.* **2014**, *14*, 3214.

[255] X. Zhou, Z. Liu, *Chem. Commun.* **2010**, *46*, 2611.

[256] S. K. Hong, J.E. Kim, S. O. Kim, B. J. Cho, in *2010 10th IEEE Conference on Nanotechnology* **2010**, 604.

[257] H. S. Ki, C. B, Jin, in *Nanoelectronics Conference (INEC), 2011 IEEE 4th International* **2011**, 1.

[258] C. Wu, F. Li, Y. Zhang, T. Guo, and T. Chen, *Appl. Phys. Lett.* **2011**, *99*, 042108.

[259] O. O. Ekiz, M. Urel, H. Guner, A. K. Mizrak, and A. Dana, *ACS Nano*, 2011, **5**, 2475.

[260] K. S. Vasu, S. Sampath, and A. K. Sood, *Solid State Commun.* **2011**, *151*, 1084.

[261] L.H. Wang, W. Yang, Q.-Q. Sun, P. Zhou, H.-L. Lu, S.-J. Ding, and D. Wei Zhang, *Appl. Phys. Lett.* **2012**, *100*, 063509.

[262] H. D. Kim, M. J. Yun, J. H. Lee, K. H. Kim, T. G. Kim, *Sci. Rep.* **2014**, *4*, 4614.

[263] C. L. He, Z. W. Shi, L.C. Zhang, W. Yang, R. Yang, D. X. Shi, G. Y. Zhang, *ACS Nano* **2012**, *6*, 4214.

[264] I. Kim, M. Siddik, J. Shin, K. P. Biju, S. Jung, H. Hwang, *Appl. Phys. Lett.* **2011**, *99*, 042101.

[265] X. Dong, W. Huang, and P. Chen, *IEEE Trans. Nanotechnol.* **2010**, *99*, 1.

[266] S. K. Hong, J. E. Kim, S. O. Kim, B. J. Cho, *J. Appl. Phys.* **2011**, *110*, 044506.

[267] Z. R. Wang, V. Tjoa, L. Wu, W. J. Liu, Z. Fang, X. A. Tran, J. Wei, W. G. Zhu, H. Y. Yud, *J. Electrochem. Soc.* **2012**, *159*, 177.

[268] K. C. Chang, R. Zhang, *IEEE Electron Device Lett.* **2013**, *34*.

[269] X. L. Li, H. L. Wang, J. T. Robinson, H. Sanchez, G. Diankov, H. J. Dai, *J. Am. Chem. Soc.* **2009**, *131*, 15939.

[270] F. Zhao, J. Liu, X. Huang, X. Zou, G. Lu, P. Sun, S. Wu, W. Ai, M. D. Yi, X.

Y. Qi, L. Xie, J. Wang, H. Zhang, W. Huang, *ACS Nano* **2012**, *6*, 3027.

[271] S. K. Pradhan, B. Xiao, S. Mishra, A. Killam, A. K. Pradhan, *Sci. Rep*. **2016**, *6*, 26763.

[272] N. T. Ho, V. Senthilkumar, Y. S. Kim, *Solid-State Electron*. **2014**, *94*, 61.

[273] B. L .Hu, R. Quhe, C. Chen, F. Zhuge, X. J. Zhu, S. S. Peng, X. X. Chen, L. Pan, Y. Z. Wu, W. Zheng, Q. Yan, J. Lu, R. W. Li, *J. Mater. Chem.* **2012**, *22*, 16422.

[274] J. C. Jin, J. Lee, E. Lee, E. Hwang, H. Lee, *Chem. Commun*. **2012**, *48*, 4235.

[275] G. Liu, X. D. Zhuang, Y. Chen, B. Zhang, J. H. Zhu, C. X. Zhu, K. G. Neoh, E. T. Kang, *Appl. Phys. Lett.* **2009**, *95*, 253301.

[276] X. D. Zhuang, Y. Chen, G. Liu, P. P. Li, C. X. Zhu, E. T. Kang, K. G. Noeh, B. Zhang, J. H. Zhu, Y. X.Li, *Adv. Mater*. **2010**, *22*, 15, 1731.

[277] L. Valentini, M. Cardinali, E. Fortunti, J. M. Kenny, *Appl. Phys. Lett.* **2014**, *105*, 153111.

[278] S. Pinto, R. Krishna, C. Dias, G. Pimentel, G. N. P. Oliveira, J. M. Teixeira, P. Aguiar, E. Titus, J. Gracio, J. Ventura, J. P. Araujo, *Appl. Phys. Lett.* **2012**, *101*, 063104.

[279] J. Liu, Z. Yin, X. Cao, F. Zhao, A. Lin, L. Xie, Q. Fan, F. Boey, H. Zhang, W. Huang, *ACS Nano* **2010**, *4*, 3987.

[280] CareRAMM public summary http://emps.exeter.ac.uk/media/universityofexeter/emps/careramm/D4.4_Public_summary_of_project_results_from_the_third_year_of_the_project.pdf

[281] C. Casiraghi, J. Robertson, A. C. Ferrari, *Mater. Today* **2007**, *10*, 44

[282] A. C. Ferrari, *Surf. Coat. Technol*. **2004**, *180*, 190.

[283] P. J. Fallon, V. S. Veerasaamy, C. A. Davis, J. Robertson, G. A. J. Amaratunga, W. I. Milne, J. Koskinen, *Phys. Rev. B* **1993**, *48*, 4777.

[284] M. C. Polo, J. L. Andujar, A. Hart, J. Robertson, W. I. Milne, *Diamond Relat. Mater*. **2000**, *9*, 663.

[285] A. Sebastian, A. Pauza, C. Rossel, R. M. Shelby, A. F. Rodriguez, H. Pozidis, E. Eleftheriou, *New J. Phys.* **2011**, *13*, 013020.

[286] F. Kreupl, R. Bruchhaus, P. Majewski, J. B. Philipp, R. Symanczyk, T. Happ, C. Arndt, M. Vogt, R. Zimmermann, A. Buerke, A. P. Graham, M. Kund, *IEDM 2008 Technical Digest* **2008**, *15* , 521.

[287] P. Peng, D. Xie, Y. Yang, C. Zhou, S. Ma, T. Feng, H. Tian, T. Ren, *J. Phys D: Appl. Phys.* **2012**, *45*, 365103.

[288] D. Fu, D. Xie, T. T. Feng, C. H. Zhang, J. B. Niu, H. Qian, L. T. Liu, *IEEE Electron Device Letters* **2011**, *32*, 80.

[289] J. Xu, D. Xie, T. Feng, C. Zhang, X. Zhang, P. Peng, D. Fu, H. Qian, T.-l. Ren, L. Liu, *Carbon* **2014**, *75*, 255.

[290] Y. Chai, Y. Wu, K. Takei, H.-Y. Chen, S. Yu, P. C. H. Chan, A. Javey, H.-S. P. Wong, *IEEE Trans. Electron. Dev*. **2011**, *58*, 3933.

[291] B. Ren, L. Wang, L. Wang, J. Huang , K. Tang, Y. Lou , D. Yuan, Z. Pan, Y. Xia, *Vacuum* **2014**, *107*, 1.

[292] K. Antonowicz, A. Jesmanowicz, J. Wieczorek, *Carbon* **1972**, *10*, 81.

[293] A. C. Ferrari and J. Robertson, *Philosophical Transactions of the Royal Society A-mathematical Physical and Engineering Sciences* **2004**, *362*, 2477.

[294] C. A. Santini, A. Sebastian, C. Marchiori, V. P. Jonnalagadda, L. Dellmann, W. W. Koelmans, M. D. Rossell, C. P. Rossel, E. Eleftheriou, *Nat. Communications*. **2015**, *6*, 1.

[295] H. Chen, F. Zhuge, B. Fu, J. Li, J. Wang, W. Wang , Q. Wang, L. Li, F. Li, H. Zhang, L. Liang, H. Luo, M. Wang, J. Gao, H. Cao, H. Zhang, Z. Li, *Carbon* **2014**, *76*, 459.

[296] V. K. Nagareddy, A. K. Ott , C. Dou, T. Tsvetkova, M. Sandulov, M. F. Craciun, A. C. Ferrari, C. D. Wright, submitted (2016).

[297] S. Zhang, J. Zhou, D. Zhang, B. Ren, L. Wang, J. Huang, L. Wang, *Vacuum* **2016**, *125*, 189.

[298] M. Pyun, H. Choi, J. B. Park, D. Lee, M. Hasan, R. Dong, S. J. Jung, J. Lee, D. J. Seong, J. Yoon, H. Hwang, *Appl. Phys. Lett*. **2008**, *93*, 212907.

[299] H. Choi, M. Pyun, T. W. Kim, M. Hasan, R. Dong, J. Lee, J. B. Park, J. Yoon, D. J. Seong, T. Lee, H. Hwang, *IEEE Electron Dev. Lett.* **2009**, *30*, 302.

[300] D. I. Kim, J. Yoon, J.-B. Park, H. Hwang, Y. M. Kim, S. H. Kwon, K. H. Kim, *Appl. Phys. Lett*. **2011**, *98*, 152107.

[301] W. W. Koelmans, T. Bachmann, F. Zipoli, A. K. Ott, C. Dou, A. C. Ferrari, O. Cojocaru-Mirédin, S. Zhang, M. Wuttig, V. K. Nagareddy, M. F. Craciun, A. Alexeev, C. D. Wright, V. P. Jonnalagadda, A. Curioni, A. Sebastian, E. Eleftheriou, Carbon-based resistive memories, IEEE (IMW),1-4 (**2016**).

[302] T. A. Bachmann, A. M. Alexeev, W. W. Koelmans, F. Zipoli, A. K. Ott, C. Dou, A. C. Ferrari, V. K. Nagareddy, M. F. Craciun, V. P. Jonnalagadda, A. Curioni, A. Sebastian, E. Eleftheriou, C. D. Wright, IEEE NMDC **2016**.

[303] F. Kreupl, Carbon Memory Assessment, White paper for the ITRS meeting on emerging research devices (ERD) in Albuquerque, New Mexico, on August 25-26, **2014**.

[304] X. Zhao, H. Xu, Z. Wang, L. Zhang, J. Ma, Y. Liu, *Carbon* **2015**, *91*, 38.

[305] W. Dai, P. Ke, A. Wang, *J. Vac. Sci. Technol. B* **2013**, *31*, 031207.

[306] J. Park, M. Jo, J. Lee, S. Jung, W. Lee, S. Kim, S. Park, J. Shin, H. Hwang, *Microelectron. Eng.* **2011**, *88*, 935.

[307] X. Gao, X. Zhang, C. Wan, J. Wang, X. Tan, D. Zeng, *Diamond & Related Mater.* **2012**, *22*, 37.

[308] A. K. Ott, C. Dou, U. Sassi, I. Goykhman, A. Katsounaros, D. Yoon, X. Chen, J. Wu, A. Lombardo A. C. Ferrari, submitted (2016)

[309] Y. Chai, A. Hazeghi, K. Takei, H. Y. Chen, P. C. H. Chan, A. Javey, and H. S. P. Wong, *International Electron Devices Meeting - Technical Digest*, **2010**, 210.

[310] D. Fu, D. Xie, C.-H. Zhang, D. Zhang, J.-B. Niu, H. Qian, L.-T. Liu, *Chin. Phys. Lett*. **2010**, *27*, 098102.

[311] Y. He, J. Zhang, X. Guan, L. Zhao, Y. Wang, H. Qian, Z. Yu, *IEEE Transactions on electron devices,* **2010**, *57*, 3434.

[312] S. Qin, J. Zhang, D. Fu, D. Xie, Y. Wang, H. Qian, L. Liu, Z. Yu, *Nanoscale* **2012**, *4*, 6658.

[313] C. D. Wright, P. Hosseini, and J. A. Vazquez Diosdado , Adv. Funct. Mater. 2013, 23, 2248.

[314] Y. V. Pershin, M. Di Ventra, *Advances In Physics* **2011**, *60*, 145.

[315] K. Sangwan, D. Jariwala, I. S. Kim, K. S. Chen, T. J. Marks, L. J. Lauhon, M. C. Hersam, *Nat. Nanotechnol*. **2015**, *10*, 403.

[316] P. F. Cheng, K. Sun, Y. H. Hu, *Nano Lett*. **2016**, *16*, 572.

[317] X. Zhang, H. Qiao, X. Nian, Y. Huang, X. Pang, *J. Mater. Sci. Mater. Electron*. **2016**, 27, 7609.

[318] C. X. Hao, F. S. Wen, J. Y. Xiang, S. J. Yuan, B. C. Yang, L. Li, W. H. Wang, Z. M. Zeng, L. M. Wang, Z. Y. Liu, Y. J. Tian, *Adv. Funct. Mater.* **2016**, *26*, 2016.

[319] A. Ambrosi, Z. Sofer, M. Pumera, *Chem. Commun*. **2015**, *51*, 8450.

[320] J. Liu, Z. Zeng, X. Cao, G. Lu, L. H. Wang, Q. L. Fan, W. Huang, H. Zhang, *Small* **2012**, *8*, 3517.

[321] S. Ali, J. Bae, C. H. Lee, *In Proceedings of SPIE* **2015**, *9553*, 95530T.

[322] K. Ali, J. Ali, S. M. Mehdi, K. Choi, Y. J. An, *Appl. Surf. Sci.* **2015**, *353*, 1186.

[323] S. T. Han, Y. Zhou, B. Chen, C. Wang, L. Zhou, Y. Yan, J. Zhuang, Q. Sun, H. Zhang, V. A. L. Roy, *Small* **2015**, *12*, 390.

[324] S. M. Shinde, G. Kalita, M. Tanemura, *J. Appl. Phys*. **2014**, *116*, 214306.

[325] J. Mangalam, S. Agarwal, A. N. Resmi, M. Sundararajan, K. B. Jinesh, *Org. Electron.* **2016**, *29*, 33.

[326] Z. Yin, Z. Zeng, J. Liu, Q. He, P. Chen, H. Zhang, *Small* **2013**, *9*, 727.

[327] A. A. Bessonov, M. N. Kirikova, D. I. Petukhov, M. Allen, T. Ryhänen, M. J. a Bailey, *Nat. Mater.* **2015**, *14*, 199.

[328] X. Y. Xu, Z. Y. Yin, C. X. Xu, J. Dai, J. G. Hu, *Appl. Phys. Lett*. **2014**, *104*, 033504.

[329] K. Qian, R. Y. Tay, V. C. Nguyen, J. X. Wang , G. F. Cai, T. P. Chen , E. H. T. Teo, P. S. Lee, *Adv. Funct. Mater.* **2016**, *26*, 2176.

[330] N. D. Zhigadlo, *J. Cryst. Growth* **2014**, *402*, 308.

[331] D. Golberg, P. M. F. J. Costa, O. Lourie, M. Mitome, X. Bai, K. Kurashima, C. Zhi, C. Tang, and Y. Bando, *Nano Lett*. **2007**, *7*, 2146.

[332] C. W. Chang, D. Okawa, A. Majumdar, and A. Zettl, *Science* **2006**, *314*, 1121.

[333] B. Ilhan, M. Kurt, H. Ertuk, *Exp. Therm. Fluid Sci*. **2016**, *77*, 272.

[334] P. Y. Huang, C. S. R. Vargas, A. M. V. D. Zande, W. S. Whitney, M. P. Levendorf, J. W. Kevek, S. Garg, J. S. Alden, C. J. Hustedt, Y. Zhu, J. Park, P. L. McEuen, D. A. Muller, *Nature* **2011**, *469*, 389.

[335] A. L. Gibb, N. Alem, J. H. Chen, K. J. Erickson, J. Ciston, A. Gautam, M. Linck, A. Zettl, *J. Am. Chem. Soc*. **2013**, *135*, 6758.

[336] Y. Hattori, T. Taniguchi, K. Watanabe, K. Nagashio, *ACS Nano* **2015**, *9*, 916.

[337] Y. F. Ji, C. B. Pan, M. Y. Zhang, S. B. Long, X. J. Lian, F. Miao, F. Hui, Y. Y. Shi, L. Larcher, E. Wu, M. Lanza, *Appl. Phys. Lett.* **2016**, *108*, 012905.

[338] N. Jain, R. B. Jacobs-Gedrim, B. Yu, *Mater. Res. Soc. Symp. Proc.* **2014**, *1658*, DOI: 10.1557/opl.2014.503.

[339] J. D. Wood, S. A. Weels, D. Jariwala, K. S. Chen, E. Cho, V. K. Sangwan, X. L. Liu, L. J. Lauhon, T. J. Marks, M. C. Hersam, *Nano Lett.* **2014**, *14*, 6964.

[340] D. Hanlon, C. Backes, E. Doherty, C. S. Cucinotta, N. C. Berner, C. Boland, K. Lee, P. Lynch, Z. Gholamvand, A. Harvey, S. F. Zhang, K. P. Wang, G. Moynihan, A. Pokle, Q. M. Ramasse, N. McEvoy, W. J. Blau, J. Wang, S. Sanvito, D. D. Regan, G. S. Duesberg, V. Nicolosi, J. N. Coleman, *Nat. Commun.* **2015**, *6*, 8563.

[341] T. W. Hickmott, *J. Appl. Phys.* **1962**, *33*, 2669.

[342] J. G. Simmons, R. R. Verderber, *Proc. R. Soc. London Ser. A* **1967**, *301*, 77.

[343] R. Degraeve, B. Kaczer, G. Groeseneken, *Microelectron. Reliab.* **1999**, *39*, 1445.

[344] E. Miranda, J. Sune, R. Rodriguez, M. Nafria, X. Aymerich, *Appl. Phys. Lett.* **1998**, *73*, 490.

[345] M. Ahmad, S. A. Han, D. H Tien, J. Jung, Y. Seo, *J. Appl. Phys.*,**2011**, 110, 054307.

[346] J. J. Yang, M. X. Zhang, J. P. Strachan, F. Miao, M. D. Pickett, R. D. Kelley, G. M. Ribeiro, R. S. Williams, *Appl. Phys. Lett*. **2010**, *97*, 232102.

[347] Y. B. Kim, S. R. Lee, D. Lee, C. B. Lee, M. Chang, J. H. Hur, M. J. Lee, G. S.

Park, C. J. Kim, U. Chung, I. K. Yoo, K. Kim, , **2011** Symposium on VLSI Technology.

[348] C. H. Cheng, A. Chin, F. S. Yeh, 2010 Symposium on VLSI Technology Digest of Technical Papers **2010**, 85.

[349] Sen Liu, N. D. Lu, X. L. Zhao, H. Xu, W. Banerjee, H. B. Lv, S. B. Long, Q. J. Li, Q. Liu, M. Liu, *Adv. Mater*. **2016**, *0,* 1.

[350] X. Cao, X. M. Li, X. D. Gao, W. D. Yu, X. J. Liu, Y. W. Zhang, L. D. Chen, X. H. Cheng, *J. Appl. Phys.* **2009**, *106*, 073723.

[351] B. Zhang, G. Liu, Y. Chen, L. J. Zeng, C. X. Zhu, K. G. Neoh, C. Wang, E. T. Kang, *Chem. Eur. J.* **2011**, *17*, 13646.

[352] A. Midya, N. Gogurla, S. K. Ray, *Current Appl. Phys*. **2015**, *15*, 706.

[353] A. N. Aleshin, P. S. Krylova, A. S. Berestennikova, I. P. Shcherbakova, V. N. Petrova, V. V. Kondratievb, S. N. Eliseeva, *Synthetic Metals* **2016**, *217*, 7.

[354] Y. Sun, J. Lu, C. Ai, D. Wen, *Phys. Chem. Chem. Phys*. **2016**, *18*, 11341.

[355] A. Thakre, H. Borkar, B. P. Singha, A. Kumar, *RSC Adv.* **2015**, *5*, 57406.

[356] S. Valanarasu, I. Kulandaisamy, A. Kathalingam, J. K. Rhee, T. A. Vijayan, R. Chandramohan, *J. Nanosci. Nanotechnol.* **2013**, *13*, 6755.

[357] O. O. Kapitanova, G. N. Panin, O. V. Kononenko, A. N. Baranov, T. W. Kang, *Journal of the Korean Physical Society* **2014**, *64*, 1399.

[358] G. Khurana, P. Misra, N. Kumar,S. Kooriyattil, J. F Scott, R. S Katiyar, *Nanotechnology* **2016**, *27*, 015702.

[359] J. R. Rani, S. I. Oh, J. M. Woo, J. H. Jang, *Carbon* **2015**, *94*, 362.

[360] A. D. Yu, C. L. Liu and W. C. Chen, *Chem. Commun.* **2012**, *48*, 383.

[361] H. Y. Wu, C. C. Lin, C. H. Lin, *Ceram. Int.* **2015**, *41*, S823.

[362] X. Huang, B. Zheng, Z. Liu, C. Tan, J. Liu, B. Chen, H. Li, J. Chen, X. Zhang,

Z. Fan, W. Zhang, Z. Guo, F. Huo, Y. Yang, L. H. Xie, W. Huang, H. Zhang, *ACS Nano* **2014**, *8*, 8695.

[363] C. Tan, X. Qi, Z. Liu, F. Zhao, H. Li, X. Huang, L. Shi, B. Zheng, X. Zhang, L. Xie, Z. Tang, W. Huang, H. Zhang, *J. Am. Chem. Soc*. **2015**, *137*, 1565.

[364] Z. Wei, Y. Kanzawa, K. Arita, Y. Katoh, K. Kawai, S. Muraoka, S. Mitani, S. Fujii, K. Katayama, M. Iijima, T. Mikawa, T. Ninomiya, R. Miyanaga, Y. Kawashima, K. Tsuji, A. Himeno, T. Okada, R. Azuma, K. Shimakawa, H. Sugaya, T. Takagi, R. Yasuhara, K. Horiba, H. Kumigashira, M. Oshima, *IEEE IEDM*, 15-17 Dec, **2008**.

FIGURES

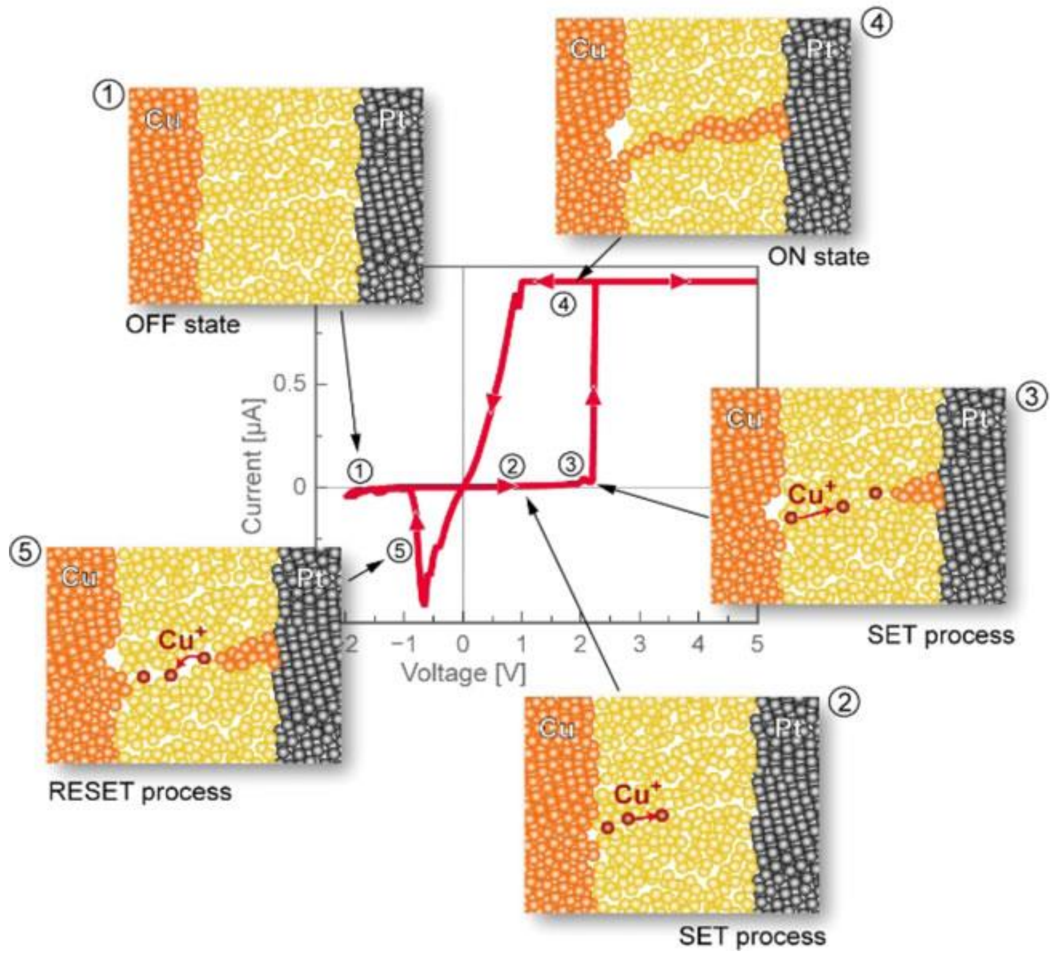

Fig. 1: Current–voltage characteristics of ECM/CBRAM cell with schematic presentation of the related physical processes. Reproduced with permission from [34]. Copyright from IOP Publishing Ltd 2011.

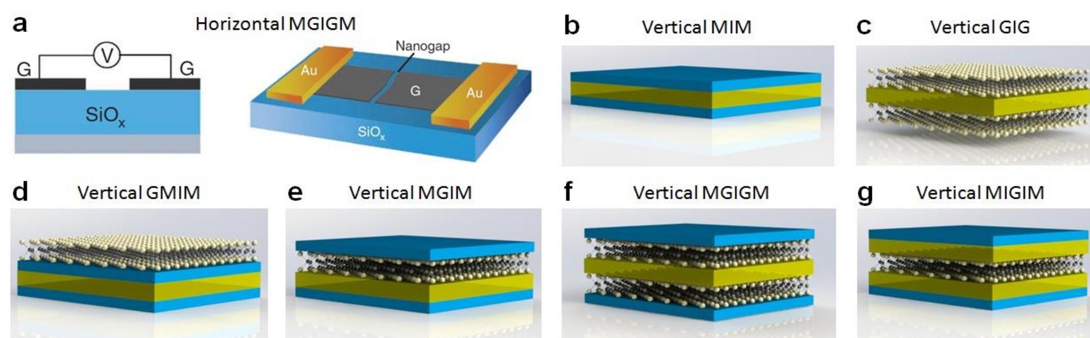

Fig. 2: Different device structures proposed in GRMs-based RRAM technology. M indicates metal, I indicates insulator, and G indicates GRM. The electric field in (b-g) is always applied between the top and bottom layers.

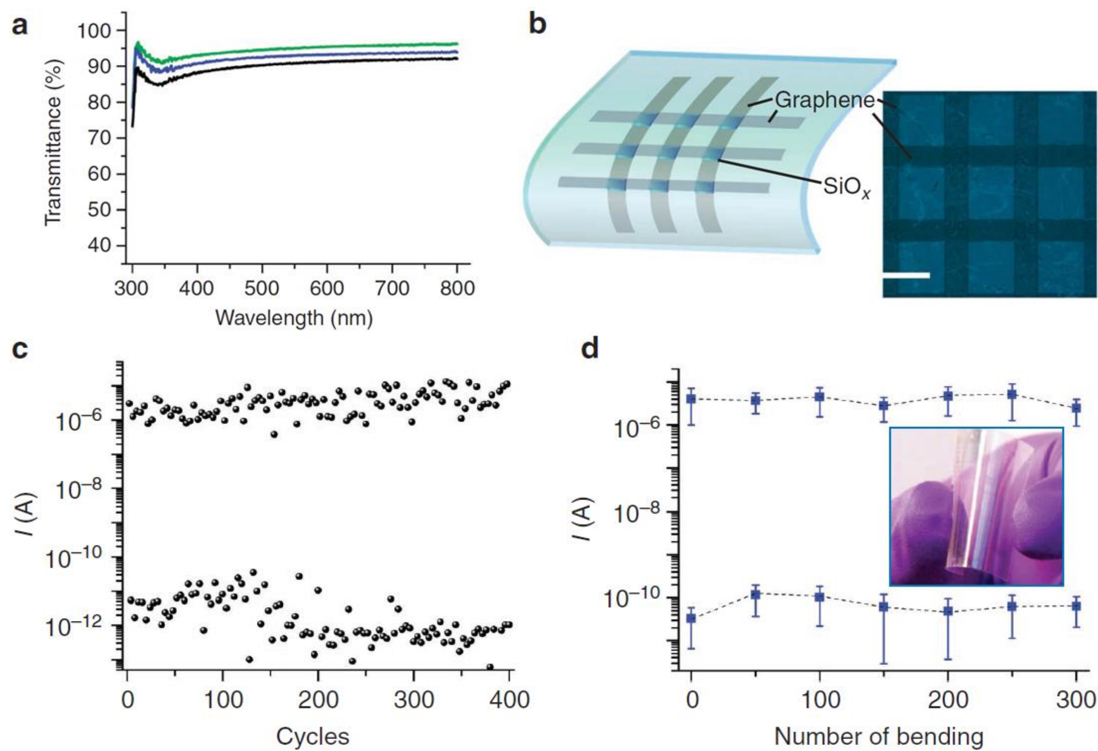

Fig. 3: (a) High transparency of SLG/SiO_2/SLG RRAM on glass substrate [105]. (b) (Left panel) Schematic SLG/SiO*x*/SLG crossbar structures on a plastic (fluoropolymer) substrate and (right panel) optical image [105]. Scale bar, 20 μm. (b) Optical image of the SLG/SiO*x*/SLG pillar structures with the inset showing the schematic image. Scale bar, 100 μm [105]. (c) Endurance measured from one of the crossbar devices using + 5 and + 14 V as set and reset voltages. The programming current is not shown here and the memory states (current) were recorded at + 1 V. [105] (d) Current levels of both ON and OFF memory states (read at + 1 V) from a crossbar device during repeated bending of the plastic substrate to r_b~0.6cm. The inset shows transparent memories using the pillar structures on the plastic substrate. Reproduced with permission from [105]. Copyright from Nature Publishing Group, 2012.

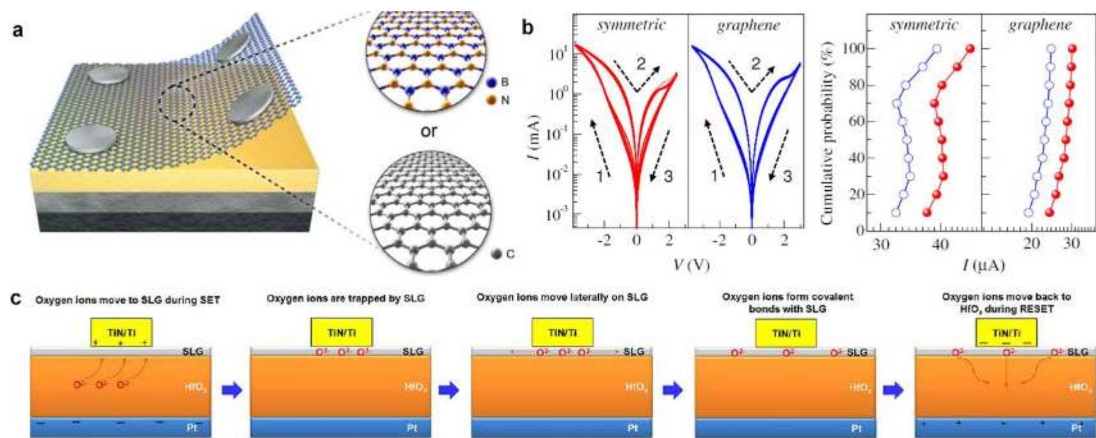

Fig. 4: (a) Schematic of SLG inserted between the top electrode and insulating film of a RRAM cell [107]. (b) Resistance switching I–V characteristics of a symmetric Al–WO_3–Al and a Al(SLG)–WO_3–Al device. Cumulative probability of the HRS current at ±0.5 V for both configurations [107]. (c) Schematic diagrams of oxygen ions movement in MGIM structures. The diagrams represent (from left to right) elementary steps of the process including movement of oxygen ions to SLG during SET, capture of oxygen ions by SLG, movement of oxygen ions laterally on SLG, formation of covalent bond with SLG, followed by movement of oxygen ions back to HfO_X during reset [217]. (a) and (b) are reproduced with permission of [107]. Copyright from Elsevier 2015. (c) is reproduced with permission from [217]. Copyright from American Chemical Society 2013.

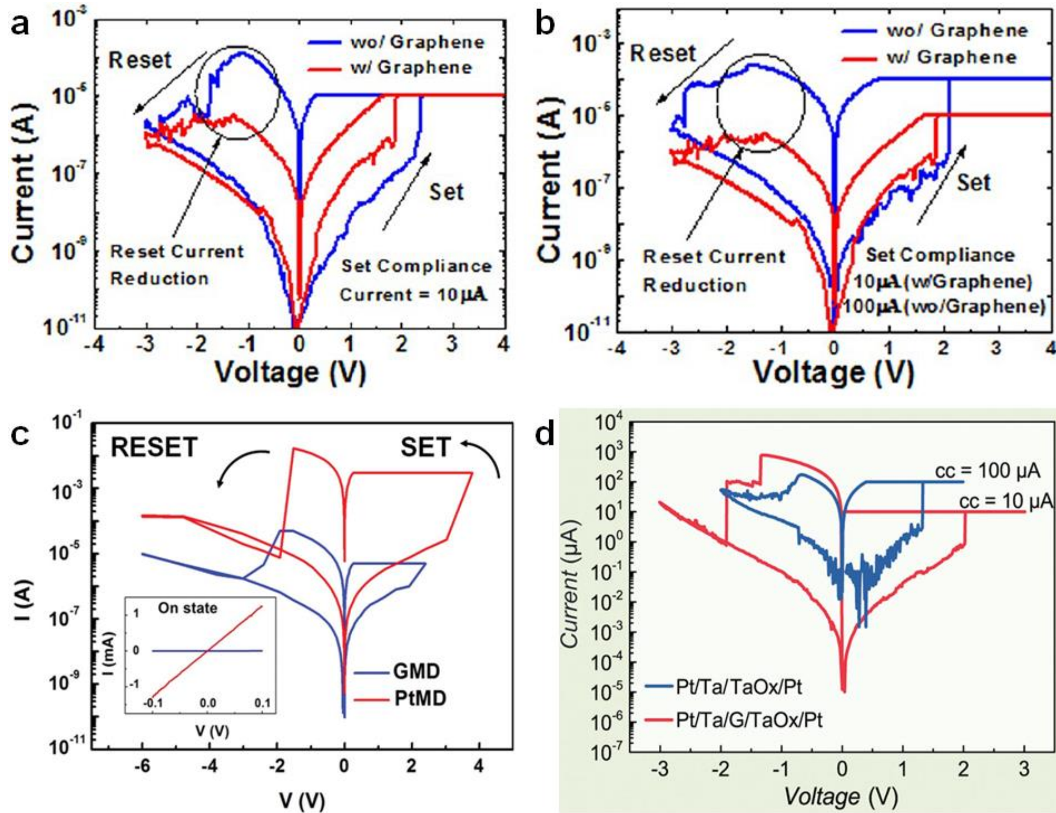

Fig. 5: (a) Typical resistive switching behaviour of Ti/SLG/HfO_X/Pt (red) and Ti/HfO_X/Pt RRAMs under the same current limitation [217]. (b) Typical resistive switching behaviour for the same devices but using optimal testing conditions [217]. 10 and 100 μA currents are applied to achieve steady switching. (a) and (b) are reproduced with permission from [217]. Copyright from American Chemical Society 2013. (c) Switching curves of typical TiO_2 based memristive devices using SLG and Pt electrodes, with a SET current compliance of 5 μA and 3 mA. The arrows point to the switching directions. Inset: small-bias I – V curves for both devices in the ON state, showing different resistance. Reproduced with permission from [196]. Copyright from Wiley-VCH 2014. (d) I–V curve comparison between a Pt/Ta/TaO_X/Pt cell with SLG inserted between the Ta and the TaO_X layers (red) and one cell without (blue) in logarithmic scale. The cell without SLG needs higher HRS currents for stable switching. That with SLG offers higher I_{ON}/I_{OFF} and HRS current reduction. Reproduced with permission from [55]. Copyright from Wiley-VCH 2015.

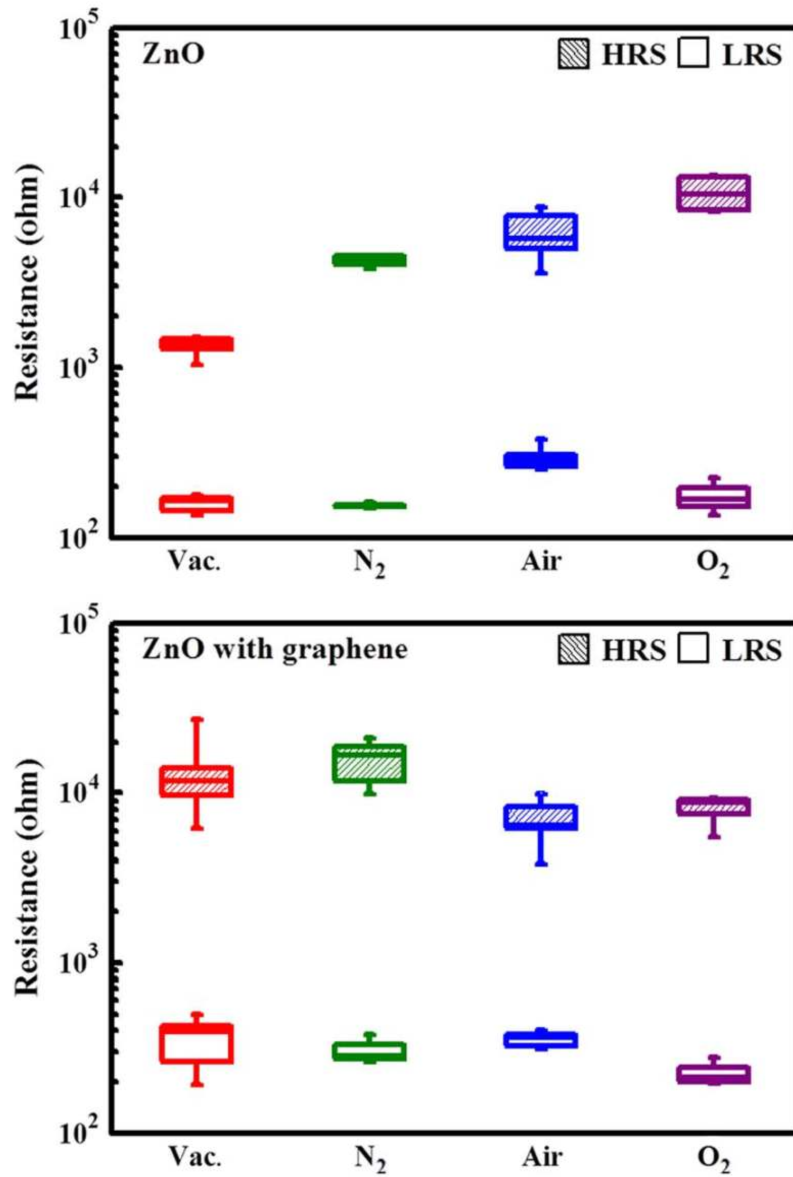

Fig. 6: Atmosphere-dependent resistance in HRS and LRS of ZnO RRAMs with and without SLG electrodes. The bottom and the top of the box are the 25th percentile and the 75th percentile, the band near the middle of the box is the 50th percentile, and the ends of the whiskers represent the 10th percentile and the 90th percentile. Reproduced with permission from [74]. Copyright from IEEE 2013.

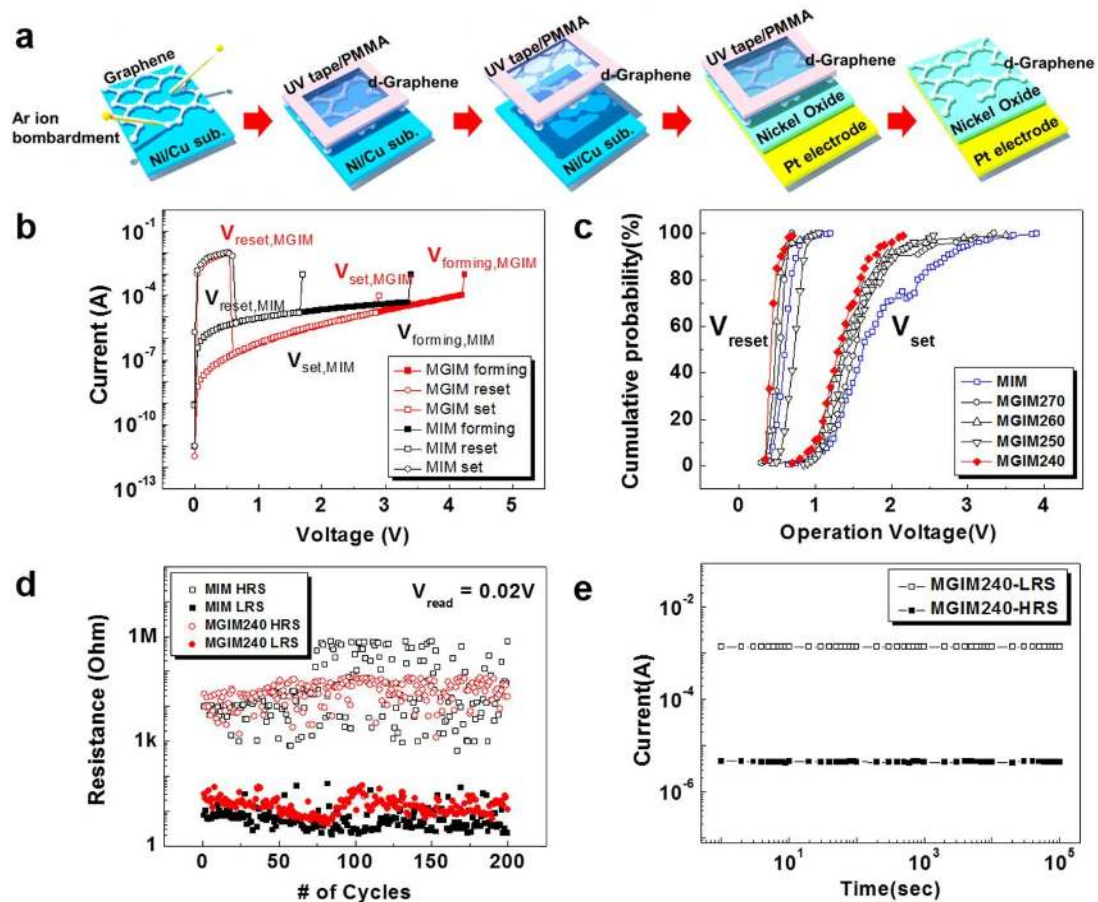

Fig. 7: (a) Illustration of fabrication process for MGIM structure using functionalized SLG prepared before transfer.[170] (b) Initial current-voltage characteristics of the MGIM and conventional MIM structures.[170] (c) Cumulative probability of switching voltages, Vset and Vreset, for MGIM structures with SLG irradiated with Ar+ ions at 240 eV (MGIM240), 250 eV (MGIM250), 260 eV (MGIM260), and 270 eV (MGIM270) as well as a MIM structure. [170] (d) Change in resistance states for MGIM240 and MIM, measured at room temperature and atmospheric pressure. [170] (e) Retention characteristics of MGIM240 measured at 85 °C in a vacuum of 1 mTorr as well as ambient atmospheric condition under reading voltage~0.1 V. Reproduced with permission from [170]. Copyright from Nature Publishing group 2015.

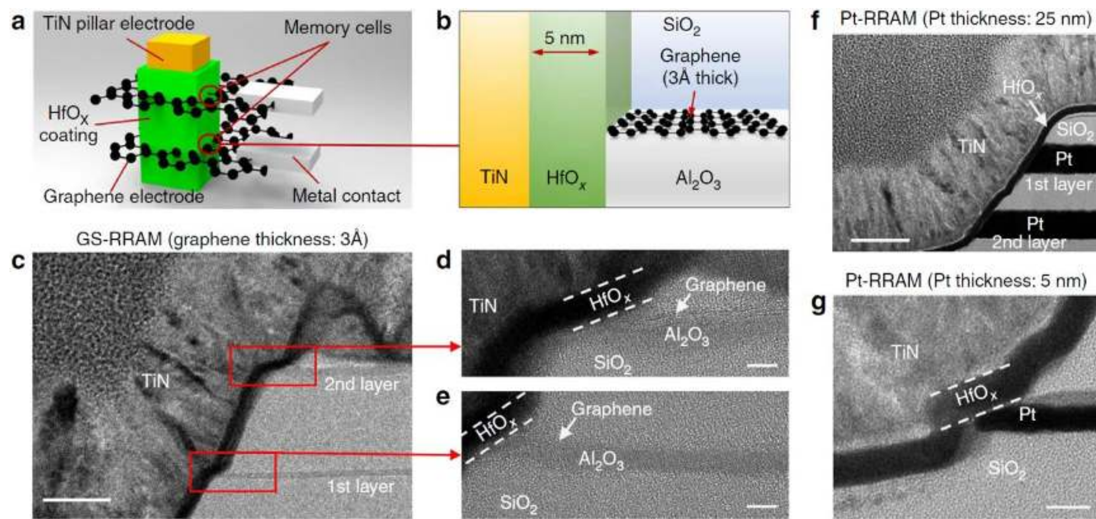

Fig. 8: (a) SLG-based RRAM in a vertical cross-point architecture. The RRAM cells are formed at the intersections of the TiN pillar electrode and the SLG plane electrode. The resistive switching HfOx layer surrounds the TiN pillar electrode and is also in contact with SLG [113]. (b) Schematic cross-section of the SLG-based RRAM [113]. (c) High-resolution TEM image of the two-stack GS-RRAM structure. The RRAM memory elements are highlighted in red. Scale bar, 40 nm [113]. (d,e) First and second layer of GS-RRAM with SLG on top of Al_2O_3. Scale bars, 5 nm [113]. (f, g) TEM image of the two-stack Pt-based RRAMs. Scale bars, 40nm (f) and 5nm (g). Reproduced with permission from [113]. Copyright from Nature Publishing Group 2015.

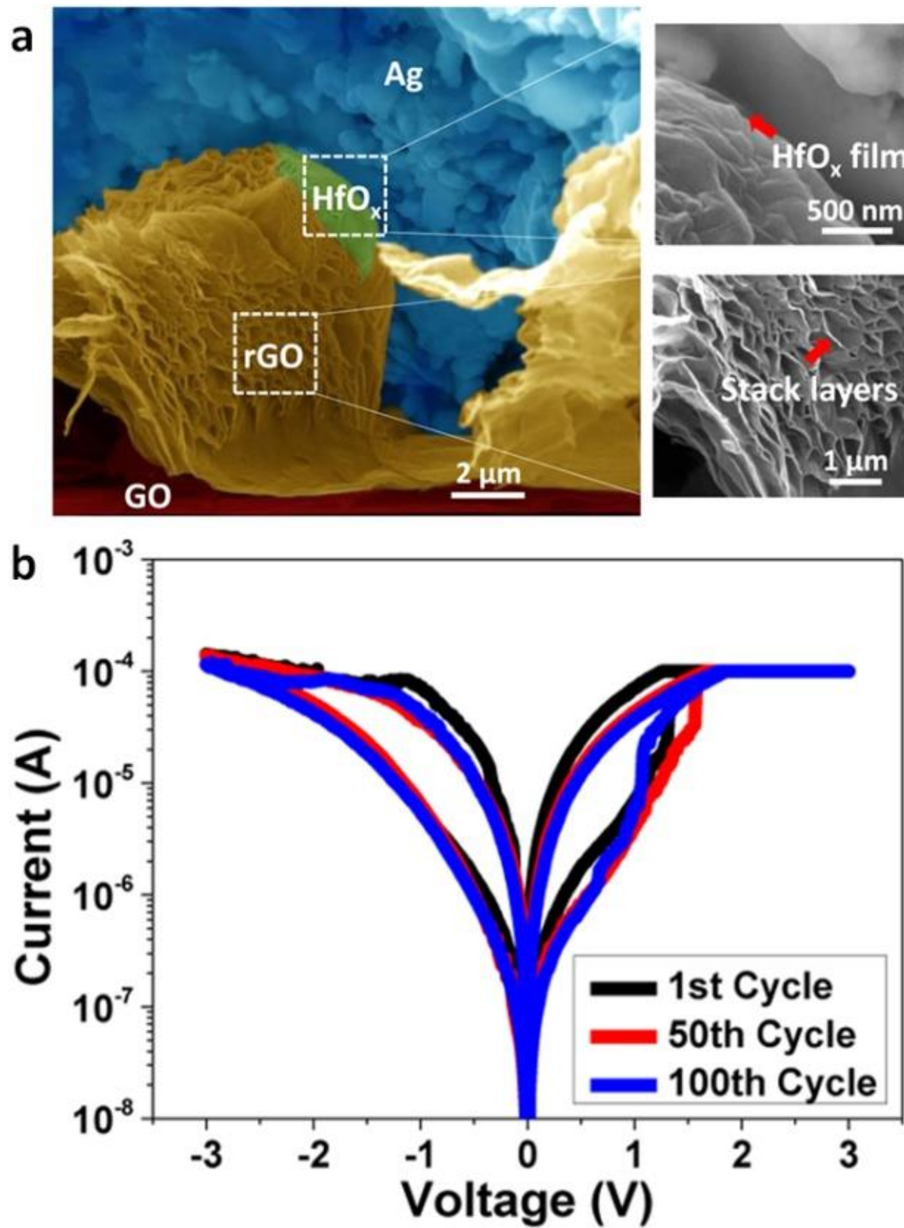

Fig. 9: (a) Cross-sectional SEM image displaying the folded, aggregated and misaligned nature of GRMs used in RRAM technologies. The insets highlight HfO_X films and stacked RGO layers, respectively [254]. (b) RS behaviour of LSG-RRAM at the first, 50th and 100th cycle, respectively. Reproduced with permission from [254]. Copyright from American Chemical Society 2014.

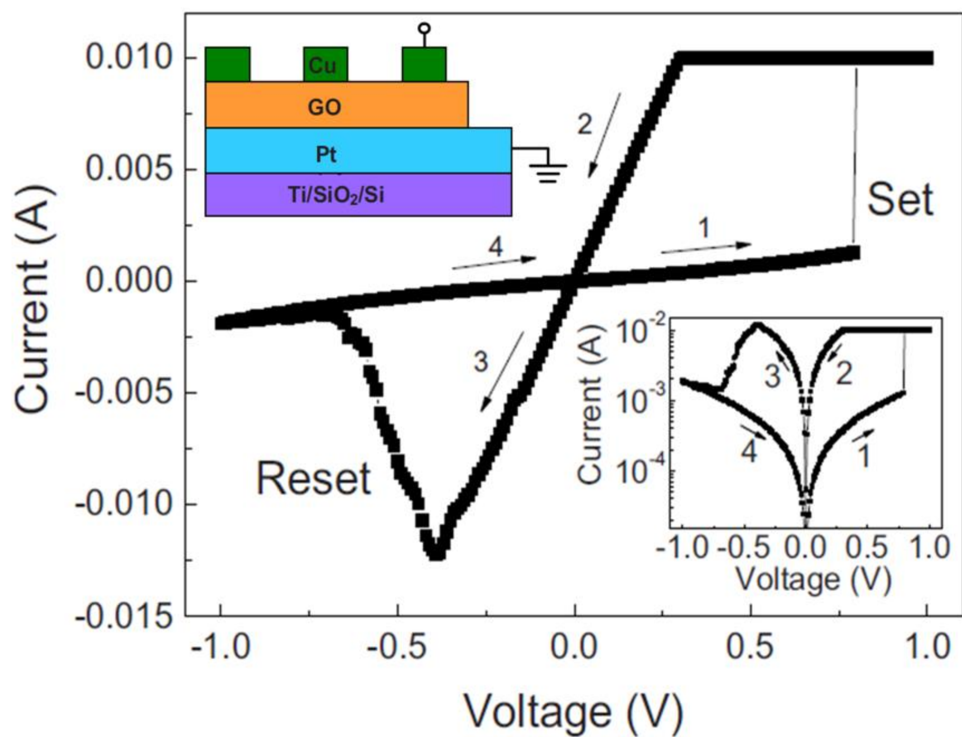

Fig. 10: *I-V* characteristics of the Cu/GO/Pt RRAM cell showing RS. The arrows indicate the sweep direction. The insets show the *I-V* characteristics in semilogarithmic scale and the schematic configuration. Modified and reprinted with permission from [241]. Copyright from American Institute of Physics 2009.

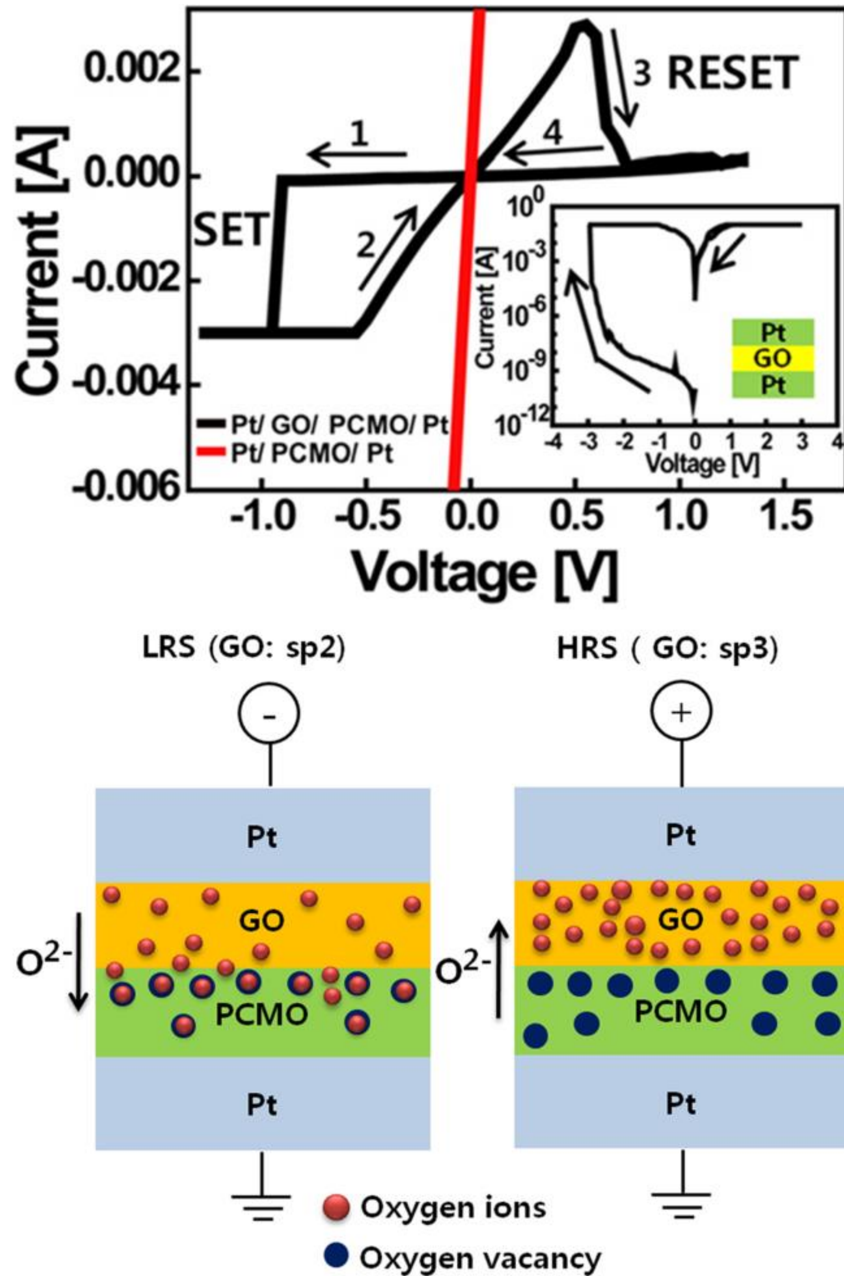

Fig. 11: (Top) Typical *I-V* hysteresis curves of GO/PCMO and PCMO cells. The inset shows the *I-V* hysteresis for the Pt/GO/Pt device [264]. (Bottom) Proposed switching mechanism in LRS (left) and HRS (right) for the GO/PCMO devices. Reproduced with permission from [264]. Copyright from American Institute of Physics 2011.

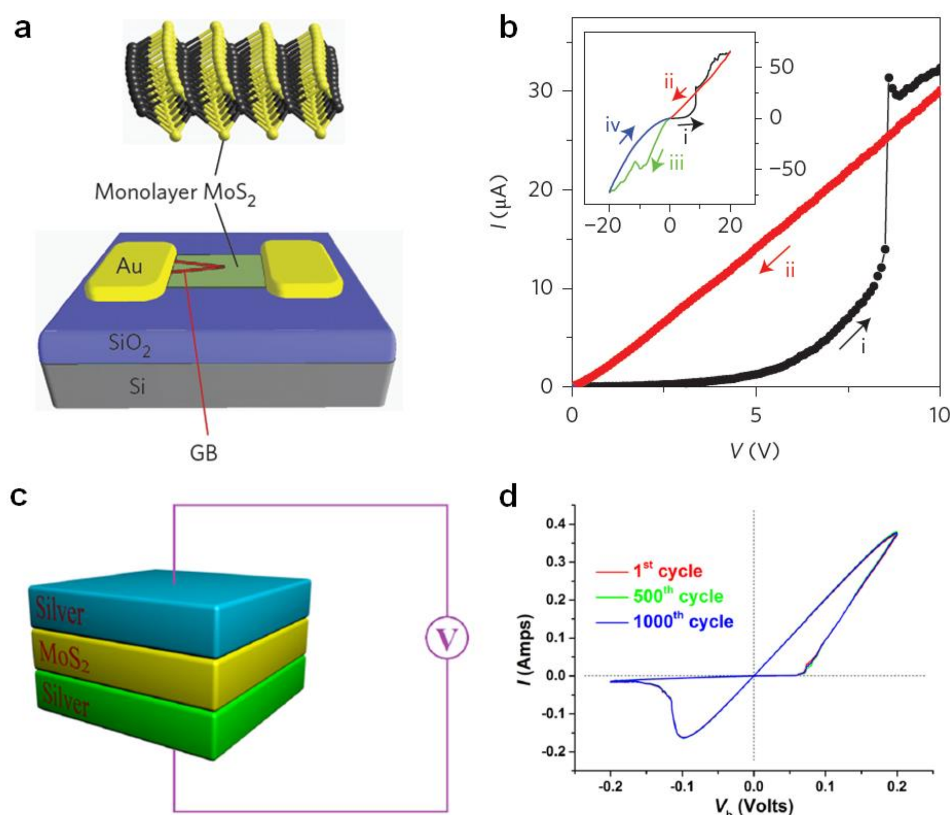

Fig. 12: (a) Schematic horizontal MoS_2 RRAM cell with two GBs connected to one of the electrodes and intersecting at a vertex within the channel [315]. (b) Partial *I–V* characteristics of an electroformed intersecting-GB memristor (channel length, L = 7 μm) obtained immediately after electroforming [315]. The set process occurs at V_{set} = 8.3 V with an abrupt twofold increase in current. Inset: Full *I–V* characteristics of one switching cycle. Measurements were performed at a sweep rate of 1 V s^{-1} and V_g = 40 V under vacuum (pressure <2 × 10^{-5} torr). The voltage was swept in the order 0 V → 20 V → 0 V → −20 V → 0 V, as shown by the coloured arrows with the four sweeps labelled as i, ii, iii and iv. (a) and (b) are reproduced with permission from [315]. Copyright from Macmillan Publishers Limited 2015. (c) Schematic structure of vertical Ag/MoS_2/Ag RRAM cell from [316]. (d) Typical *I−V* characteristic of Ag/MoS_2/Ag switch at the 1st (red), 500th (green), and 1000th (blue) cycle at room temperature. (c) and (d) are reproduced with permission from [316]. Copyright from American Chemical Society 2015.

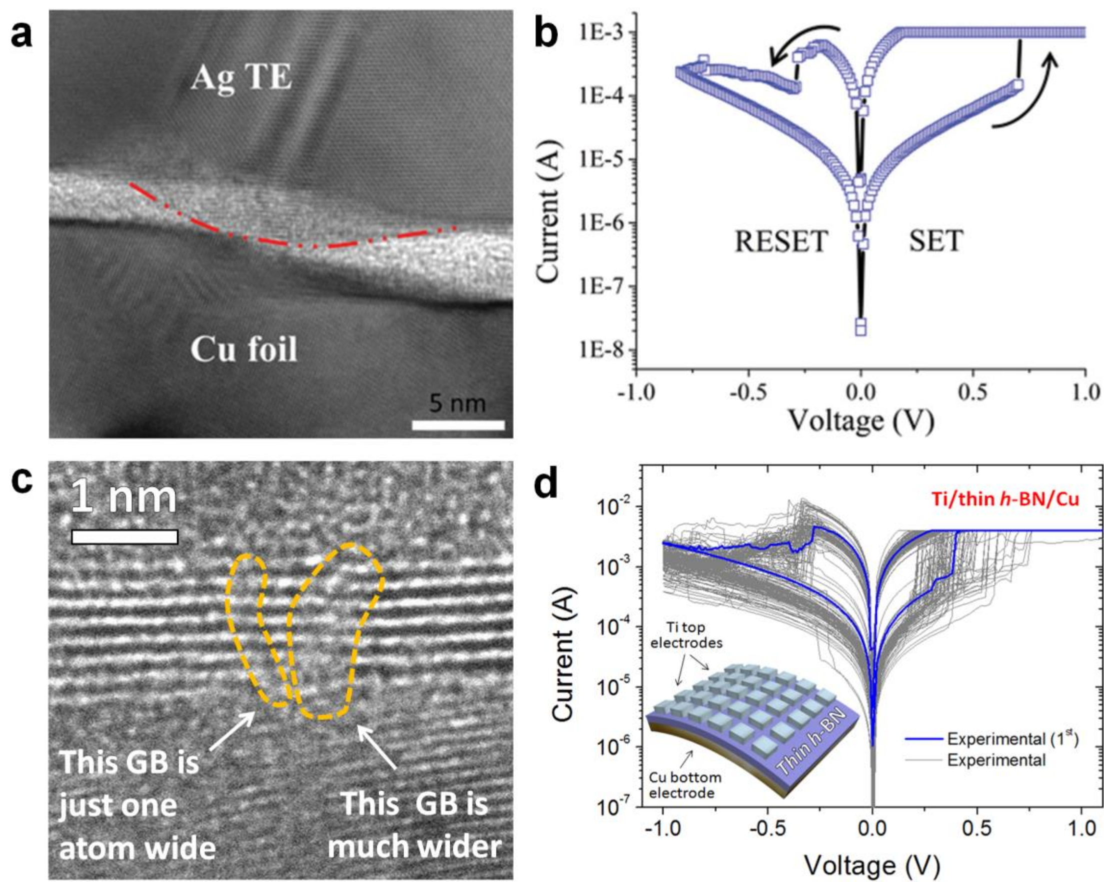

Fig. 13: (a) TEM image of a complete conducting filament. The thinnest region of the filament is at the *h*-BN/Cu foil interface [329]. (b) Switching characteristics of the Au/*h*-BN/Cu foil/PET devices. (a) and (b) are reproduced with permission from [329]. Copyright from WILEY-VCH 2016. (c) Cross-section TEM image of truly layered Ti/*h*-BN/Cu stacks [163]. (d) I-V curve collected on a 100 μm × 100 μm capacitor under a constant bias of 2.5V. (d) is reproduced with permission from [163]. Copyright from Wiley-VCH 2016.

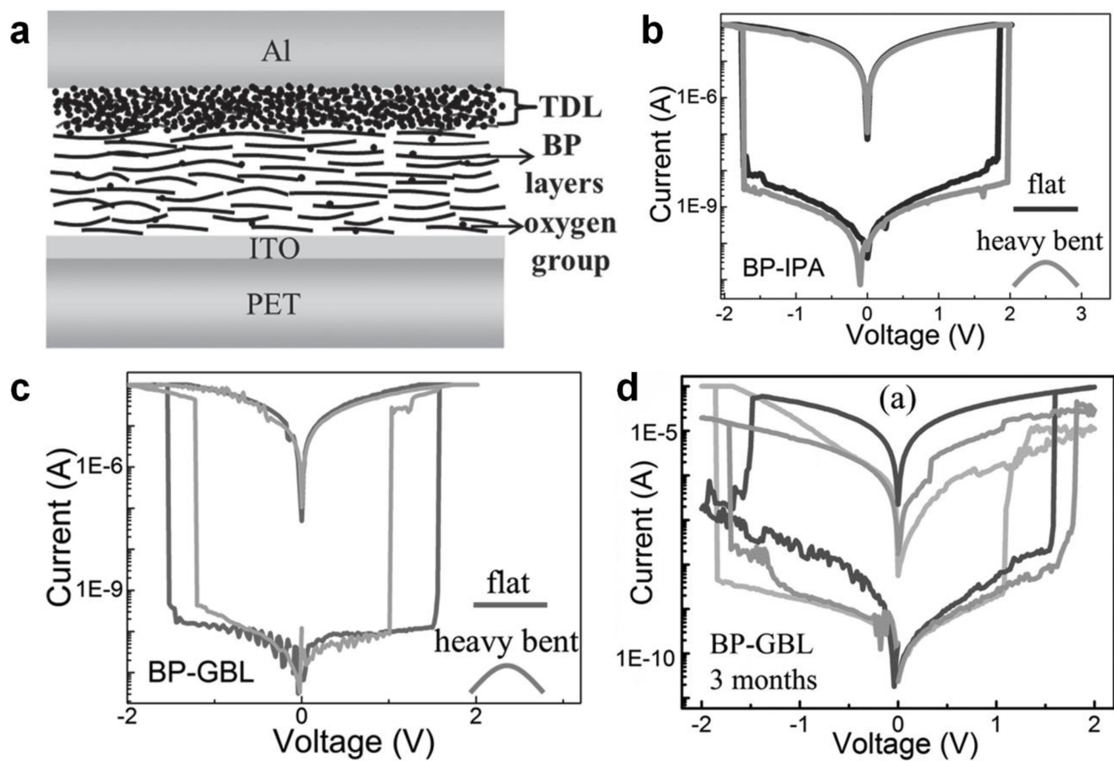

Fig. 14: (a) Shematic illustration of RRAM-BP cross-section. *I–V* characteristics for the RRAM-BP device of BP-IPA (b), and BP-GBL (c) in the flat and bent conditions [318]. Typical *I–V* curves obtained in the repeated voltage sweeping cycles for the RRAM-BP devices fabricated with the BP-GBL (d). Reproduced with permission from [318]. Copyright from Wiley-VCH 2016.

Table 1: Technology requirements for RRAM according to ITRS [2] vs. best performances reported for TMO-based and GRMs-based RRAM. The parameters highlighted in italics in GRMs-based RRAM columns indicate that they do not fit the technology requirements (although they are the highest reported). The ION/IOFF ratio is not strictly a technology requirement, but it is a reference parameter usually compared in RRAMs

Parameter	**Technology requirements**	**TMOs based RRAMs**			**GRMs based RRAMs**		
		Best performances	**Device structure**	**Ref.**	**Best performances**	**Device structure**	**Ref.**
Operating voltages	< 1V	0.3V	Ti/HfO_2/TiN	41	~ -0.6	ITO/GO/Ag	251
		0.1V	Pt/Ni/Al_2O_3/SiO_2/Si	43	~ 0.4V	Ti/*h*-BN/Cu	163
		-0.2V (set) / 0.5V (reset)	Pt/TiO_2/Pt	111	~ 0.7V	Al/GO/Al	253
Power consumption	~ 10 pJ/transition	0.1 pJ/transition	TiN/Hf/HfO_X/TiN	31	~ 100 pW	Gr/TiOx/Al_2O_3/TiO_2/Gr	185
		0.1-7 pJ/transition	Al/Ti/Al_2O_3/s-CNT	44	-	-	-
Switching times	< 10 ns/transition	300 ps	TiN/TiO_X/HfO_X/TiN	32	10 ns (set) / 1 ns (reset)	W/ta-C/W	286
		<10 ns	Al/Ti/Al_2O_3/s-CNT	44	5 ns (set) / 5 ns (reset)	Pt/RGO–th/Pt	273
		~ ns level	Cu/Al_2O_3/aSi/Ta	45	< 10s	PEN/Ti/Pt/GO/Ti/Pt	280
Endurance	$>10^9$ cycles	10^{12} cycles	Pt/Ta_2O_{5-X}/TaO_{2-X}/Pt	33	2×10^{13} cycles @ 75°C	W/ta-C/W	286
		5×10^9 cycles	Pt/TaO_X/Pt	364	*10^8*	*Al/PFCF/RGO/ITO*	*351*
		$>10^{12}$ cycles	Ta/TaO_X/TiO_2/Ti	111	*10^3 **	*Ag/MoS_2/Ag*	*316*
		10^{10} cycles	Pt/TaO_X/Ta	346	*> 650*	*Ti/h-BN/Cu*	*163*
		10^{11} cycles	W/AlO/TaO_X/ZrO_X/Ru	347	-	-	-
Data retention	>10 years	>10 years@ 85°C	Pt/Al_2O_3/HfO_2/Al_2O_3/TiN/Si	46	*> 10^7 s (115 days)*	*Al/GO/ITO*	249
		>10 years @ 85°C	Pt/TaOx/Pt	364	-	-	-

MIM cell Size	576 nm^2	5 nm^2	TaN/TiN/Zr/HfO_2/CAFM tip	296	8.5 nm^2	Pt/ta-C/C-AFM tip	296
		10 nm × 10 nm	TiN/Hf/HfO_X/TiN	31	-	-	-
I_{ON}/I_{OFF} ratio	10^6	3×10^6	Ni/GeO/STO/TaN	348	~ 10^9	Ag/ZrO_2/SLG/Pt	349
		2×10^6	Pt/Gd_2O_3/Pt	350	> 10^6	Ti/*h*-BN/Cu	163

Table 2: Graphene based RRAM devices with transparency and/or flexibility capability. In the column named *Flexible*, r_b and C are the bending radius and number of RS cycles collected during the test (respectively). For the *Transparent* column, the percentages correspond to light transmittance, and *Yes* mans that the authors claim that the structure is transparent but didn't quantify it. This will be valid for all tables in this manuscript showing such information.

Device structure	Fabrication method	Device area	I_{ON}/I_{OFF}	Set V [V]	Retention [s]	Endurance [cycles]	Power consumption [µW]	Switching time [ns]	Transparent	Flexible	Ref.
MLG/Dy_2O_3/ITO	CVD (Transfer)	80 - 3×10^4 [µm^2]	>10^5	0.4	>10^4	>100	4.4	60 (set) 60 (reset)	80%	No	192
ITO/SLG/ZnO/ITO	CVD (Transfer)	200 µm in diameter	20	-	10^4	>100	-	-	Yes	No	74
PS/SLG/PMMA/ SLG/PMMA *	CVD (Transfer)	500 µm in diameter	L1 10^4 L2: 10^6	L1: -2 L2: -4	10^4 s	1	-	-	Yes	No	116
Al/PMMA/MLG/ PMMA/ITO/PET	CVD (Transfer)	18-27 µm in diameter	4.4×10^6	3.4	1×10^5	1.5×10^5	-	-	Yes	r_b = 10 mm C = 1.5×10^5	195
MLG/PI:PCBM/Al	CVD (Transfer)	-	~ 10^6	4	1×10^4	>30	-	-	92%	r_b = 4.2 mm C = 1×10^4	75
Ti/Pt/TiO_2/G/PEN (G thickness not mentioned)	CVD (Transfer)	36×36 [µm^2]	10^2	2	10^6	1	3 (set) 94 (reset)	-	Yes	r_b = 10 mm C = 100	196
BLG/SiO_X/BLG/ITO	CVD (Transfer)	100 µm in diameter	10^5 **	5	-	100	-	-	90%	No	105
BLG/SiO_X/BLG/Polymer	CVD (Transfer)	100 µm in diameter	10^6	5	-	400	-	-	Yes	r_b = 12 mm C = 300	105

* This device shows multilevel RS. Depending on V_{SET} used the I_{ON}/I_{OFF} ratio changes. We give the parameters for both levels.
** This value is not well supported in Ref. [116], the *I-V* curve only shows 1-2 orders of magnitude, while the *R* vs. *Cycle* plot shows ~ 10^5. The *I-V* curve should be shown.

Table 3: Switching in GO based devices

Device Structure	Device area	I_{ON}/I_{OFF}	Set V [V]	Retention [s]	Endurance [cycles]	Ref.
Pt/GO/Cu	100 µm in diameter	500	~ 0.7	$>10^4$	>100	[241]
Pt/GO/Cu	100 µm in diameter	~ 1250	0.8 ~ 1.2	$>10^4$	>100	[245]
Pt/GO/Ti	100 µm in diameter	~ 650	0.8 ~ 1.2	$\sim10^5$	>100	[245]
Pt/GO/Ag	100 µm in diameter	~ 100	0.5 ~ 1	$\sim10^5$	~100	[245]
Pt/GO/Au	100 µm in diameter	~ 40	0.6 ~ 0.8	$\sim10^5$	>100	[245]
Si/GO/Al	600×600 [μm^2]	110	-5.5	10^3	~100	[250]
Ge/GO/Al	600×600 [μm^2]	76	-8.7	10^3	>100	[250]
Al/GO/Al	-	10^3	0.7	-	-	[253]
ITO/GO/Al	180 µm in diameter	10^3	-1.6	10^7	>100	[249]
ITO/GO/Ag	-	10^4	-0.6 ± 0.2	$>10^3$	-	[242]
ITO/GO/Ag	80 µm in diameter	<10	0.6	-	-	[133]
Ag/GO/Ag	-	10	6.7	$>10^3$	-	[251]
p-Si/GO/Ag	50 ~ 150 µm in diameter	10^4	3.5	$>10^3$	>100	[247]
Al/GO/Au/GO/ITO	-	10^2	-	-	10^4	[243]

Table 4: Switching in RGO based devices

Device structure	Device area	I_{ON}/I_{OFF}	Set V [V]	Retention [s]	Endurance [cycles]	Switching time [ns]	Ref.
PET/ITO/RGO+PVA+Au NP/Al	-	$>10^3$	0.44	$>10^4$	-	-	[352]
ITO/RGO/ITO	50 µm in diameter	-	2	10^5 @ 85°C	$>10^5$	30 (set) 30 (reset)	[262]
Au/RGO/ITO	-	10^3	2	10^5 s	-	-	[270]
Al/GO/ITO	~3 mm in diameter	10^5	-	$>10^4$	-	25 (set) 25 (reset)	[260]
Al/RGO/Al	-	10	-	$>10^6$	>100	-	[272]
Al/RGO/Al	100 µm in diameter	10^2	0.6	$>10^4$	>250	-	[271]
Pt/RGO–th/Pt	100 µm in diameter	$>10^4$	1.9 ~ 3.9	$>10^5$	>350	5 (set) 5 (reset)	[273]
Al/PFCF/RGO/ITO	0.4 mm in diameter	10^4	-1.2V	10^4	10^8	-	[351]
Al/RGO-ferrocene/ITO	0.04 mm in diameter	10^3	-	10^3 s	10^3	-	[274]
Ag/HfO_X/LSG (laser-scribed RGO)	-	10	-	10^4	100	-	[254]

Table 5: Switching in GO and RGO-polymer and mixed structures

Device structure	Device area	I_{ON}/I_{OFF}	Set V [V]	Retention [s]	Endurance [cycles]	Ref.
ITO/TPAPAM-GO/Al	0.4×0.4 [mm²]	10^3	-1	$>10^4$	10^8	[276]
ITO/GO-PVK/Al	-	$>10^3$	-2	$>10^4$	10^8	[275]
PET/ITO/PVK:Gr(GO)/Al	-	-	0.2 ~ 0.4	-	Not reversible	[353]
ITO/PVA+GO/Al	200 µm in diameter	10^4	-0.75	10^4	$>10^4$	[354]
ITO/PVDF-GO/Al	0.0004 [cm²]	10^4	3.6 ~ 4.1	-	-	[355]
Al/CuO/GO/CuO/Al	-	-	3.0	-	-	[244]
ITO/PMMA/GO/PMMA/Al	30 µm in diameter	$>10^3$	-1.7	10^4	$>10^5$	[356]
Gr/GO/ZnONR/Nb	-	10^3	-	-	>50	[357]
ITO/GOAu/Al	200 µm in diameter	10^6	-1	10^4	>300	[358]
ITO/GO-FeO/Pt	-	5×10^3	0.9	10^5	>1100	[359]
ITO/FPA-rGO/Al	0.04 [mm²]	10^3	1.6	$>10^3$	$>10^3$	[274]
Al/GO-PFCz-ITO	0.16 ~ 0.0225 [mm²]	10^3	0.38	$>10^4$	10^8	[351]
Au/PrGODMF/ITO	-	100	-	>1000	100	[128]
Ag/PI/GO:PI/PI/ITO	-	1000	5	1400	130	[258]
Pt/GO/PCMO/Pt	-	10^2	-0.75	10^4	150	[264]
Al/PS-b.P4VP-GO/ITO	0.4×0.4mm²	10^4	~ 6	$>10^4$	10^8	[360]
Al/P3HT:PCBM/rGO/glass	-	10^6	-	-	-	[140]
Pt/Zr:SiO*x*/C:SiO*x*/TiN	-	100	-	-	-	[268]
rGO/P3HT:PCBM/Al	-	10^4 -10^5	-	-	-	[279]
PET/rGO/MoS_2-PVP/Al	-	~ 10^2	-	-	-	[320]

Table 6: Switching in GO and RGO on flexible substrate

Device structure	Device area	I_{ON}/I_{OFF}	Set V [V]	Retention [s]	Endurance [cycles]	Switching time [ns]	Ref.
PET/ITO/GO/Al	300 µm in diameter	280	2.2	10^4	>100	-	[261]
PES/Al/GO/Al	50 µm × 50 µm	>100	-2.5	5×10^4	~ 100	-	[126]
PES/ITO/GO/ITO	150 µm in diameter	10	0.7 ~ 1	10^5	-	-	[361]
PET/ITO/GO/ZnO nanorods/Al	200 µm in diameter	~ 100	1 ~ 4.8	10^4	>200	-	[246]
PET/ITO/GO/Al	200 µm in diameter	~ 100	3.9	-	-	-	[246]
PET/ITO/GO/Ag	0.026 [mm^2]	5	-0.14	~10^3	13	-	[139]
PET/ITO/RGO+PVA+Au NP/Al	-	>10^3	-0.44	>10^4	-	-	[352]
Pt/RGO–th/Pt	100 µm in diameter	>10^4	1.9 ~ 3.9	>10^5	>350	<5 ns	[273]
Al/RGO/Al	100 µm in diameter	10^2	-0.6	>10^4	>250	-	[271]
PEN/Ti/Pt/GO/Ti/Pt	100 nm × 100 nm	-	3.5	>10^5	>10^3	<10 (set)	[280]
Al/GO/ITO	180 µm in diameter	10^3	-1.6	10^7	>100	-	[249]

Table 7: Hydrogenated amorphous carbon

Device structure	Device area	I_{ON}/I_{OFF}	Set V [V]	Retention [s]	Endurance [cycles]	Power consumption [μW]	Critical field [V/cm]	Switching time [ns]	Ref.
Cr/a-C:H:(B)/Au	-	10^2	-	-	-	-	5×10^5	-	[84]
Pt/a-C:H/Cu (Ag orAu)*	100 μm in diameter	>100	1.1	$>10^5$	110	-	-	-	[85]
TiN/a-C:H/Cu (Pt, W) **	49 ± 11 nm in diameter	$>10^3$	4.1	57,600	15	-	-	30 (set) <30 (reset)	[86]
TiN/a-C: H /Pt	0.36 to 16 [μm²]	100	1.5	10,000 @85°C	10^7	-	-	-	[87]

* The Cu electrode has been also replaced by Ag and Au, and the resulting devices also show resistive switching. It was found that the ON/OFF ratio (R) and switching threshold voltages (V) vary as follows: $R_{Cu}>R_{Ag}>R_{Au}$ and $V_{Cu}>V_{Au}>V_{Ag}$.

** This report used devices with Cu, Pt or W electrodes. From the paper, it is unclear to which electrode correspond the performances indicated.

Table 8: Doped amorphous carbon

Device structure	Device area	I_{ON}/I_{OFF}	Set V [V]	Retention [s]	Endurance [cycles]	Power consumption [µW]	Switching time [ns]	Ref.
W/a-CO_x/Pt,Ti,W	100 nm in diameter	$>10^2$	-	10^4 @ 85°C	$>10^4$	-	40 (set) 4(reset)	[294, 301]
Pt/a-$CN_{0.15}$/Cu	100 µm in diameter	1	0.6	$>10^6$	10^3	-	-	[295]
FTO/a-C:Co/Al	-	25	-	$>10^5$	-	-	-	[297]
Pt/a-C:Cu/Cu	0.1 × 0.1 [µm²]	10^2	0.7	10^4 @ 85°C	$>10^3$	-	-	[298, 299]
Pt/a-C:Cu/Pt	30x30 [µm²]	-	0.7	-	-	-	-	[300]
Pt/a-C:N/C-AFM tip	12 nm diameter	-	3	-	-	-	-	[296]
Pt/a-C:Si/C-AFM tip	-	-	3.5	-	-	-	-	[296]

Table 9: ta-C and a-C

Device structure	Device area	I_{ON}/I_{OFF}	Set V [V]	Retention [s]	Endurance [cycles]	Power consumption [µW]	Critical field [V/cm]	Switching time [ns]	Ref.
n-Si/a-C/C-AFM tip	-	10 @80K	5	3000	20	-	-	–	[307]
TiN/a-C (sp^2rich)/ C-AFM tip (PtSi)	20~30 nm in diameter	-	1~2	-	Not reversible	-	-	-	[285]
Pt/ta-C/C-AFM tip	8.5 nm in diameter	-	12V pulse amplitude	-	-	-	-	5 (set)	[296]
W/ta-C/W	150 nm in diameter	$>10^3$	1~3	-	2.3×10^{13} @ 75°C	-	-	10 (set) 1 (reset)	[286]
Ag/a-C/CNT	0.001 [μm^2]	40-200	5.4~7.5	$>10^6$	31	-	-	-	[290]
Al/a-C/Cu	-	3	<3	10^5	-	-	-	-	[291]
Al/ta-C/W	2500 [μm^2]	10	<1	$>10^5$	120	-	-	-	[287]
Pt/a-C/Cu,Ag	50x50 [μm^2]	-	0.18@0K	10^4@85°C	-	-	-	-	[306]
Pt/a-C/Cu	500µm in diameter	100	0.1	10^8	-	-	-	-	[304]
Pt/a-C/Cu	100µm in diameter	>70	1	-	110	-	-	-	[305]
Pt/ta-C/W	50-500 nm in diameter	>300	0.8	-	-	-	5×10^7	50 (set) 4 (reset)	[301,288,289]

Table 10: Transition Metal dichalcogenides based RRAMs

Device structure	Fabrication method	I_{ON}/I_{OFF}	Retention [s]	Endurance [cycles]	Power consumption [µW]	Switching time [ns]	Transparent	Flexible	Ref.
PMMA-MoS_2/MLG/SiO_2/Si	CVD (Transfer)	2.5×10^3	-	-	-	-	NO	NO	[317]
Ag/$MoSe_2$/FTO	Hydrothermal	12	>50	-	-	-	NO	NO	[315]
Au/MoS_2/SiO_2/Si	CVD	10^3	-	-	-	-	NO	NO	[326]
Ag/MoS_2/Ag	LPE (spin coating)	10^3	-	10^3 *	-	-	NO	NO	[316]
Ag/MoS_2-MoO_x/Ag	Modified Langmuir–Blodgett	$>10^6$	-	>8000s	10 nW	-	NO	YES	[327]
Al/MoS2-GO/ITO	LPE (spin coating)	10^2	-	-	-	-	NO	NO	[326]
RGO/ZIF-8 coated MoS_2/RGO	LPE (spin coating)	7×10^4	-	1.5×10^3s	-	-	NO	YES	[362]
RGO/MoS_2-P123/RGO	LPE (spin coating)	5.5×10^2 s	>50	4×10^3s	-	-	NO	NO	[363]
PET/RGO/MoS_2-PVP/Al	Polymer-assisted exfoliation	~ 10^2	-	-	-	-	NO	YES	[320]
RGO/MoS_2/ITO/Si	Hydrothermal	10^4	-	$>5.5 \times 10^3$ s	-	-	NO	NO	[328]

* This value is not well supported in Ref. [316]. The authors only show the 1st, 500th and 1000th *I-V* curves, and no *R* vs *Cycle* or Weibul plot is shown. Moreover the top electrodes of those devices are made by drying Ag paint on the spin coated MoS_2 using a shadow mast. More rigorous processes and better characterization is needed to confirm such performances.

Table 11: *h*-BN based RRAM devices.

Structure	Fabrication method	Bipolar RS under positive set	Forming process needed	V_{SET} [V] I_{SET} [A]	V_{RESET} [V] I_{RESET} [A]	I_{ON}/I_{OFF}	Endurance cycles	Retention time	Bipolar RS under negative set	Threshold RS	Ref.
Ti/hBN/Cu	CVD (no transfer)	YES	NO	0.4V 4×10^{-4}A	-0.3V 4×10^{-3}A	10	> 350	-	NO	YES	[163]
Ti/hBN/Cu	CVD (no transfer)	YES	NO	0.7V 4×10^{-6}A	-0.7V 10^{-2}A	10^4	> 600	-	YES	YES	[164]
Ti/hBN/CuNi	CVD (no transfer)	YES	YES	0.7V 4×10^{-3}A	-0.4V 2×10^{-2}A	15	-	-	NO	NO	[163]
Ti/hBN/CuNi	CVD (no transfer)	YES	YES	6V 10^{-3}A	-2V 10^{-1}A	10^6	-	-	YES	NO	[163]
Ti/hBN/ITO	CVD (transfer)	YES	NO	0.4V 2×10^{-4}A	-0.3V 10^{-3}A	10	> 180	-	NO	NO	[163]
Ti/MLG/hBN/MLG/Au	CVD (transfer)	YES	YES	2.3V 10^{-3}A	-0.6V 4×10^{-2}A	10^3	> 450	4×10^4 s	NO	NO	[163]
Al/hBN/WO_3/Al	CVD (transfer)	-	-	-	-	<10	~80	3×10^4	-	-	[107]
Ag/hBN/Cu/PET *	CVD (no transfer)	-	YES	-	-	100	550	3×10^3 s	-	-	[329]
Au/Ti/hBN/Cu *	CVD (no transfer)	-	YES	-	-	-	>100	-	-		[329]
Au/Ti/SLG/hBN/SiO_2/Si	MC	-	-	-	-	10^3	-	10^5 s	-	-	[338]

* The layered structure of the BN in Ref. [329] is not well supported. From their cross sectional TEM pictures it looks like an amorphous hBN film (see Figure 13).

Table 12: Black phosphorous based RRAM devices

Device structure	Fabrication method	I_{ON}/I_{OFF}	Retention [s]	Endurance [cycles]	Power consumption [μW]	Switching time [ns]	Transparent	Flexible	Ref.
Al/TDL/BP/ITO/PET	LPE (spin coating)	$\sim 3 \times 10^5$	-	10^5 s	-	-	NO	YES	[318]
(PET)/Au/BPQD-PVP/Ag	LPE (spin coating)	6×10^4	-	1100 s	-	-	NO	YES	[119]

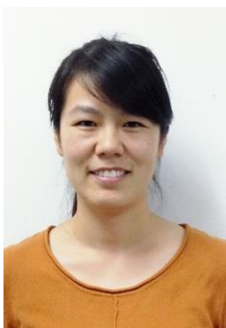

Fei Hui received a Bachelor degree in Chemistry from Huanghuai University in 2013. She is currently pursuing her PhD at Soochow University. Her research mainly focuses on two dimensional materials and their integration in resistive random access memories. Fei Hui has developed a patent on graphene-coated nanoprobes that has received 1M$ investment. In 2016 she received the Royal Society of Chemistry travel award.

Mario Lanza is Young 1000 Talent Professor and research group leader at Soochow University. He received his PhD in Electronic Engineering in 2010 at the Universitat Autonoma de Barcelona. During his PhD, he was visiting scholar at the Deggendorf Institute of Technology under a DAAD grant (where he worked in a project for with Infineon Technologies), and at The University of Manchester under a Ministry of Education grant. He was NSFC postdoctoral fellow at Peking University, and Marie Curie postdoctoral fellow at Stanford University. His research focuses on the

development of advanced electronic devices using graphene and related materials. Prof. Lanza has published over 75 research papers, including Science and Advanced Materials, and is a member of the editorial board of Nature Scientific Reports and Wiley-VCH (CRT). In 2016 he was ranked world top 2 Young Investigator in the field of Nanotechnology by Elsevier.